GEORGIA INSTITUTE OF TECHNOLOGY
OFFICE OF CONTRACT ADMINISTRATION

NOTICE OF PROJECT CLOSEOUT

Closeout Notice Date 05/07/91

Project No. E-21-T25_____ Center No. 10/24-6-R6583-T25_

Project Director JOY E B_____ School/Lab ELEC ENGR_____

Sponsor AIR FORCE/GRIFFISS AFB, NY_____

Contract/Grant No. F30602-88-D-0025-0025_____ Contract Entity GTRC

Prime Contract No. _____

Title SILICON-ON-INSULATOR PHOTONICS_____

Effective Completion Date 900430 (Performance) 900530 (Reports)

Closeout Actions Required:	Y/N	Date Submitted
Final Invoice or Copy of Final Invoice	Y	_____
Final Report of Inventions and/or Subcontracts	Y	_____
Government Property Inventory & Related Certificate	N	_____
Classified Material Certificate	Y	_____
Release and Assignment	Y	_____
Other _____	N	_____

Comments_____

_____

Subproject Under Main Project No. _____

Continues Project No. _____

Distribution Required:

Project Director	Y
Administrative Network Representative	Y
GTRI Accounting/Grants and Contracts	Y
Procurement/Supply Services	Y
Research Property Managment	Y
Research Security Services	Y
Reports Coordinator (OCA)	Y
GTRC	Y
Project File	Y
Other _____	N
_____	N

NOTE: Final Patent Questionnaire sent to PDPI.

CONTRACT FUNDS STATUS REPORT (DD FORM 1586)
CONTRACT NUMBER F30602-88-D-0025
QUARTER: MAY-JUN '88

	CURRENT QUARTER FUNDING		$0.00
	CURRENT QUARTER EXPENDITURES		$0.00
	CONTRACT CEILING		$4,200,000.00
	FUNDING TO DATE	-	$0.00
*	PENDING COMMITMENTS	-	$766,000.00
	AVAILABLE FUNDING		$3,434,000.00
	FUNDING TO DATE		$0.00
	YTD EXPENDITURES	-	$0.00
	OUTSTANDING EXPENDITURES		$0.00

*	C-8-2120	WESTINGHOUSE/BEAUDET	$56,000.00
	C-8-2129	RENSSELAER/DAS	$100,000.00
	E-8-7066	UNIV OF PENN/STEINBERG	$100,000.00
	E-8-7124	BOSTON COLLEGE/McFADDEN	$35,000.00
	E-8-7125	BRANDEIS UNIV/HENCHMAN	$23,000.00
	E-8-7126	PENN STATE/CASTLEMAN	$22,000.00
	A-8-1631	UNIV OF PENN/STEINBERG	$100,000.00
	B-8-3617	GA WASHINGTON UNIV/MELTZER	$100,000.00
	B-8-3618	GA WASHINGTON UNIV/BERKOVICH	$100,000.00
	C-8-2492	GA TECH/SMITH	$50,000.00
	A-8-1203	GA TECH/HUGHES	$80,000.00
		TOTAL PENDING	$766,000.00

CONTRACT FUNDS STATUS REPORT (DD FORM 1586)
CONTRACT NUMBER F30602-88-D-0025
QUARTER: JUL-SEPT '88

CURRENT QUARTER FUNDING			$698,034.00
DO # 0001	$56,000		
0002	$95,141		
0003	$78,854		
0004	$230,000		
0005	$45,561		
0006	$25,000		
0007	$20,000		
0008	$98,374		
0009	$29,403		
0010	$19,701		
	$698,034		
CURRENT QUARTER EXPENDITURES			$0.00
CONTRACT CEILING			$4,200,000.00
FUNDING TO DATE		-	$698,034.00
* PENDING COMMITMENTS		-	$426,563.00
AVAILABLE FUNDING			$3,075,403.00
FUNDING TO DATE			$698,034.00
YTD EXPENDITURES		-	$0.00
OUTSTANDING EXPENDITURES			$698,034.00

* DO # 0001	INCREMENTAL FUNDING		$90,729.00
0002	INCREMENTAL FUNDING		$66,680.00
0003	INCREMENTAL FUNDING		$54,154.00
0004	INCREMENTAL FUNDING		$20,000.00
C-8-2400	STATE UNIV OF NY/FAM		$95,000.00
C-8-2402	RENSSELAER/SAULNER		$100,000.00
TOTAL PENDING			$426,563.00

CONTRACT FUNDS STATUS REPORT (DD FORM 1586)
CONTRACT NUMBER F30602-88-D-0025
QUARTER: OCT-DEC '88

	CURRENT QUARTER FUNDING		$120,834.00
	DO # 0004	$66,680	
	0006	$54,154	
		$120,834	
	CURRENT QUARTER EXPENDITURES		$28,740.82
	CONTRACT CEILING		$4,200,000.00
	FUNDING TO DATE	-	$818,868.00
*	PENDING COMMITMENTS	-	$784,729.00
	AVAILABLE FUNDING		$2,596,403.00
	FUNDING TO DATE		$818,868.00
	YTD EXPENDITURES	-	$28,740.82
	OUTSTANDING EXPENDITURES		$790,127.18

*	DO # 0001	INCREMENTAL FUNDING	$90,729.00
	0007	INCREMENTAL FUNDING	$20,000.00
	C-8-2400	STATE UNIV OF NY/FAM	$95,000.00
	C-8-2402	RENSSELAER/SAULNER	$100,000.00
	B-9-3592	UNIV OF CA/DAVIS/LEVITT	$60,000.00
	N-9-5514	SOHAR INC./HECHT	$50,000.00
	C-9-2015	NCS/O'NEAL	$100,000.00
	A-9-1120	HITEC, INC./KAZAKOS	$75,000.00
	E-9-7057	UNIV OF TX/ARLINGTON/FUNG	$40,000.00
	E-9-7093	MONTANA STATE/JOHNSON	$34,000.00
	S-9-7552	ALFRED UNIV/SYNDER	$20,000.00
	C-9-2404	STANFORD UNIV/WIDROW	$100,000.00
		TOTAL PENDING	$784,729.00

CONTRACT FUNDS STATUS REPORT (DD FORM 1586)
CONTRACT NUMBER F30602-88-D-0025
QUARTER: JAN-MAR '89

CURRENT QUARTER FUNDING			$574,457.00
DO # 0001	$90,729		
0011	$75,000		
0012	$75,000		
0013	$59,989		
0014	$49,989		
0015	$70,000		
0016	$43,750		
0017	$30,000		
0018	$22,000		
0019	$38,000		
0020	$20,000		
	$574,457		
CURRENT QUARTER EXPENDITURES			$86,324.15
CONTRACT CEILING			$4,200,000.00
FUNDING TO DATE		-	$1,393,325.00
* PENDING COMMITMENTS		-	$594,651.00
AVAILABLE FUNDING			$2,212,024.00
FUNDING TO DATE			$1,393,325.00
YTD EXPENDITURES		-	$115,064.97
OUTSTANDING EXPENDITURES			$1,278,260.03

* DO # 0007	INCREMENTAL FUNDING		$20,000.00
0011	INCREMENTAL FUNDING		$19,568.00
0012	INCREMENTAL FUNDING		$24,700.00
0015	INCREMENTAL FUNDING		$29,783.00
0016	INCREMENTAL FUNDING		$31,250.00
0017	INCREMENTAL FUNDING		$10,000.00
0018	INCREMENTAL FUNDING		$12,000.00
0019	INCREMENTAL FUNDING		$12,000.00
C-8-2404	STANFORD UNIV/WIDROW		$100,000.00
N-9-5732	GRIFFIN		$25,000.00
A-9-1476	BOWDOIN COLLEGE/CHONACKY		$20,350.00
E-9-7110	UNIV OF LOWELL/SALES		$50,000.00
S-9-7559	UNIV OF MICHIGAN/ROBINSON		$20,000.00
B-9-3621	SRI/LUNT		$20,000.00
N-9-5308	KAMAN SCIENCES		$100,000.00
E-9-7119	DARTMOUTH COLLEGE/CRANE		$100,000.00
	TOTAL PENDING		$594,651.00

CONTRACT FUNDS STATUS REPORT (DD FORM 1586)
CONTRACT NUMBER F30602-88-D-0025
QUARTER: APR-JUN '89

CURRENT QUARTER FUNDING			$160,350.00
DO # 0021	$25,000		
0022	$45,000		
0023	$20,350		
0024	$50,000		
0025	$20,000		
	$160,350		
CURRENT QUARTER EXPENDITURES			$318,963.82
CONTRACT CEILING			$4,200,000.00
FUNDING TO DATE		-	$1,553,675.00
* PENDING COMMITMENTS		-	$718,994.00
AVAILABLE FUNDING			$1,927,331.00
FUNDING TO DATE			$1,553,675.00
YTD EXPENDITURES		-	$434,028.79
OUTSTANDING EXPENDITURES			$1,119,646.21

* DO # 0007	INCREMENTAL FUNDING		$20,000.00
0011	INCREMENTAL FUNDING		$19,568.00
0012	INCREMENTAL FUNDING		$24,700.00
0015	INCREMENTAL FUNDING		$29,783.00
0016	INCREMENTAL FUNDING		$31,250.00
0017	INCREMENTAL FUNDING		$10,000.00
0018	INCREMENTAL FUNDING		$12,000.00
0019	INCREMENTAL FUNDING		$12,000.00
0022	INCREMENTAL FUNDING		$54,693.00
B-9-3621	SRI/LUNT		$20,000.00
N-9-5308	KAMAN SCIENCES		$100,000.00
E-9-7119	DARTMOUTH COLLEGE/CRANE		$100,000.00
N-9-5740	CHRISTIANSON		$15,000.00
N-9-5317	UNIV OF CO/NORGARD		$50,000.00
S-9-7625	UNIV OF CA/DAVIS/KOWELL		$20,000.00
N-9-5314	KAMAN SCIENCES		$100,000.00
N-9-5315	KAMAN SCIENCES		$100,000.00
	TOTAL PENDING		$718,994.00

CONTRACT FUNDS STATUS REPORT (DD FORM 1586)
CONTRACT NUMBER F30602-88-D-0025
QUARTER: JUL-SEP '89

CURRENT QUARTER FUNDING			$476,000.00
DO # 0017	$10,000		
0026	$15,000		
0027	$20,000		
0028	$50,000		
0029	$40,000		
0030	$30,000		
0031	$20,000		
0032	$66,000		
0033	$70,000		
0034	$85,000		
0035	$70,000		
	$476,000		
CURRENT QUARTER EXPENDITURES			$415,422.69
CONTRACT CEILING			$4,200,000.00
FUNDING TO DATE		-	$2,029,675.00
* PENDING COMMITMENTS		-	$253,994.00
AVAILABLE FUNDING			$1,916,331.00
FUNDING TO DATE			$2,029,675.00
YTD EXPENDITURES		-	$849,451.48
OUTSTANDING EXPENDITURES			$1,180,223.52

* DO # 0007	INCREMENTAL FUNDING		$20,000.00
0011	INCREMENTAL FUNDING		$19,568.00
0012	INCREMENTAL FUNDING		$24,700.00
0015	INCREMENTAL FUNDING		$29,783.00
0016	INCREMENTAL FUNDING		$31,250.00
0018	INCREMENTAL FUNDING		$12,000.00
0019	INCREMENTAL FUNDING		$12,000.00
0022	INCREMENTAL FUNDING		$54,693.00
N-0-5703	UNIV OF SOUTHERN FLA/WILSON		$50,000.00
	TOTAL PENDING		$253,994.00

CONTRACT FUNDS STATUS REPORT (DD FORM 1586)
CONTRACT NUMBER F30602-88-D-0025
QUARTER: OCT-DEC '89

CURRENT QUARTER FUNDING				$292,994.00
DO #	0001	$9,000	C-8-2129	
	0011	$19,568	C-8-2400	
	0012	$24,700	C-8-2402	
	0015	$29,783	C-9-2015	
	0016	$31,250	A-9-1120	
	0018	$12,000	E-9-7093	
	0019	$62,000	C-9-2109	
	0022	$54,693	C-9-2404	
	0028	$50,000	N-9-5308	
		$292,994		

CURRENT QUARTER EXPENDITURES		$286,691.16
CONTRACT CEILING		$4,200,000.00
FUNDING TO DATE	-	$2,322,669.00
* PENDING COMMITMENTS	-	$595,000.00
AVAILABLE FUNDING		$1,282,331.00
FUNDING TO DATE		$2,322,669.00
YTD EXPENDITURES	-	$1,136,142.64
OUTSTANDING EXPENDITURES		$1,186,526.36

*	DO # 0007	S-8-7592	INCREMENTAL FUNDING	$20,000.00
	0029	E-9-7119	INCREMENTAL FUNDING	$60,000.00
	0030	N-9-5317	INCREMENTAL FUNDING	$20,000.00
	0034	N-9-5314	INCREMENTAL FUNDING	$15,000.00
	0016	N-9-5315	INCREMENTAL FUNDING	$30,000.00
	N-0-5703	UNIV OF SOUTHERN FLA/WILSON		$50,000.00
	A-0-1102	UNIV OF CA/SMOOT, BARBER, GT		$100,000.00
	P-0-6011	NCSU/VANDERLUGT		$100,000.00
	C-0-2456	NEW JERSEY INST/BAR-NESS		$100,000.00
	P-0-6014	STEVENS INST/ZMUDA		$100,000.00
	TOTAL PENDING			$595,000.00

WAITING FOR PROPOSALS:
P-0-6018 UAH/CAULFIELD
P-0-6021 GT/SUMNERS
P-0-6022 CORNELL UNIV/TANG
B-0-3353 ROCHESTER INST/LASKY

CONTRACT FUNDS STATUS REPORT (DD FORM 1586)
CONTRACT NUMBER F30602-88-D-0025
QUARTER: JAN-MAR '90

CURRENT QUARTER FUNDING				$114,301.00
DO #	0007	$9,000	S-8-7592	
	0029	$19,568	E-9-7119	
	0030	$24,700	N-9-5317	
	0036	$29,783	P-0-6014	
	0037	$31,250	P-0-6011	
		$114,301		
CURRENT QUARTER EXPENDITURES				$376,743.62
CONTRACT CEILING				$4,200,000.00
FUNDING TO DATE				- $2,436,970.00
* PENDING COMMITMENTS				- $532,800.00
AVAILABLE FUNDING				$1,230,230.00
FUNDING TO DATE				$2,436,970.00
YTD EXPENDITURES				- $1,512,886.26
OUTSTANDING EXPENDITURES				$924,083.74

* DO#	0034	N-9-5314	INCREMENTAL FUNDING	$15,000.00
	0035	N-9-5315	INCREMENTAL FUNDING	$30,000.00
	0037	P-0-6011	INCREMENTAL FUNDING	$10,000.00
	N-0-5703	UNIV OF SOUTHERN FLA/WILSON		$50,000.00
	A-0-1402	UNIV OF CA/SMOOT, BARBER, GT		$100,000.00
	C-0-2456	NEW JERSEY INST/BAR-NESS		$100,000.00
	P-0-6021	GT/SUMNERS		$100,000.00
	P-0-6022	CORNELL UNIV/TANG		$30,800.00
	B-0-3353	ROCHESTER INST/LASKY		$20,000.00
	P-0-6018	UAH/CAULFIELD		$77,000.00
TOTAL PENDING				$532,800.00

WAITING FOR PROPOSALS:
P-0-6018 UAH/CAULFIELD
P-0-6021 GT/SUMNERS
P-0-6022 CORNELL UNIV/TANG
B-0-3353 ROCHESTER INST/LASKY

GEORGIA INSTITUTE OF TECHNOLOGY
SCHOOL OF ELECTRICAL ENGINEERING
ATLANTA, GEORGIA 30332

TELEPHONE: (404) 894-

November 21, 1989

Mr. David R. Trujillo
Solar Energy Research Institute
1617 Cole Blvd.
Golden, CO 80401-3393

SUBJECT: Contract No. XX-8-181551 under DE-ACO2-83CH10093
Project Director: A. Rohatgi

Dear Mr. Trujillo:

Enclosed please find copies of the Monthly Contract Management Report for the period 10/1/89-10/31/89 on the above referenced contract.

If you have any questions, please feel free to contact me.

Sincerely,

Pam Majors
Research Administrator

pm
Enclosure

cc: Mr. Bhushan Sopori

FORM DOE 536
(1/78)

CONTRACT MANAGEMENT SUMMARY REPORT

FORM APPROVED
OMB NO. 38R-0190

1. Contract Identification	2. Reporting Period	3. Contract Number
Impurity Characterization Support for Silicon	10/1/89 through 10/31/89	XX-8-18155-1

4. Contractor (Name and Address)	5. Contract Start Date	6. Contract Completion Date
Solar Energy Research Institute 1617 Cole Blvd. Golden, CO 80401-3393	10/1/88	12/1/89

7. Months	OCT	NOV	DEC	JAN	FEB	MAR	APR	MAY	JUN	JUL	AUG	SEP	OCT	NOV	DEC	8. FY 88/89

9. Cost Status

g. Cost Plan Date: 10/1/88

a. / b. B&R Numbers

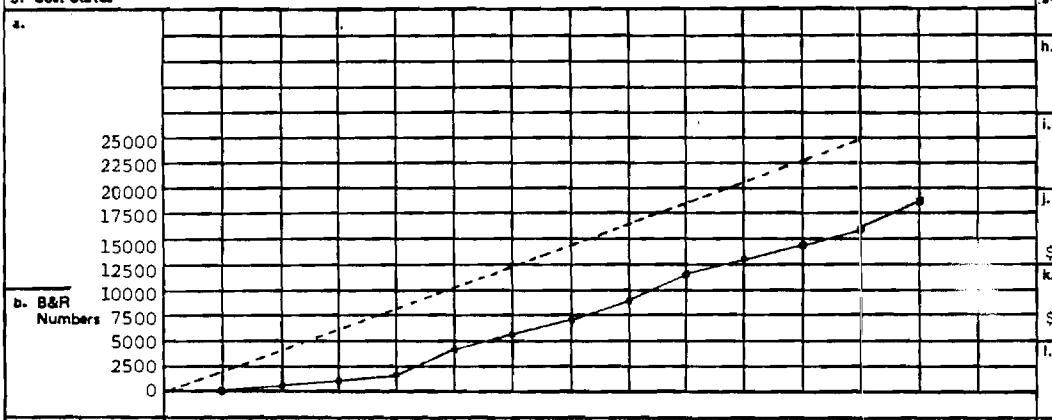

h. Planned Costs Prior FYs

i. Actual Costs Prior FYs

j. Total Estimated Costs for Contract: $25,000

k. Total Contract Value: $25,000

l. Unfilled Orders Outstanding

Accrued Costs																
c. Planned	0	2.3	2.3	2.3	2.3	2.3	2.3	2.3	2.3	2.3	2.3	2.0				
d. Actual	0	.9	.9	.4	2.3	1.1	1.7	1.7	1.7	1.7	1.7	1.7	1.7			
e. Variance	0	1.4	1.4	1.9	0	1.2	0.6	0.6	0.6	0.6	0.6	0.6				
f. Cum. Variance	0	1.4	2.8	4.7	4.7	5.9	6.5	7.1	7.7	8.3	8.9	9.5				

m. Estimate for Subsequent Reporting Period: 3,534

10. Manpower Status (Direct Labor)

e. Manpower Plan Date: 10/1/88

a.

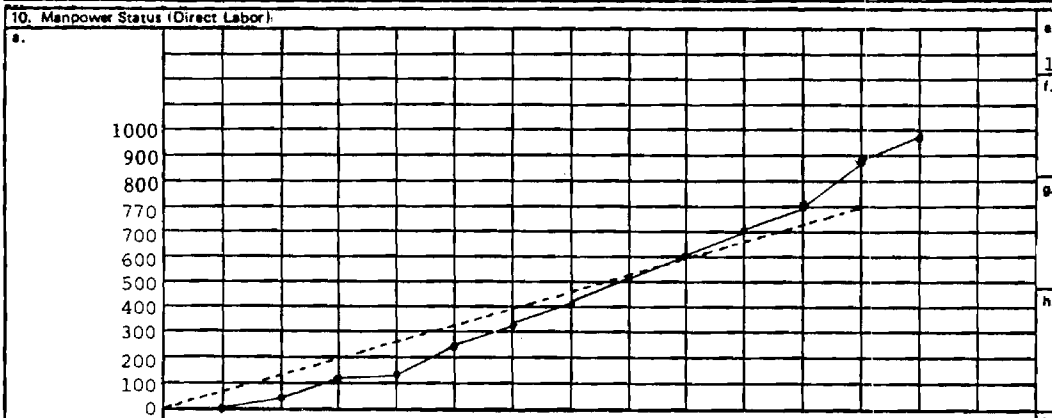

f. Planned Manpower Prior FYs

g. Actual Manpower Prior FYs

h. Total Estimated Manpower for Contract: 770

i. Total Contract Manpower: 770

Manpower																
b. Planned	0	70	70	70	70	70	70	70	70	70	70	70				
c. Actual	0	51	51	25	129	65	97	97	97	97	97	97	87			
d. Variance	0	19	19	45	(59)	5	(27)	(27)	(27)	(27)	(27)	(27)				

11. Major Milestone Status

a. Task 1. DLTS Measure.

b. Task 2. FTIR Measure.

c. Task 3. PAS Measure.

d. Task 4 PL Measure.

e.

f.

g.

h.

i.

12. Remarks

13. Signature of Contractor's Project Manager and Date	14. Signature of Government Technical Representative and Date

E-21-T[illegible]

ROME AIR DEVELOPMENT CENTER
EXPERT SCIENCE AND ENGINEERING PROGRAM
CONTRACT NO. F30602-88-D-0025

R & D STATUS REPORT

PERIOD COVERED: 6/30/89 - 9/30/89

TASK NUMBER: E-21-T15-S1

TITLE: Silicon-on-Insulator Photonics

PRINCIPAL INVESTIGATOR: Prof. Andrew L. Robinson

INSTITUTION: University of Michigan

OTHER PARTICIPANTS AND TITLES: Mr. Russell Watts, research student

A. TECHNICAL PROGRESS ACHIEVED ON EFFORT:

Designed mask set for prototype micromechanical silicon-on-insulator photonic devices:

1. On/off cantilever optical modulator
2. Doubly-supported beam modulator
3. Doubly-supported beam interferometer
4. Passive test structures for transmission loss characterization

Literature review on silicon-on-insulator photonics, micromechanical strucrtures

Began development of fabrication process

Please note that although the contract shows a start date of 6/30/89, funding was not actually available until the second week of August.

B. TRAVEL:

NONE

C. PRESENTATIONS AND PUBLICATIONS:

NONE

D. LEVEL OF EFFORT BY EACH CONTRIBUTOR (IN MAN-MONTHS OR MAN-HOURS)

Robinson: 1/2 man-month

Watts: 25 man-hours

ROME AIR DEVELOPMENT CENTER
EXPERT SCIENCE AND ENGINEERING PROGRAM
CONTRACT NO. F30602-88-D-0025

R & D STATUS REPORT

PERIOD COVERED: 10/1/89 -- 3/31/90

TASK NUMBER: E-21-~~T4~~-S1

TITLE: SILICON-ON-INSULATOR PHOTONICS

PRINCIPAL INVESTIGATOR: Prof. Andrew L. Robinson

INSTITUTION: University of Michigan

OTHER PARTICIPANTS AND TITLES: Mr. Russell Watts, research student

A. TECHNICAL PROGRESS ACHIEVED ON EFFORT:

Continued development of fabrication process. Bonding-and-etchback SOI technology was implemented for prototype test device fabrication. This process requires further optimization, but successful on initial samples. The primary remaining issue is optimization for thickness uniformity and surface smoothness.

The complete fabrication sequence was initiated on BESOI sample. Techniques for infrared alignment of waveguide patterns to underlying etched recesses (used for electrostatic activation of the micromechanical SOI photonic devices) were developed. Dry etching techniques for 5-um-thick waveguide structures are in progress.

A technical analysis of the prototype micromechanical SOI photonic devices was initiated.

B. TRAVEL: None

C. PRESENTATIONS AND PUBLICATIONS:

None

D. LEVEL OF EFFORT BY EACH CONTRIBUTOR (IN MAN-MONTHS OR MAN-HOURS)

Robinson: 1/2 man-month

Watts: 120 man-hours

FINAL TECHNICAL REPORT: SILICON-ON-INSULATOR PHOTONICS

Contract No. E-21-T25-51

Prof. Andrew L. Robinson and Russell Watts
Solid State Electronics Laboratory
Department of Electrical Engineering and Computer Science
University of Michigan
Ann Arbor, MI 48109-2122

Summary

This is the Final Report for the project on Silicon-on-Insulator Photonics, funded by the Rome Air Development Center as a subcontract from the Georgia Institute of Technology (contract no. E-21-T25-51).

The Statement of Work called for research on two topics. The first was the development in our laboratory of a silicon-on-insulator wafer fabrication technique based on the bonding-and-etchback SOI (BESOI) method. The second the development of microstructures for waveguides and active devices on BESOI substrates. The active devices were to be controlled by a novel technique for controlling the optical signals, where micromechanical structures would be manipulated to modify the path of the light. Due to problems in the first task described in more detail below, we were unable to complete the fabrication of the samples. We have identified the problems and potential solutions, which are also described below.

In addition, we have performed an analysis SOI waveguide structures in general, and of the proposed micromechanical active devices in particular. We have identified several important relationships between the physical characteristics and performance of the waveguides and micromechanical active devices, resulting in some design guidelines for these structures. These results will have a strong impact on any future work in this area.

This report consists of two sections. Sec. is a brief summary of the progress made, problems encountered, and potential solutions in the fabrication task. Sec. is a report written by Mr. Russell Watts, the student working on the project. In addition to describing the fabrication work in somewhat more detail, it presents a discussion of electromechanically induced optical effects as they relate to the proposed micromechanical photonic devices.

Fabrication Process

In our Statement of Work, we proposed to fabricate BESOI samples using the following sequence of steps:

1. Form epitaxial substrate with etch-stop layers
2. Oxidize epitaxial substrate and "handle" wafer
3. Contact epitaxial substrate and "handle" wafer, and permanently bond at elevated temperature
4. Etch back epitaxial substrate to remove original silicon and etch-stop layers; this leaves a SOI layer on "handle" wafer, which provides mechanical support for subsequent fabrication

Because our laboratory does not have the equipment necessary for growth of silicon layers, we have used outside vendors to provide this as a service. The etch-stop layers in the "seed" wafers are formed by ion implantation, which can be performed by a large number of vendors. The epitaxial growth step itself is more difficult, in that a small thermal budget is required to prevent outdiffusion of the etch stop layer. We obtained samples from Lawrence Semiconductor Laboratories in Phoenix, AZ; they use a rapid-thermal technique which results in very abrupt interfaces between the etch stop and the epitaxial layer.

The process of preparing the samples for bonding and the bonding itself (Steps2 and 3 above) is quite simple, and has not presented any difficulties. In fact, high-quality silicon wafers tend to stick together when contacted. We have not had significant problems due to voids caused by particulate

contamination. While this might be a problem for a high-volume process, it is being addressed by the companies interested in BESOI.

The primary problem we have encountered has been in the etch-back of the "seed" wafer to leave behind the SOI film. A four-step process is used[1]:

1. Rapid etching of the "seed" to remove most of the silicon substrate
2. Etching down to the p+ etch stop using EDP, which has an etch rate that is strongly doping-dependent
3. Removal of the p+ etch stop using a 1:3:8 etch, which etches heavily-doped material ($> 10^{18}\text{cm}^{-3}$) much more rapidly than more lightly-doped material
4. Final thinning of the SOI layer using a combination of isotropic chemical etching and thermal oxidation

After the third step, the surface condition of the wafer is approximately in its final state. This is where we encountered difficulty; the roughness of the wafers at this point precluded their further use for either electronic or optical structures. We estimate the short-range RMS roughness to be on the scale of 10 nm, which would cause significant propagation loss in the waveguides due to scattering at the top interface. It is believed that this roughness is related to the ion implantation parameters used in the formation of the etch-stop in the "seed" wafer. There is anecdotal evidence that the dose rate of the ion implantation can affect the roughness of the final SOI layer; high dose rates cause increased surface roughness. This information was not available at the time this project was started, and there was insufficient funding to permit optimization of the interaction between the ion implantation, the epitaxial growth, and the final quality of the sample.

In addition to the "standard" approaches used by previous researchers, we proposed to the use of electrochemical etching to provide improved SOI film uniformity, thickness control, and electrical quality. We achieved limited success with this technique, for the same reasons outlined above.

We note that BESOI wafers are now commercially available. However, these wafers would be unsuitable for SOI photonics. They have excellent surface finish, which provided by the mechanical polishing techniques used for the entire thinning process. However, the thinnest samples available are around 2 μm, and the thickness uniformity is on the order of 0.5 μm. The thickness could be reduced uniformly by thermal oxidation followed by removal of the resulting silicon dioxide layer, but the relatively poor thickness uniformity would result in corresponding variations in the waveguide thickness in a given sample. While the uniformity might be acceptable for proof-of-concept experiments in a university or research setting (we are, in fact, considering this as an interim approach to obtaining adequate material), they would be not be uniform enough for fabrication of uniform devices over an entire wafer. This problem would be solved by further advances in the mechanical thinning process, or by commercialization of a chemical thinning process similar to the one we use.

While the other commercially-available SOI techniques – zone-melting recrystallization (ZMR) and separation by implanted oxygen (SIMOX) could be used to make waveguide structures, there are some problems inherent in their use. ZMR typically have some surface undulations on the order of 10 nm, with a lateral distance scale on the order of 100 μm. Since this is a long-range "roughness" (relative to the wavelength scale under consideration), it should not add substantial scattering loss. However, the ZMR process is likely to induce non-uniform stress in the SOI film, which would

[1] "W. P. Maszara, G. Goetz, T. Caviglia and J. B. McKitterick, Bonding of silicon wafers for silicon-on-insulator", *J. Appl. Phys.*, vol. 64, no. 10, pp. 4943-4950, 1988.

make it unsuitable for micromechanical applications calling for flat suspended structures. SIMOX might have sufficiently uniform stress to make flat structures over the dimensions of interest, but as-implanted SIMOX is only about 200 nm thick; it would be necessary to use an epitaxial growth step to increase the thickness up to the 1 μmrange necessary to get light out of a waveguide structure (see page 84 in the report in Sec. below). In addition, the buried oxide can only be about 0.4 μmthick, which places a limitation on design flexibility. The well depth, which provides for the motion that would induce the desired optical effects, would essentially be fixed at whatever the SIMOX process provides.

We continue to support the BESOI approach for fabrication of material for SOI photonics, particularly in the context of the micromechanical devices described below, because it provides the best combination of micromechanical properties and design flexibility.

Report by Russell Watts

The information that follows is a report written by Mr. Russell Watts, the student working on the project. In addition to describing the fabrication work in somewhat more detail, it presents a discussion of electromechanically induced optical effects as they relate to the proposed micromechanical photonic devices. It presents an analysis SOI waveguide structures in general, and of the proposed micromechanical active devices in particular. We have identified several important relationships between the physical characteristics and performance of the waveguides and micromechanical active devices, resulting in some design guidelines for these structures. These results will have a strong impact on any future work in this area.

SILICON-ON-INSULATOR (SOI) PHOTONICS

CONTRACT NO. E-21-T25-51
COTR: Dr. Richard Soref /RADC
Prepared by: Russell Watts
Under the Direction of: Asst. Prof. Andrew L. Robinson
Department of Electrical Engineering
The University of Michigan
1990

ABSTRACT

The purpose of this investigation was to demonstrate a capability to integrate micro-machining techniques with SOI technology for the fabrication of optical waveguide structures that can be controlled electro-mechanically. A significant part of this effort was devoted to the experimental development of a process sequence for the fabrication of some representative structures that are described in this report. We also present, supported by modeling, a discussion of electro-mechanically induced optical effects as they relate to two particular structures: a silicon cantilever beam and a silicon bridge. Emphasis is focussed on the transformation of optical waveguiding properties due to elastic deformation of these structures for purposes of switching and transduction.

TABLE OF CONTENTS

CHAPTER I

INTRODUCTION

The term "Integrated optics", attributed to Miller by Nishihara et al. [1] in 1969, was used to describe techniques which combined microlithographic processes prevalent in the electronic semiconductor industry with electro-optical materials and devices to fabricate miniature optical and electro-optical processing systems. These devices have also been referred to as Optical Integrated Circuits or OIC's by some authors [1,2]. The two fundamental constituents of an Integrated Circuit (IC) are the interconnect and the devices. The analogous interconnect for an OIC is the optical waveguide. Devices can be divided into two categories: passive and functional (active) [1]. Passive devices have static optical characteristics. Examples of passive devices are lenses, power splitters, and combiners. Functional devices require some form of control input which modifies the optical characteristics of the device. Nishihara et al. have identified five methods for controlling optically guided radiation, listed in Table 1.1. Two additional methods, mechanical and electro-mechanical, have been added. An investigation of these two methods of guided wave control, using Silicon on Insulator (SOI) for waveguiding, forms the basis of this investigation.

As stated, the main topic of this directed study is the design and fabrication of electro-mechanical-optical (EMO) devices using SOI technology. The scope of this study will be limited to two active devices and the requisite optical interconnect. As shown in Figure 1.1, the optical interconnect is assumed to be adequately represented by a two dimensional waveguide consisting of a flat silicon beam of unit length having a rectangular cross section of height, Hg and width Wg, separated from a silicon substrate by a layer of silicon dioxide as shown in Figure 1.1.

TABLE 1.1 Classification of Control of Optical Guided Modes (adapted from Nishihara et al. [1])

Interaction	Effect	Phenomena	Functions
electric field to light	electrooptic effect (Pockels or Kerr)	index change	amplitude /phase modulation, optical-path direction change, deflection, diffraction, mode conversion
sound wave to light	acoustooptic effect	index change	diffraction, deflection, mode conversion, single-side band modulation
magnetic field to light	magnetooptic effect (Faraday effect)	polarization rotation	nonreciprocity, mode conversion
heat to light	thermooptic effect	index change	switching, phase modulation
light to light	nonlinear-optic effect	induced polarization	2nd harmonic generation, parametric amplification, phase conjugation
*geometry to light	mechanical deformation	alters optical path	path direction change, deflection, amplitude/phase modulation, mode conversion
* lattice spacing to light	photoelastic effect	index change	amplitude/phase modulation, mode conversion,

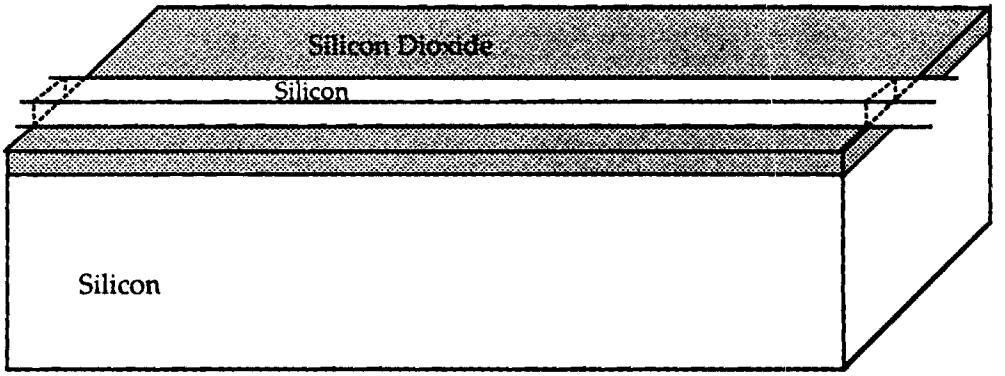

Figure 1.1 Basic Silicon on Insulator (SOI) waveguide structure

The two active devices to be studied are represented in Figure 1.2. They are representative of a class of waveguide devices that conduct light and that can undergo mechanical modification (such as deflection) by the application of an electrostatic potential between the two layers of silicon (actuation) or by application of a mechanical force (transduction), which in turn modifies the properties of the beam of light passing through the structure. Device dimensions of interest do not appear to be fundamentally limited by current silicon processing capabilities. Typical devices would be several microns to several tens of microns in width and from hundreds of angstroms up to several microns in height. One stark difference between this approach and other electro-optical effects is that because of the mechanical nature of these devices, frequency response is likely to be limited to a range from DC up to several megahertz. It must also be emphasized that the device structures under investigation have not been optimized for any particular application, but have been made as simple as possible to facilitate quantitative understanding of basic device behavior.

1.1 Motivation for SOI / EMO Devices

Although the present investigation has been limited to SOI, there is no inherent reason why this concept cannot be extended to other materials systems with the appropriate optical quality and machinability. However SOI is particularly well suited for this application. Crystalline silicon is relatively inexpensive, readily available in very pure form with low defect densities (and hence is of high optical quality), mechanically rugged, and chemically inert. The process technologies for fabrication of highly integrated structures in silicon are very mature and many intricate micro-structures have been demonstrated [3]. Optically speaking, high resistivity silicon is highly transmissive beyond 1.2 microns and has a large index of refraction, providing an excellent medium for optical waveguide fabrication. Optical waveguide structures in silicon and silicon-related materials have been

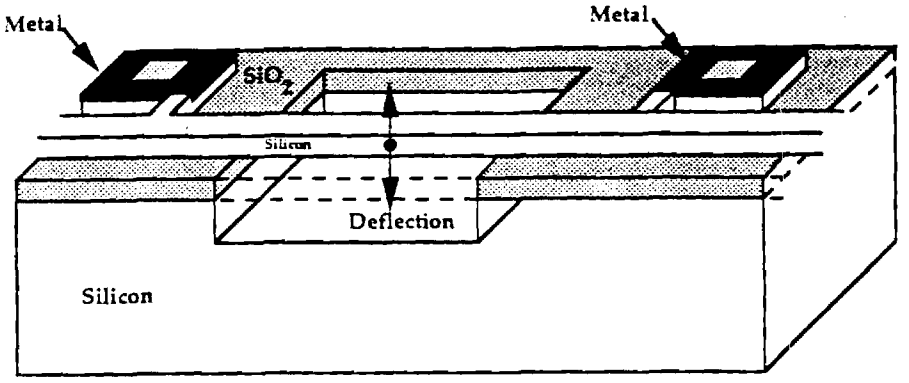

(a)

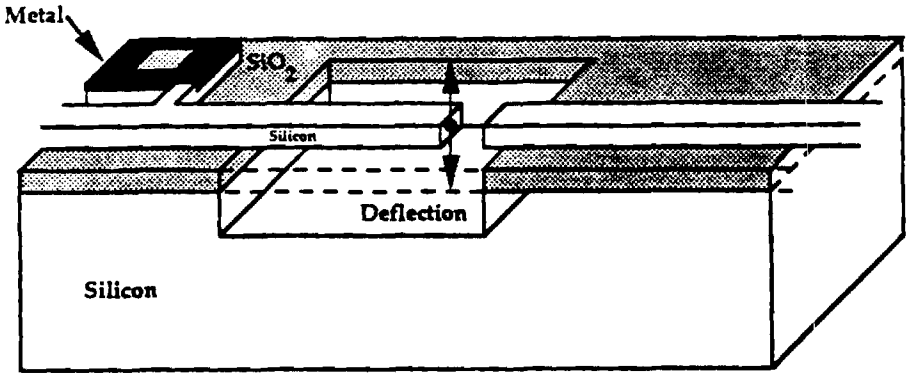

(b)

Figure 1.2 3-D Cutaway of silicon microstructures (not to scale): (a) Micro-Bridge with well lengths on the order of several hundreds of microns, (b) Micro-Cantilever beam of similar magnitude.

demonstrated. These attributes combine to make single crystal silicon a near ideal candidate for passive OIC's.

A variety of approaches have been used to develop waveguides in the 1.3 to 1.6 micron wavelength region using silicon based processes [4,5]. Several one-dimensional representations of silicon-based waveguide structures are shown in Figure 1.3. However, initial efforts employed an oxide-covered silicon substrate [only] as a surface upon which other waveguide materials such as glasses, nitrides, or polysilicon materials were deposited. In general, the oxide was required to be quite thick because of the relatively small index of the guiding material compared to that of the silicon. Thin oxides resulted in the leakage of radiation into the silicon substrate. Alternatively, some researchers used impurity doping to alter the index of refraction to form waveguiding layers directly in silicon; however, this gave rise to greater losses due to free carrier absorption [6].

Recently, interest has surfaced in SOI as a means of enhancing existing OIC capabilities by providing a high-quality, optically-isolated, crystalline silicon material for waveguide fabrication. There are a number of emerging technologies for producing thin SOI films. One process used to produce relatively thin layers (~1000s of Angstroms) is referred to as SIMOX (Separation by IMplantation with OXygen) [7]. Although efforts to produce waveguides using SIMOX as starting material have produced mixed results, it appears that this process holds significant promise for single mode waveguides requiring very thin but uniform films.

An alternative is Bonded and Thinned SOI (BTSOI—sometimes referred to as Bonded and Etched or BESOI) which results in an oxide-isolated silicon layer that is as defect free as the unprocessed bulk starting material, while also allowing for a much thicker and higher quality oxide layer if necessary; films as thin as 80±20 nanometers have been reported [8]. Haisma et al. has reported 5 ± .2 micron film uniformity over an entire wafer and expresses confidence that similar results can be obtained for 1 micron films [33]. It is therefore believed that thicker low loss multi-mode waveguides can also be readily fabricated. The BTSOI was used as a starting

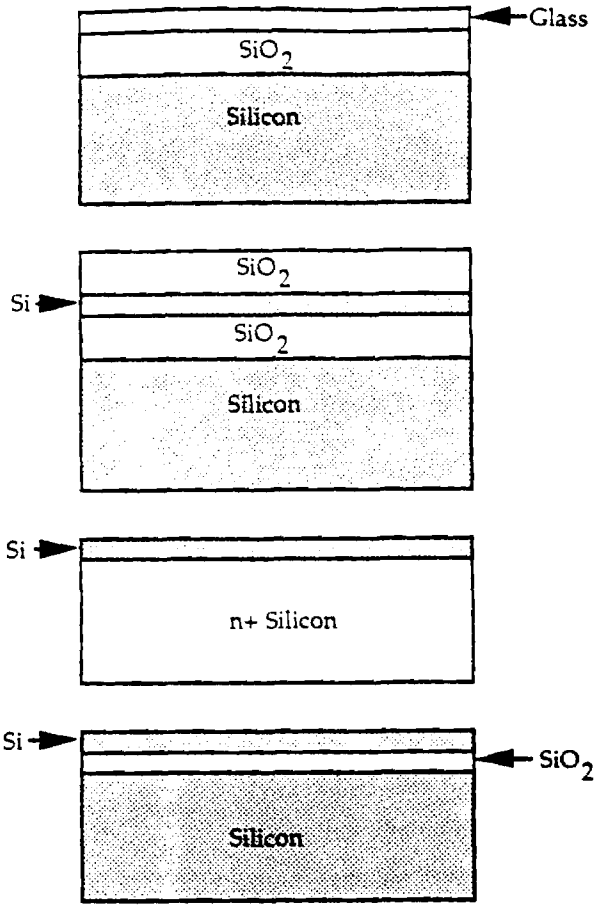

Figure 1.3 Four types of silicon compatible waveguides.

point for this investigation because of the desire to work initially with larger geometries to avoid measurement and handling difficulties associated with very small signals and minute structures. Because the quality and uniformity of the SOI film is a critical process parameter the particular BTSOI process which was used will be described in greater detail in a subsequent chapter.

Although it would appear, at first, that the choice of silicon as a waveguide material for this class of devices was motivated solely by the micro-machining capabilities which have emerged. Actually, it was the lack of a significant electro-optical effect in silicon which motivated the use of micro-mechanics as an alternative means of producing low loss large scale optical effects over reasonable dimensions [9]. Investigations have already been conducted into relevant electro-optic (EO) properties of silicon in the highly transmissive wavelength region of 1.3 to 1.6 micron [9]. One of the drawbacks of silicon is its centro-symmetric crystalline structure, which prohibits the linear EO effect commonly referred to as the Pockels Effect. As a result, investigators have resorted to the use of impurity doping and modulation of free carrier densities to control guided waves in silicon. The major drawbacks of this approach are: (1) the presence of free carriers increases absorption, and (2) large variations in free carrier density result in only relatively small variations in refractive index and consequently small phase shifts [9]. It is for these reasons that the electro-mechanical effects are being investigated.

Three important optical effects result from mechanical deformation of the waveguide and they are: (1) the path length, and hence the phase, is altered in proportion to the deflection; (2) the direction and possibly the mode of propagation can be geometrically altered; and (3) the index of refraction can be altered through the photoelastic effect [24]. Also, from the viewpoint of control efficiency, electro-mechanical actuation is electrostatic, so that holding power should be relatively small. There are two major drawbacks to this approach. First, compared to other EO control methods the time responses will be relatively slow due to the mechanical nature of the device. This will be accentuated in air where viscous damping can be

substantial. Second, a mature, quantitative understanding of the effects of mechanical deformation on the optical waveguide properties of similar integrated single crystal structures is non-existent. This latter item, combined with the complexity of the phenomena, was one of the primary reasons for attempting to fabricate and test such devices before doing any extensive modelling or device optimization.

1.2 Research Objectives and Report Organization

The primary goals of this directed study were (1) to demonstrate a new technique of guided wave control by fabricating and testing devices based on relatively mature technologies, and (2) to characterize the behavior of two classes of electro-mechanical-optical (EMO) devices, the micro-cantilever beam and the silicon micro-bridge, vis a vis two functions—switching and transduction. In particular, using a signal flow approach, the key processes which must be investigated include the introduction of light into the waveguide, the waveguiding properties of SOI structures, how these properties are affected by mechanical deformations and other chracteristics of the devices under study, and how the changes are measured (detected). The relationship between these processes and the associated design parameters is a principal component of this investigation. The fabrication sequence that has been developed is the other significant aspect of this study and is discussed in detail below.

To this end, Chapter II presents the rationale and layout for the EMO device test structures as well as a fabrication sequence, with illustrations, that will lead to the successful fabrication of these test structures. Important tradeoffs which were factored into the development of this process are also included. Chapter III begins with an overview of optical waveguide theory that is sufficiently detailed to make some first order predictions of device behavior and provides a framework for a parameterization of both passive SOI and active EMO devices. This latter analysis

provides the basis for assessing the viability of an SOI based OIC technology. Chapter IV contains a summary of our findings, a discussion of possible applications and recommendations for future investigations.

CHAPTER II

FABRICATION OF TEST STRUCTURES

The primary objective of this study was to develop a proof of concept for electro-mechanically controlled optical waveguides in SOI. A significant part of this effort was to develop a process for the fabrication of devices which can be used to demonstrate the viability of this technology. The fundamental building blocks are:

The Branch Waveguide

The Micro-Cantilever Beam (Switch)

The Micro-Bridge

The Waveguide

Each of these components have been demonstrated in some form or another, [3,4,5,6] but no one has yet to incorporate them into a single operating device.

One of the key questions is: What happens to the guided wave when the silicon waveguide is deformed? The functions which we intend to investigate with these structures are: waveguiding in a BTSOI channel waveguide, electro-mechanically induced optical switching and multiplexing, and electro-mechanical phase modulation. Other interesting experiments would entail measuring sensitivities to other parameters such as variation in the surrounding index, temperature, pressure, acoustic waves, and acceleration, to name a few.

2.1 Layout of Test Structures

At the outset of this research effort, the primary goal was to demonstrate the

concepts outlined above. In the interest of accelerating the realization of that goal, test structures were devised without extensive study of the phenomena. Heavy reliance on insight, knowledge of processing technology and on examples from the general literature resulted in the structures to be outlined below. It should be clearly understood that these structures have not been optimized for any particular application, neither actuation nor transduction. These structures were chosen specifically to facilitate the interpretation of the experimental results.

There are six test structures shown in Figures 2.1 through 2.3. In each case, three different widths were included 5, 10 and 20 microns. This should allow us to separate out volume and surface effects. Two of these are representative of complete functional integrated device structures and are shown in Figures 2.1 and 2.2. In addition to these integrated test structures, consisting of contact pads, control device (beam and well), and branches; there are other test structures which were included to isolate the effects of each of the individual components that make up the integrated test structures. These are:

(a) Branch (Figure 2.3a)

(b) Contacts (Figure 2.3b)

(c) Air gaps (Figure 2.3c)

(d) Straight Guides (Figure 2.3d)

These additional structures will help to understand the contributions of each of these components to the integrated device behavior. Test results from the straight guides can be used in conjunction with the branches to isolate the effects of the branches and provide some overall assessment of waveguide quality. The contact stubs represent the effect of the contact pad on the waveguide. The gap test structure shown in Figure 2.3(c) does not have the wells of the integrated device, thus there is no potential for misalignment. However, caution must be exercised in interpreting these results due to the presence of the higher index silicon dioxide immediately adjacent to the gap.

The height of the waveguide is process dependent. The important design

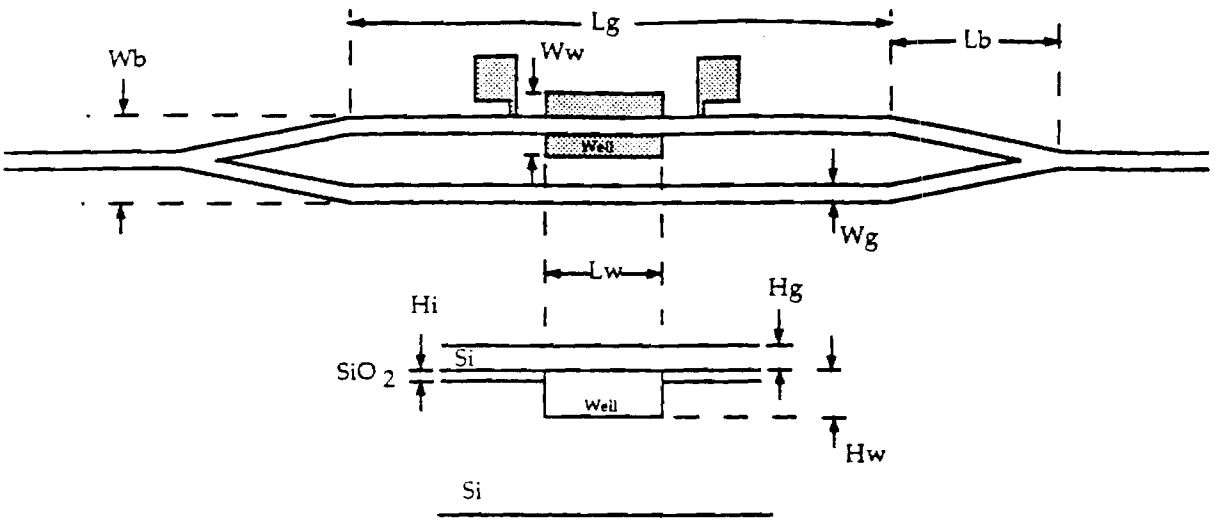

Figure 2.1 Schematic representation of a silicon micro-bridge integrated test structure.

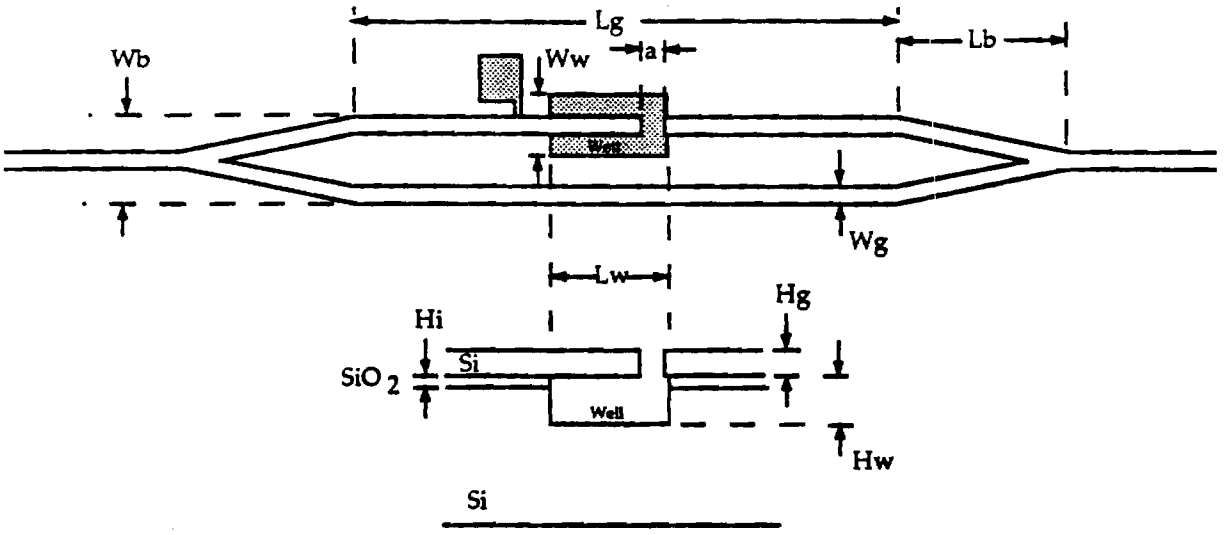

Figure 2.2 Schematic representation of a silicon micro-cantilever beam integrated test structure

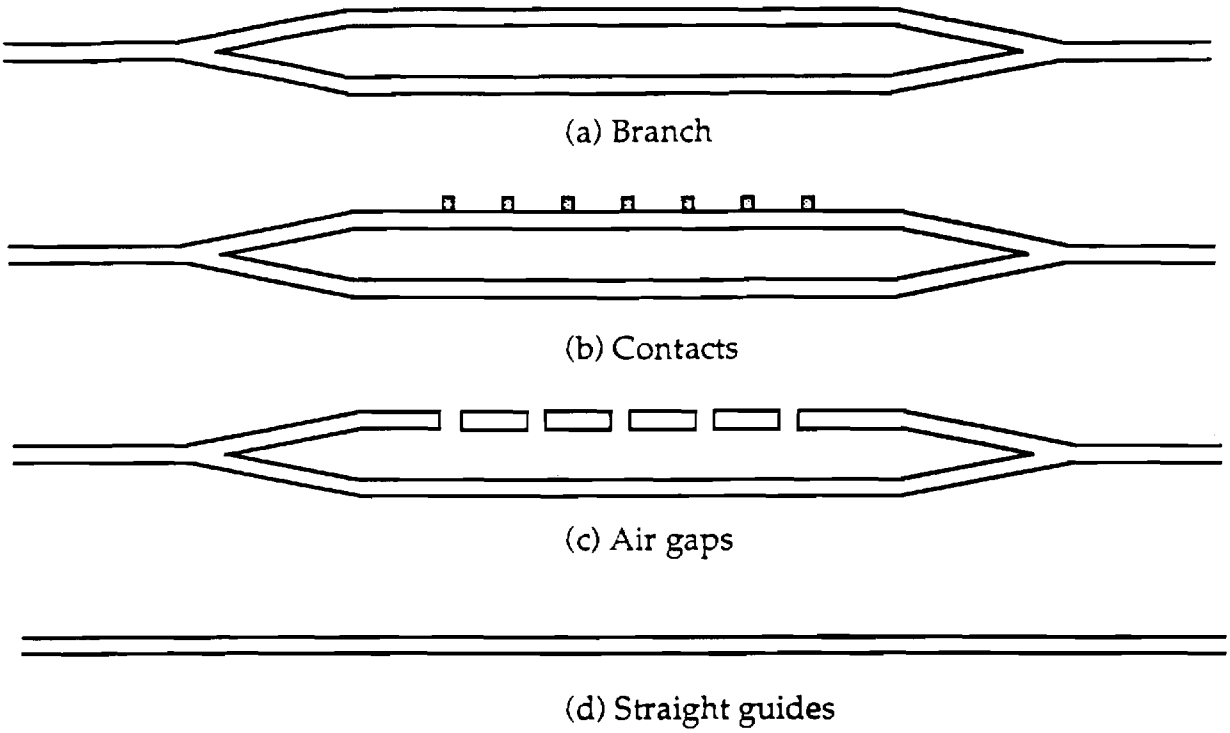

Figure 2.3 Additional test structures included to assess effects of structural components. Three different guide widths are used in each case.

TABLE 2.1 Test Structure Specifications

Parameter	Symbol	Values
guide width	Wg	5 10 20
well width	Ww	50
branch width	Wb	60 70 90
branch length	Lb	500
well length	Lw	100 200 400 100 200 400 100 200 400
guide height	Hg	6
oxide thickness	Hi	1
well depth	Hw	3
guide length	Lg	1500
beam length	l	95 195 395 95 195 395 95 195 395
gap spacing	a	5

All values in microns

layout parameters are defined in Figures 2.1 and 2.2. The test structure's values are listed in Table 2.1. These values represent an educated "best guess" for an initial experimental starting point.

2.2 Process Development

This section begins with a brief overview of the process and process requirements. The process presented here is defined specifically for BTSOI. An alternative process would be used for devices based on SIMOX or other SOI technologies. The elucidation of this process is followed by a more detailed discussion of the basic process steps and their limitations. Finally the process sequence is described and illustrated.

To produce high quality waveguiding structures a number of important constraints must be satisfied. The films must be uniform and optically smooth. The channel waveguides should have straight and smooth side walls to avoid scattering losses. This is particularly true of well guided modes with short evanescent tails that interact strongly with the surfaces. Hence, the most critical process steps are the thinning of the seed wafer and the etching of the waveguide; both have a significant impact on the optical properties of the waveguides.

The current method of thinning uses a heavily doped p++ layer about one micron thick. Every effort must be made to limit high temperature processes before the etch stop has been removed. This is necessary to limit diffusion of these impurities into the optically active layer during fabrication. Otherwise it would be difficult to effectively eliminate this layer of free carriers which would cause excessive attenuation due to absorption. This latter constraint was a significant factor in the process development.

2.2.1 Device Fabrication Processes and their Limitations

The basic process steps, listed below, are common to the silicon industry and are discussed briefly as they relate to the fabrication of the test structures. These are:

Oxidation
Photolithography
Alignment
Contacts
Bonding and Thinning, and
Etching

The two most critical steps are the bonding and thinning, and the etching of the waveguide. Some discussion of relevant experimental observations are made with regard to these last two steps because of their critical nature.

Oxidation

Oxidation is a necessary step but not a difficult one. In the bonding step of BTSOI, one of the wafers typically has an oxide. It is this oxide which forms the isolation barrier for our waveguide structure. In order to reduce leakage into the silicon substrate this layer should be as thick as possible. Due to the time required to grow thick oxides, a one to two micron layer should be considered a reasonable upper limit. Based on calculations of the effective thickness of the waveguide (to be presented later), this will be adequate for silicon guides of any height for well confined modes. The oxide thickness also forms a lower limit for the depth of the well, which must be kept reasonably shallow to facilitate low voltage deflection. A wet oxide is preferred.

Photolithography

No special precautions are required for photolithography for this fabrication sequence. If finer geometries are necessary then higher resolution photolithographic processes will be required. Because mask irregularities are often reproduced when highly selective etches are used, edge smoothness is one aspect of the photolithographic process that is important for fabrication of waveguides, that is often ignored for electronic devices operating at relatively low voltages.

Alignment

From the geometries and sizes used for these test structures a two dimensional vernier type alignment target was used. It provided adequate alignment precision. Infrared (IR) alignment is necessary for the initial alignment after bonding and thinning of the seed wafer, because it must be aligned to the covered well structures in the handle wafer. The viability of this step has been experimentally verified. During this verification process, it was noted that alignment is much easier if the lower wafer is double polished and is optically smooth. No absorption problems were encountered from the heavily doped etch stop. The first alignment step after thinning must not be metallization because metal is opaque in the IR. However once an alignment structure has been established on the surface, the use of conventional optical aligners is acceptable.

Contacts

The only special requirements for the contacts are that they must survive the waveguide etch for deep etches because there is insufficient material remaining to adequately utilize conventional photolithographic processes after waveguide delineation. An initial investigation into a titanium metal layer with a chlorine based dry etch proved unacceptable for etch depths of several microns. It is not

known whether this would also be true for depths of several thousand angstroms. Alternatively, aluminum is inert to fluorine-based dry etches but must later be selectively removed above the waveguide to avoid excess absorption, while not be removed from the contact pads. To overcome these constraints we use a three metal contact consisting of aluminum/titanium/aluminum. The aluminum protects the titanium during dry etching, while the titanium protects the bottom aluminum layer during the waveguide etch mask removal.

Bonding and Thinning

Numerous techniques are under development for producing SOI thin films. Because of the importance of maintaining good uniformity over large areas, this step is one of the most critical and one of the more difficult to control. Film thickness uniformity in SIMOX is quite good and presently appears to be the only commercially available method for producing very thin films. The film thickness, quality and the thickness of the buried SiO_2 layer are limited by the oxygen implant energies and one's ability to reduce the implant damage with a post anneal step. Processess for producing thicker bulk quality films have been described in the literature and are referred to as Bonded and Thinned Silicon on Insulator (BTSOI), because the polished surfaces of two wafers are bonded together and the back of one is removed (thinned) by etching [8,10] or by polishing [33]. The thinned wafer is referred to as the seed wafer, while the unetched wafer is the called the handle wafer. The bonding is straightforward, although it must be performed with very clean surfaces because even micron-size particles trapped between the two bonded surfaces produce relatively large voids. When an etch stop is present the thermal bonding step (in fact any high temperature processes) must be limited, in temperature and duration, to avoid diffusion of the etch stop into the waveguide layer.

The etching process which we employ involves two highly selective

chemical etches: EDP which uses a heavily doped p++ etch stop, and "1-3-8" which is used to selectively remove the p++ layer. These two etching techniques have been discussed in the literature [8,12,13]. Despite the very high selectivity of these chemical etches, it is difficult to obtain uniform films. In large part, this appears to be due to the large variation in thickness of the initial seed wafer. It may be necessary to obtain wafers that have parallel surfaces initially, to obtain the type of films which seem attainable based on the selectivity of the etches. Highly uniform films have been reported [8]. The success of the process is highly dependent on details of the processes used to form the etch stop and grow the epitaxial layer. Another potential improvement may result from the use of electrochemical etching techniques in combination with mechanical polishing of the waveguide layer [14]. Ultimately, once the thinning process is refined, the thickness of the layers may only be limited by the degree of control of current epitaxial technologies.

Etching

It is desireable to have a highly anisotropic, non-crystallographic etch for silicon that is capable of producing straight and uniform sidewalls, which does not attack the underlying oxide. In general, reactive ion etching, sputter etching and ion beam milling have the capability of producing the required geometries. However, for deep etches, one of the more significant problems is finding a mask that will stand up to highly energetic etchants over long periods of time. This will become less of a problem when thinner waveguides are being fabricated (several thousand angstroms).

2.2.2 Device Fabrication Sequence

The fabrication sequence for these structures require only four masks; wells, implants, contacts, and waveguides. The process is outlined below. Only those

details relevant to the resultant structure are included. Composition of solvents, time periods, types of resists, etc are not included unless they are critical to the successful fabrication of the device. A total of nine steps are discussed. Each step has an equivalently labeled illustration(s) associated with it. This illustrated version of the fabrication sequence is found in Figure 2.4 (a) through (i). The fabrication steps are:

(a) Oxidation of n+-substrate

A wet oxide is grown on a n+ handle wafer. The thickness of the oxide should be no less than .5 microns with 1 micron a reasonable value.

(b) Pattern and Etch Well Oxide

This handle wafer is patterned and windows are opened in the oxide for etching the wells using Buffered HF.

(c) Etch Silicon Well

The wells are etched to the required depth using EDP.

(d) Bond Wafer

The handle wafer is then bonded to the seed wafer. The seed wafer is a p- wafer with a 1 micron thick heavily doped p+ implanted layer. The concentration must exceed 5.0E+19 acceptors per centimeter cubed to act as an effective etch stop. A p- layer is epitaxially grown on this wafer. The thickness of this epitaxial layer is the approximate height of the waveguide. The seed and handle wafers are cleaned and dried (not baked) immediately before bonding, because residual water adhering to the surface aids in bonding. The two wafers are aligned, contacted, and are then thermally bonded at 900 degrees for 30 minutes. The time and temperature must be minimized to avoid diffusion of the p+ dopants into the guiding layer.

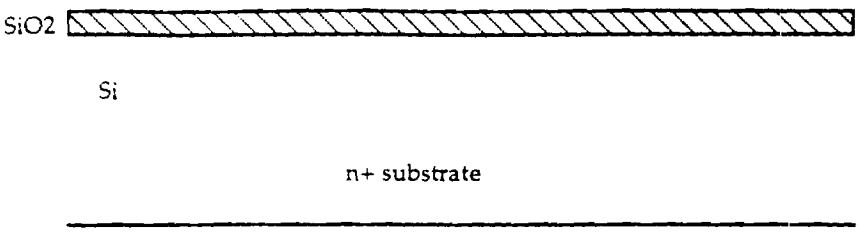

(a) Oxidation

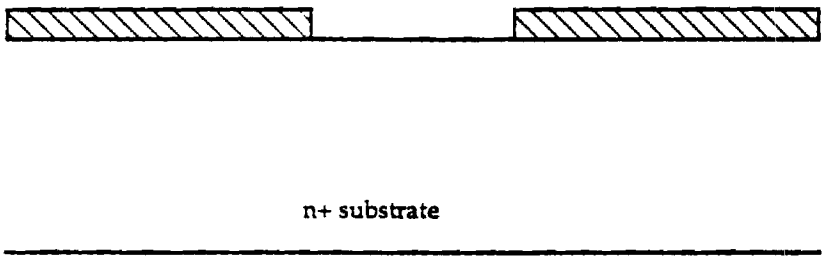

(b) Pattern and Etch Oxide

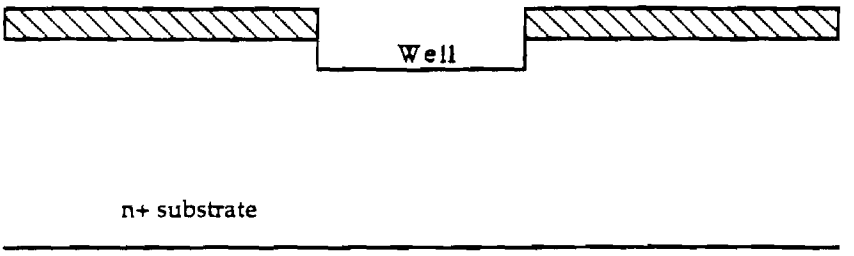

(c) Etch SiliconWell

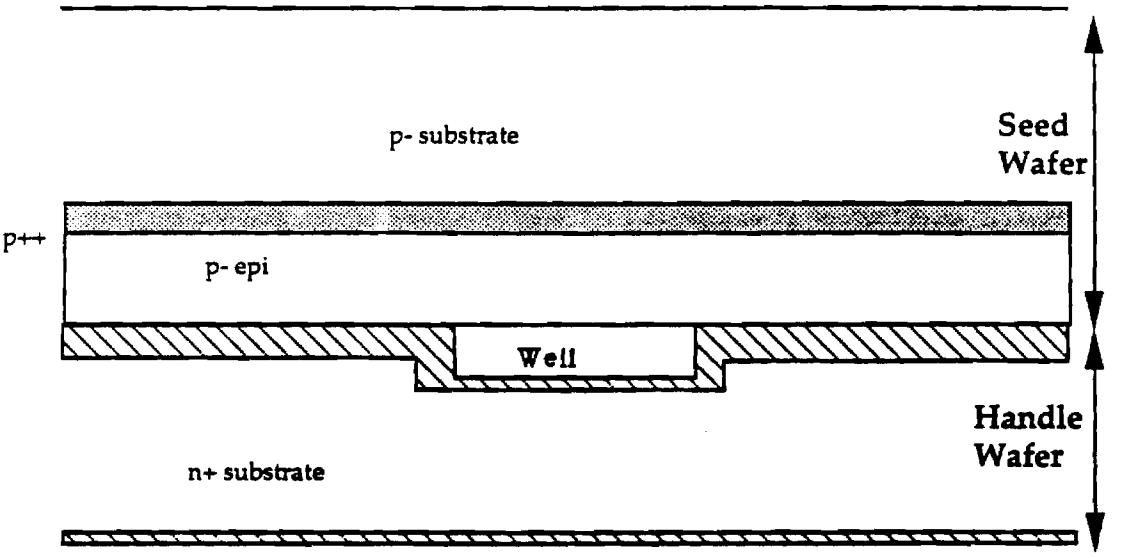

(d) Bond Wafers

(e) Thin Wafer

The bonded wafers are thinned in a three step process. A fast ISO etch is used to remove the bulk of the material. This is followed by a slower but more selective EDP etch until the etch stop is reached. Finally, the etch stop is removed using an HDP or "1-3-8" etch leaving the guiding layer on the handle wafer. (Removal of the etch stop is optional. It simplifies the process since no contact diffusion is then necessary; however, this comes at the expense of increased losses due to free carrier absorption.)

(f) Grow Oxide and Pattern for Contact Diffusion

A thin oxide (1000 angstroms) is grown on the layer and the wafer is patterned using an IR aligner to align the contacts with the subsurface wells, previously etched in the handle wafer. Windows are opened for a p++ contact diffusion. This oxide provides the surface relief necessary to pattern the metal contacts after diffusion.

(g) Metallization and Pattern Metal

After the contact diffusion, a three layer metal structure is sputtered onto the wafer. The bottom layer is 5000 angstroms of aluminum followed by a layer of titanium (1000 angstroms) and then another 1500 angstrom layer of aluminum. The contacts are patterned and the surrounding aluminum and titanium are removed. The remaining aluminum layer will be used as an etch mask for the waveguides.

(h) Pattern and Etch Waveguides

The waveguides are patterned on the remaining aluminum layer and the surrounding aluminum and oxide are removed. The silicon is etched until the oxide is reached using a fluorine based dry etch which does not attack the aluminum etch mask.

(i) Remove Etch Mask

The final step is to remove the aluminum etch mask. Removing the remaining oxide is optional. It has been assumed here that the oxide has been removed. The hypothetical cross section of a completed device is shown in Figure 2.5. It assumes a 5 micron epi-layer and that the p++ etch stop has not been removed.

Process Results

The waveguide etch has not yet been implemented. An investigation was undertaken to use a chlorine based dry etch, with limited success. A fluorine based dry etch will be tried next. The waveguide etch must be the last step, when relatively large step heights are involved, to avoid problems with photolithographic processes. One other important constraint is that the handle and seed wafer bonding surfaces must be flat and kept very clean.

A significant obstacle to the success of the BTSOI process has been residual roughness of the thinned films. Both the EDP and the 1-3-8 etch have been used, with a final roughness (short-range variation) estimated at about 100 Å. Reflections of the surface are too diffuse to permit use of single-wavelength ellipsometery to determine the thickness, or of spectroscopic ellipsometry to estimate the surface roughness. We speculate that this may be due to non-optimal conditions during implantation of the buried etch stop; other researchers have reported similar problems. However, these problems are not fundamental in nature and can clearly be overcome by a more detailed development procedure.

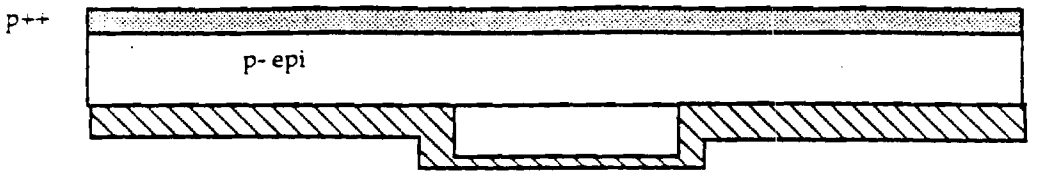

(e) Thin Wafer

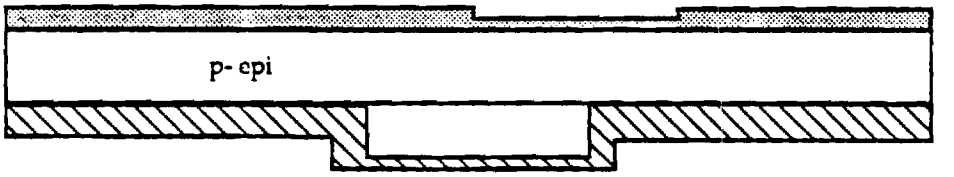

(f) Etch Contact

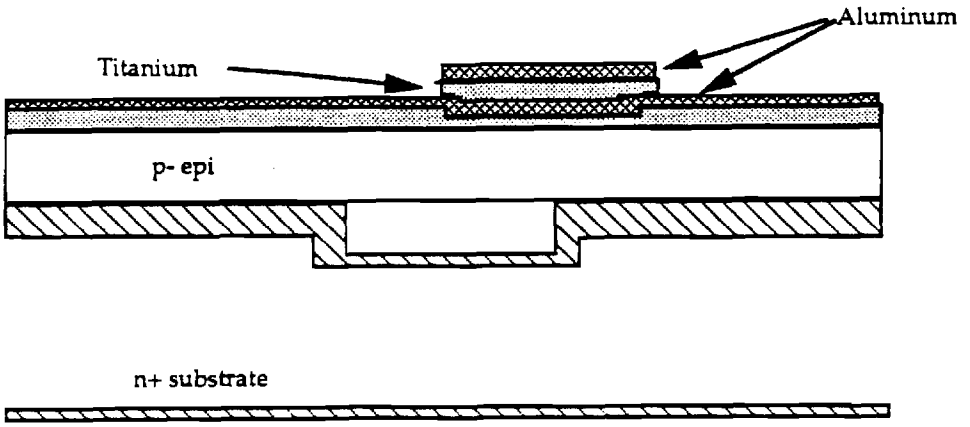

(g) Metallization and Pattern

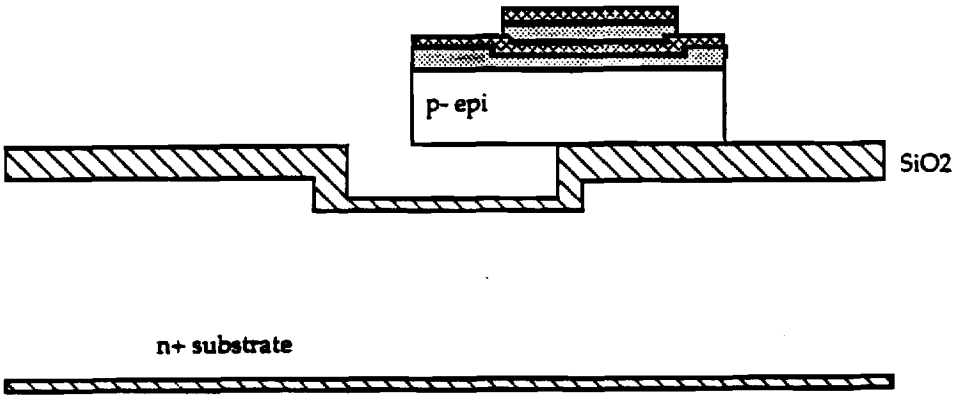

(h) Pattern and Etch Waveguide

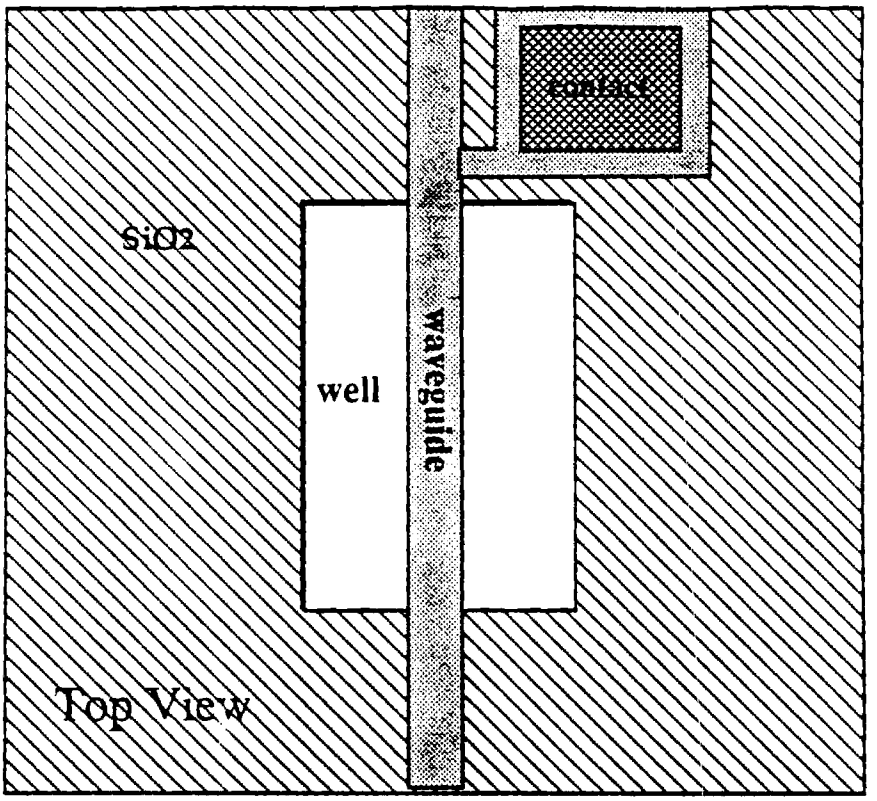

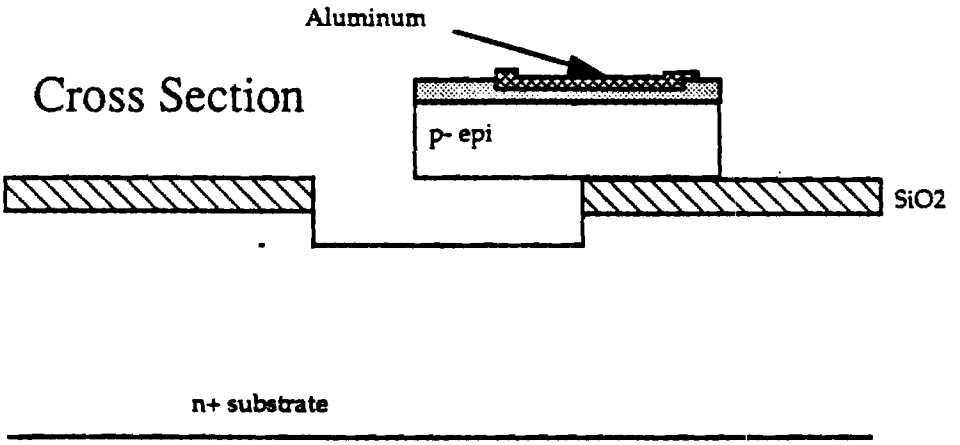

(i) Remove Etch Mask

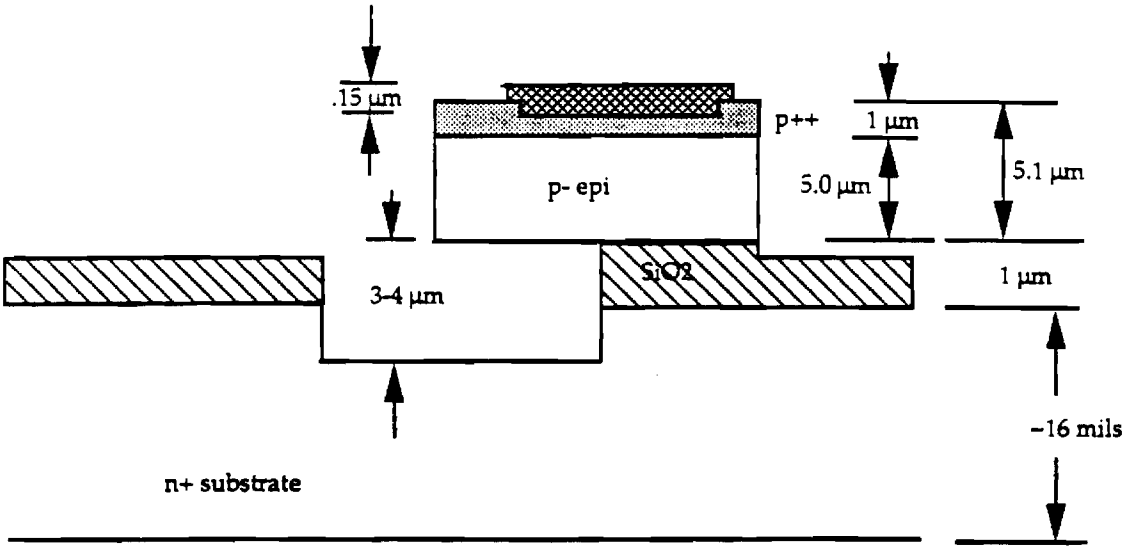

Figure 2.5 Hypothetical cross section of a completed device

CHAPTER III

WAVEGUIDING IN SOI

Three basic device structures presented in Chapter I (Figures 1.1 and 1.2.) provide a basis for OIC technology in SOI. These devices have been redrawn in Figure 3.1. The simplest of the three devices is the dielectric waveguide structure shown in Figure 3.1 (a). Kogelnik defines several channel guide geometries [15]; he refers to this geometry as a "raised strip". A straight section of raised strip channel waveguide is the fundamental structure which will be analyzed to determine the important relationships between key design variables and optical propagation in SOI waveguides. An idealized cross section is shown in Figure 3.2 in conjunction with a cross section more representative of the actual physical realization of the device. Initially, we intend to examine the relevant waveguiding properties of the idealized raised strip where the cladding is air (or vacuum), the film is silicon, and the substrate material is silicon dioxide. Other passive structures that are critical to all but the simplest of OICs include branched waveguides and curved sections. These interconnect structures will also be discussed. We will also discuss how processing and fabrication limitations cause the waveguiding characteristics of SOI based devices to depart from the ideal.

Active structures, used to modulate an optical carrier in the waveguide, are also an essential element of OIC technology. Electro-optical effects, predominately used in non-silicon based materials, are small or non-existent in silicon. Free carrier effects have been demonstrated as a viable means of signal modulation in silicon waveguides [6]. However, the presence of large numbers of free carriers causes significant attenuation. Micro-mechanical structures may offer an alternative method of signal modulation. If we create a cavity or well underneath a portion of the waveguide we have a structure like that in Fig. 3.1 (b); where the portion of the guide suspended over the well is now suspended in air and is free to move in the

W_g = Width of guide

H_g = Height of guide

W_w = Width of well

L_w = Length of well

H_i = Thickness of insulating layer

H_w = Depth of well

a = Gap length

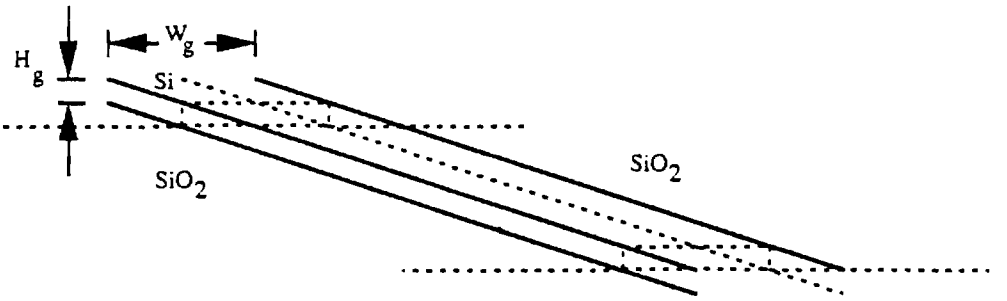

(a)

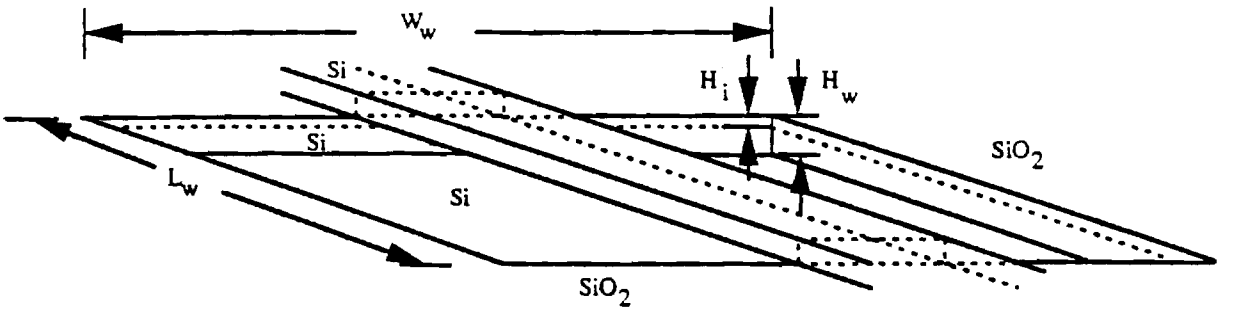

(b)

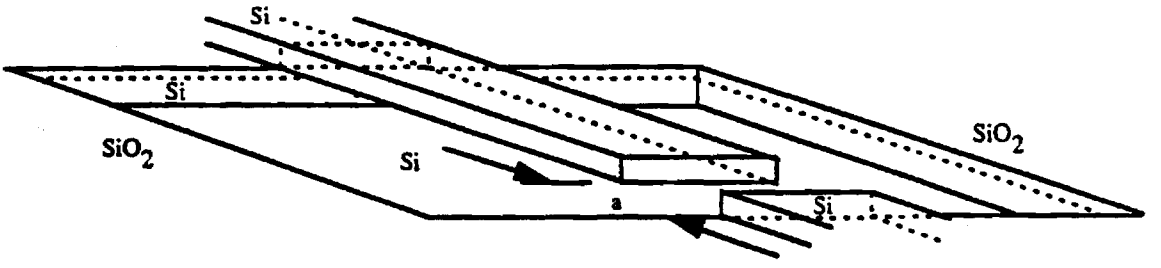

(c)

Figure 3.1 Basic EMO device structures: (a) Simple raised strip channel guide, (b) Micro-bridge a
(c) Cantilever beam

n_s = Index of substrate (Silicon Dioxide)

n_f = Index of film (Silicon)

n_c = Index of Cladding (Air or Vacuum)

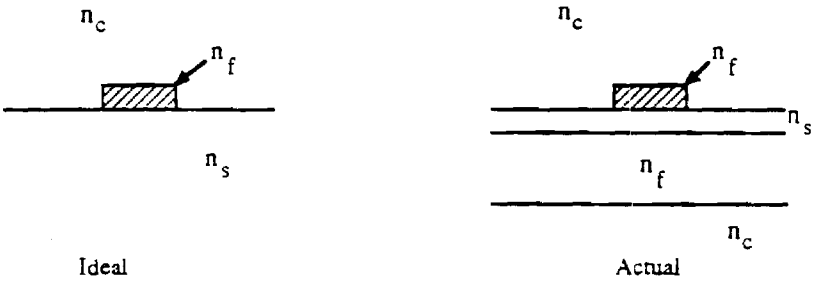

Figure 3.2 Cross section of a Raised Strip Channel Guide

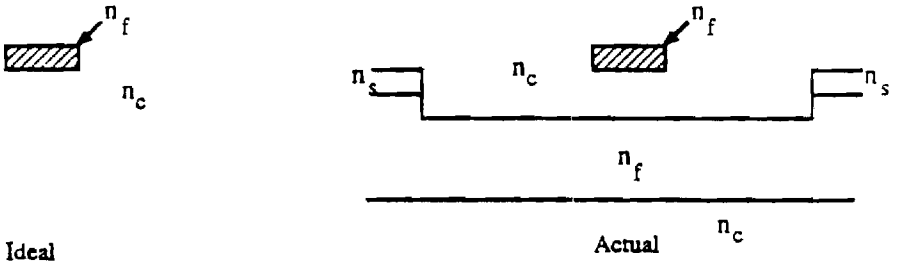

Figure 3.3 Cross Sections of a Buried Channel Guide

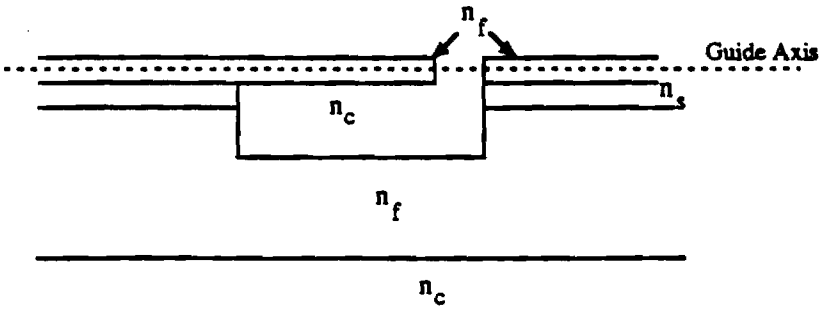

Figure 3.4 Side View of a Cantilever Beam

vertical direction. We refer to this structure as a micro-bridge. The deflection of the bridge causes the guided wave to be altered in a prescribed way. Because of the bridge's rectangular cross section its movement is preferentially up/down or side to side. Planar processing tends to favor wide thin structures to such an extent that we will focus on the case where the movement is only up and down. An idealized and an actual cross section of the micro-bridge structure are shown in Fig 3.3. This geometry can be referred to as a "buried channel" if we allow that it is "buried" in air. From a waveguiding viewpoint, one significant difference that this structure exhibits with respect to the raised strip is that it is symmetric with regard to the indices of refraction.

If we remove a portion of the bridge over the well, then we have a structure like that in Figure 3.1 (c), which we refer to as a cantilever beam; where one end is free to move. Like the bridge, we will focus our attention on the case where the beam's motion is up and down (into and out of the well). Analytically, the cantilevered waveguide structure progresses from a raised strip to a buried waveguide that terminates abruptly over the well and is separated from another section of raised strip waveguide by a small distance, a, which we refer to as the gap. The distinctive properties of the micro-cantilevered structure are a direct consequence of this gap and thus the gap will provide the primary focus for the analysis of this structure. Otherwise, the cross section of the beam is essentially the same as the bridge and is shown in conjunction with a side view of the structure in Fig. 3.4. Conceptually one can envision this device functioning as a pipe, where light is sprayed out of the end in a direction orthogonal to the end face of the beam. The amount of light which enters the adjacent section of waveguide will depend on how the cantilever beam and raised strip axes are aligned.

Three SOI waveguide structures have been introduced. In each case, there are two variants, an idealized one and an experimental one. We will perform the bulk of our analysis for the ideal case and show how, and under what circumstances, the actual structure's behavior departs from the ideal. We will use the raised strip

structure of Fig 3.1(a) and Fig. 3.2 to investigate the optical properties of an SOI channel waveguide. The micro-bridge structure in Fig. 3.1 (b) and 3.3 will provide the basis for investigating electromechanical properties of SOI waveguides and how they relate to waveguide signal transmission. Discussion of the cantilever beam structure shown in Fig. 3.1 (c) and 3.4 will focus specifically on the salient properties of the gap and the electromechanical properties of the cantilever beam. Finally, system level tradeoffs concerning the use of such structures for fabrication of OICs will be examined as well as their applicability to switching and transduction.

3.1 Passive Structures in SOI

The primary structure under consideration for optical waveguiding is a raised strip channel waveguide. This is a three dimensional structure. Referring to the cross sectional drawing shown in Figure 3.2, this structure is typically considered to have three layers, while our case actually has a five layer structure, as shown. It will be shown later that if the oxide layer is thick enough then this structure's waveguiding behavior can be effectively defined by the three upper layers: the substrate, film, and the cover, and their respective indices of refraction. In support of subsequent discussions we define three axes as shown in Figure 3.5. The axes are x (the vertical direction), y (the transverse or horizontal direction), and z (the direction of beam propagation or longitudinal direction). From these definitions and from Figures 3.1 and 3.2, it can be seen that the indices of refraction of the three dimensional structure are symmetric in the y direction and asymmetric in the x direction.

Unlike propagation of light in an unbounded medium, it is the nature of waveguides that only propagating waves which meet certain boundary (resonance) conditions can propagate in a waveguide. These resonance conditions define discrete propagation modes which depend on the geometry and bulk properties of the guide and the wavelength of light. Hence, we define the optical waveguide

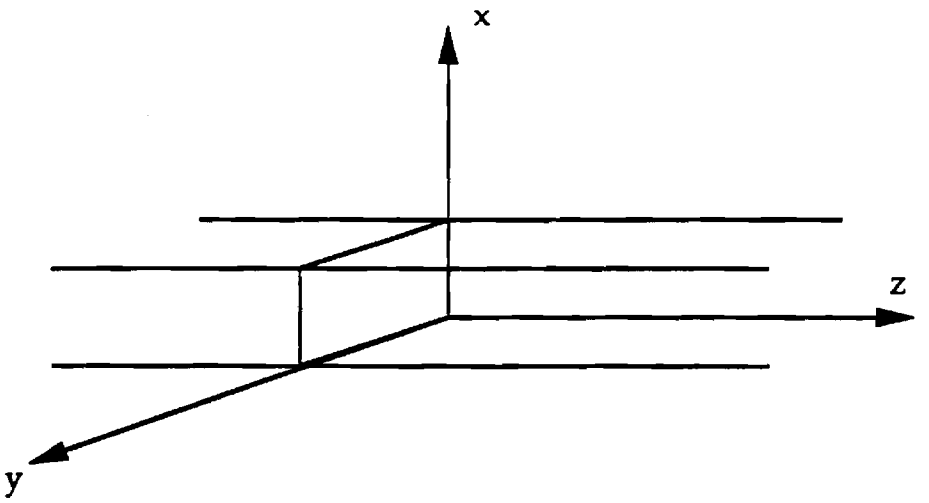

Figure 3.5 Cartesian Coordinate System Referenced to the Waveguide

behavior in terms of its wavelength and mode. There are two common approaches used to describe propagation of a guided wave: the electromagnetic (EM) and ray optics approaches. In the electromagnetic approach, a propagating mode would be defined by time independent electric and magnetic fields which propagate along the waveguide with a velocity characterized by a propagation constant, β, for example. In the ray optics approach a mode would be defined by the same propagation constant and the angle of propagation. The present discussion will be limited primarily to the ray optics approach because it provides a more intuitive understanding. It can also be shown to be fully equivalent to the electromagnetic approach. Using the ray optics approach, we intend to articulate the waveguiding nature of the raised strip channel for SOI, by first defining the key relationships between the design variables and the beam propagation parameters. Secondly, we will then consider important second-order effects which limit performance. One drawback of the ray optics approach is that it does not provide power flow information directly; therefore, we will occasionally exploit the EM approach to obtain this information. Our goal is to establish the relationship between process variables and optical waveguide behavior in this simple SOI structure as a basis for engineering more sophisticated SOI structures in the broader context of present and future OIC applications.

3.1.1 Waveguide Fundamentals

Our goal here is to investigate the waveguide properties of a particular material system, namely SOI. It is not our goal to develop the theory of dielectric waveguides. Therefore, we present only those principles which are relevant to our discussion, introducing equations from the literature without derivation, as necessary, to characterize waveguide behavior in the particular structure defined here. The interested reader is referred to any of the introductory texts for their derivation.

We begin by assuming that we have a rectangular waveguide fabricated of zero-defect, undoped single crystal silicon. The waveguide dimensions consist of a height, Hg, width, Wg, and is of infinite length (in other words, we ignore the I/O problem) residing on a silicon dioxide surface of infinite thickness. In contrast, the oxide thickness is actually limited to a few microns and the film itself can be characterized by a distribution of dopants, and defects, as well as surface and interface properties (these latter parameters represent second order effects associated with loss mechanisms). In addition to the geometry, the optical properties depend on the indices of refractions. The values we use are:

Silicon:	$n_f = 3.5$
Air:	$n_c = 1.0$
Silicon Dioxide:	$n_s = 1.5$

Other relevant physical constants are included in Table 3.1.

We consider the light source to be monochromatic, ignoring both finite beam width and finite bandwidth effects to simplify our analysis without any significant loss of generality. The wavelength used for all calculations is 1.3 μm. This wavelength was selected because of the availability of sources and silicon's low absorption at this wavelength.

Our development follows closely that of Kogelnik, focussing initially on two dimensional asymmetric slab waveguide theory, that is, we will ignore the width of the guide for the time being [15]. We begin with Snell's law, which is used to define the relationship between incident, reflected and transmitted components of a wave at a dielectric boundary. Snell's law is simply the result of the application of appropriate boundary conditions and Maxwell's equations at a dielectric interface.

Snell's Law:

$$n_1 \sin(\theta_1) = n_2 \sin(\theta_2)$$

Figure 3.6 shows the properties of reflection and refraction at the interface between

TABLE 3.1 Relevant Silicon and Silicon Dioxide Material Constants [30,31]

Property	Symbol	Units	Si	SiO_2
Crystal Structure			Diamond	Amorphous
Density	ρ	$g\ cm^{-3}$	2.328	2.19
Index of Refraction	n		3.4975	1.46
Coefficient of linear thermal expansion	α'	K^{-1}	2.5×10^{-6}	5×10^{-7}
Young's modulus	Y	$dyne\ cm^{-2}$	1.9×10^{12}	$.731 \times 10^{12}$
Poisson Ratio	υ		.18	

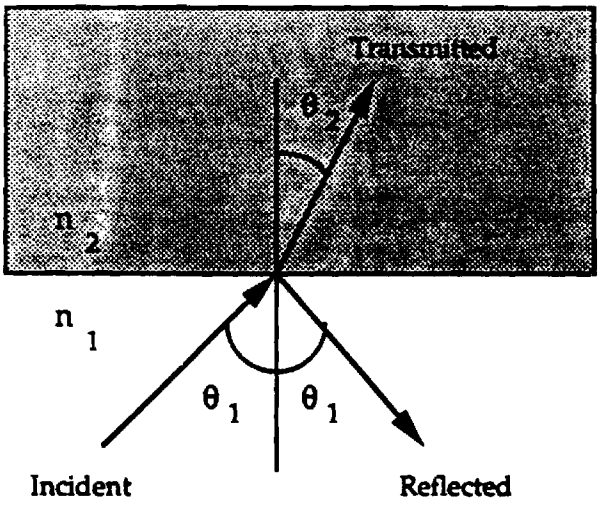

Figure 3.6 Transmission of light across a dielectric interface

two media of index n_1 and n_2. The arrows are assumed to represent the direction of propagation of plane waves. The use of arrows in this manner is representative of the Ray-Optics model. The amplitudes of the incident, transmitted and reflected wave have complex coefficients which depend on the polarization of the incident wave. The application of Maxwell's equations with the appropriate boundary conditions also gives the relationship between these coefficients. The actual time varying field solutions to the wave equation in a slab waveguide are given by equations of the form:

$$A \exp[-jkn_1(\pm x \cos\theta + z \sin\theta + \omega t)]$$

At present, the time dependence is of little importance here and will not be considered further.

We note from Snell's law that if n_1 is greater than n_2, then at some angle, θ_c, the wave is totally reflected as given by;

Condition for Total Internal Reflection (TIR)

$$\sin\theta_c = \frac{n_2}{n_1}$$

The TIR of this wave produces a polarization-dependent phase shift given by the following equations for each of the polarization states.

Transverse Electric (TE)

$$\phi_{TE} = \tan^{-1}\left(\frac{\sqrt{n_1^2 \sin^2(\theta_1) - n_2^2}}{n_1 \cos(\theta_1)}\right)$$

Transverse Magnetic (TM)

$$\phi_{TM}=\tan^{-1}\left(\frac{n_1^2}{n_2^2}\frac{\sqrt{n_f^2\sin^2(\theta_1)-n_2^2}}{n_1\cos(\theta_1)}\right)$$

For the remainder of this discussion, emphasis will be placed on the TE modes. Generalization to the TM modes is straightforward with only minor changes to the equations to be presented.

Referring to the structure shown in Figure 3.7, we have represented the propagation of light in a waveguide as a series of rays bouncing back and forth between the top and the bottom of the guide. At each reflection, the light undergoes a phase shift, defined previously, that is different for top and bottom due to the asymmetry of the guide. This will be true provided the mode angle, θ_m, is greater than the critical angle, θ_c. The critical angle at the silicon/air interface is 16°. The critical angle at the silicon/silicon dioxide interface is 24°. In this case, the critical angle for the asymmetric dimension of the guide will be determined by the silicon dioxide layer because it has an index that is closer to that of the silicon. The mode angle should not be confused with its complement, α_m, which is the angle formed by the propagation vector and the axis of the guide. We will refer to this latter angle as the "launch angle". Rays with "mode" angles less than or equal to 16 degrees would not be confined to the waveguide and are termed radiative modes while rays with mode angles between 16 and 24 degrees would not be confined by the oxide layer but would be confined by the silicon substrate/air interface resulting in a substrate mode. We will only be concerned with modes confined to the silicon film. The propagation of these waves is characterized by a vector pointing in a direction normal to a surface of constant phase, having a magnitude given by:

$$kn_f = \frac{2\pi}{\lambda} n_f$$

where

λ = wavelength of radiation

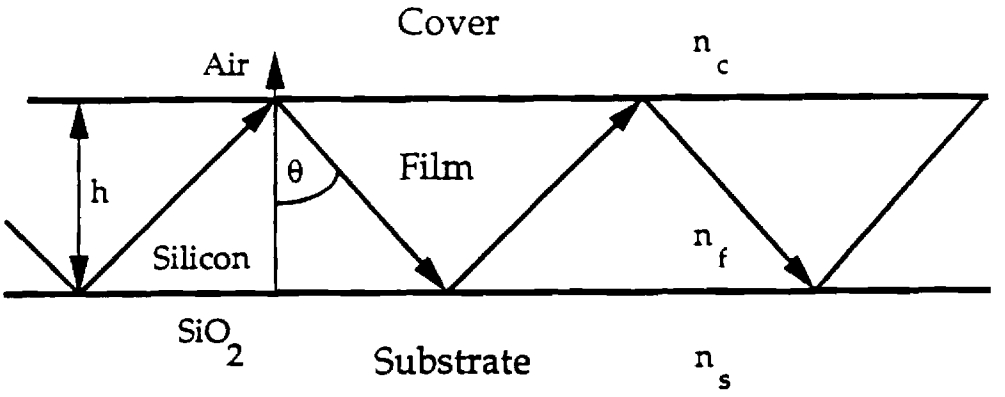

Figure 3.7 Ray optic model of light propagation in a waveguide

Noting that the path between reflections also represents a phase difference given by,

$$\phi = k\, n_f\, h \cos(\theta)$$

a guided mode exists when the sum of these phase shifts is an integer multiple of 2π. Thus the dispersion relation or "Transverse Resonance Condition" which defines the guided modes is given by

$$\frac{2\pi n_f h \cos(\theta)}{\lambda} - 2\phi_c - 2\phi_s = 2m\pi$$

We also define two other quantities which we shall use again as follows:

The propagation constant

$$\beta = k n_f \sin(\theta)$$

The effective guide index,

$$N = n_f \sin(\theta)$$

Having introduced the key relationships for defining modal behavior in a slab waveguide, we can immediately make several observations. First, for a given wavelength and height there are a finite number of guided modes, and each mode is associated with a specific propagation constant and mode angle. For the SOI waveguide structure, the mode angle for the lowest order mode is shown as a function of waveguide height in Figure 3.8 (a). The number of modes as a function of height is also shown at the top of the graph. At 5 microns over 25 modes are possible. The dependence between the mode angle and the mode for a waveguide of fixed height (Hg=2 μm) is shown in Figure 3.8(b). Because different modes propagate

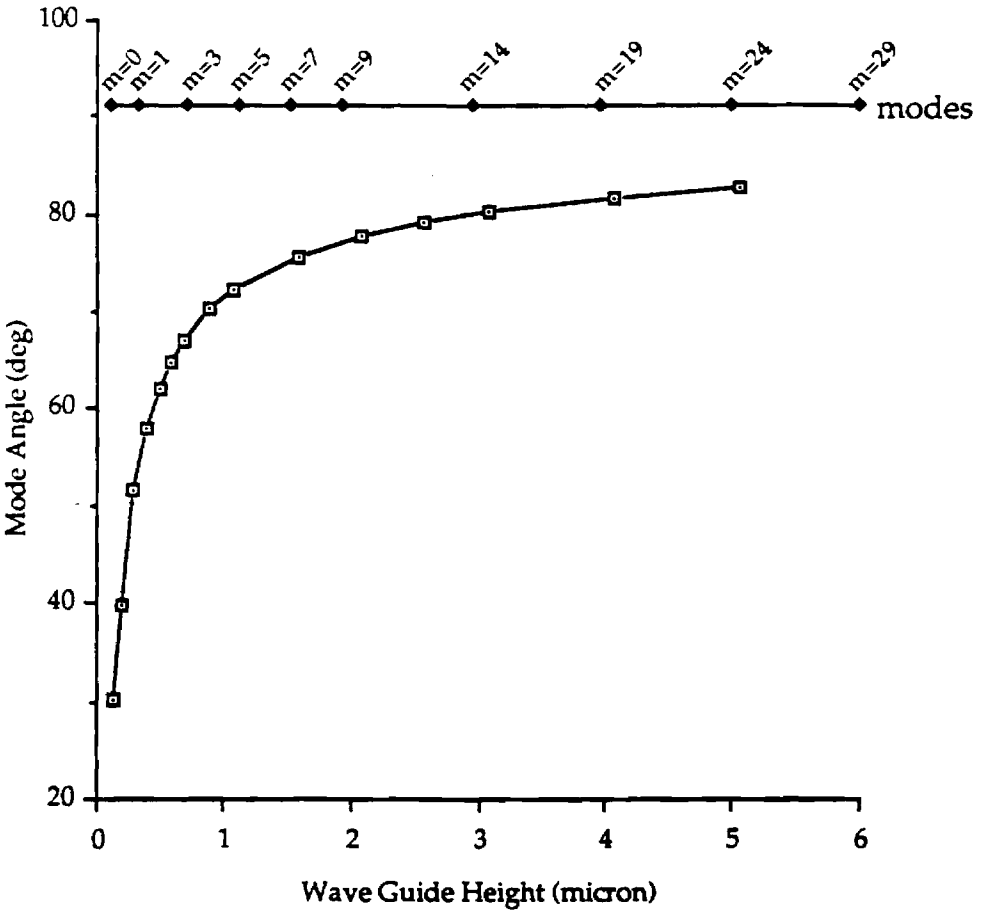

Figure 3.8 (a) Mode Angle m=0 as a Function of Waveguide Height

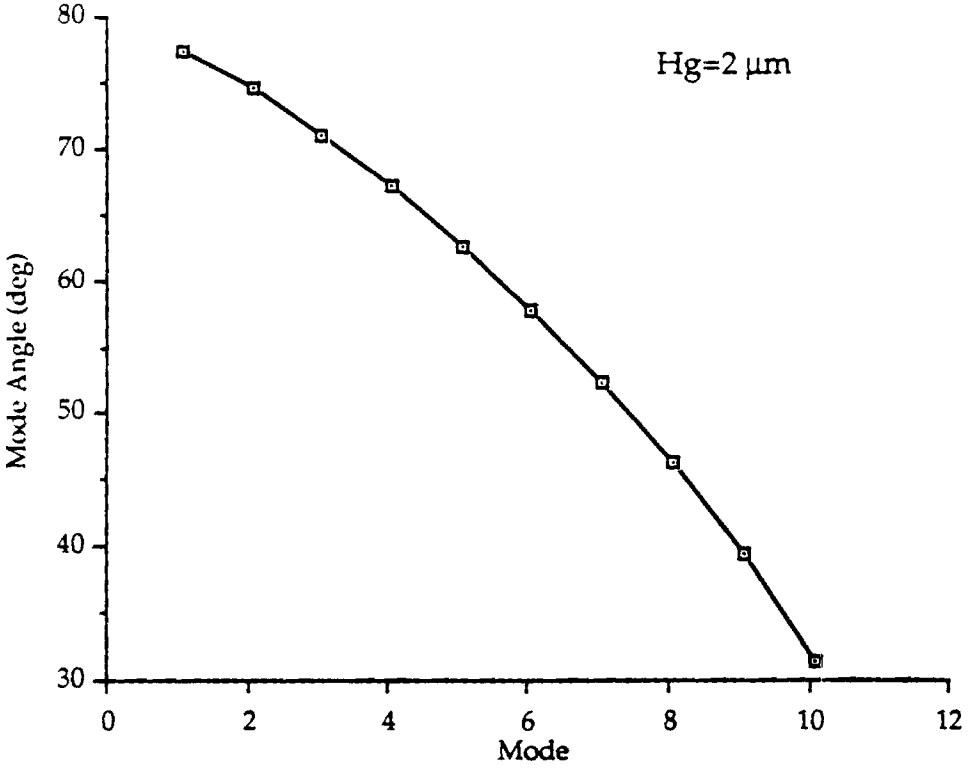

Figure 3.8 (b) Mode Angle Versus Mode at Constant Height

signals at different velocities, multimode propagation causes significant pulse spreading, thus it is desirable to fabricate a guide where only a single mode can propagate. Single-mode-only operation in SOI is possible for film heights between 200 and 2000 angstroms.

Having elucidated the basic parameters of the slab waveguide we now reconsider the effect of the second finite dimension. Noting that the width of the guide will tend to be larger than the height, there is motivation to treat the raised strip as a slab waveguide; this would facilitate an analytical treatment of its behavior. This assumption would be entirely appropriate if the horizontal dimension were large with respect to diffractive spreading due to the finite aperture of the source. This is not the case for the channel waveguides being studied here. However, reasonable approximations have been made to analytically extend the two dimensional results to the three dimensional case, such as Marcatili's shadow method and the "effective index" method [15]. Marcatili's method has shown that for well confined modes this type of structure can be treated to first order as two orthogonal systems by ignoring the shaded regions shown in Figure 3.9 [15]. This method can quite accurately predict the actual field configurations. The effective index method provides a second order method for predicting the propagation constant. The existence of such techniques provides justification to continue with the two dimensional analysis, noting that reasonably accurate extrapolation can be made to the three dimensional case.

Evanescent Waves

The simple ray model implies that the wave is entirely confined to the waveguide. The fields actually extend beyond the limits of the guide. An example of the electric field intensity for the fundamental TE mode of propagation is shown in Figure 3.10. To fully appreciate some of the important phenomena to be discussed later, we must reexamine propagation at the film interface. At this interface, the ray

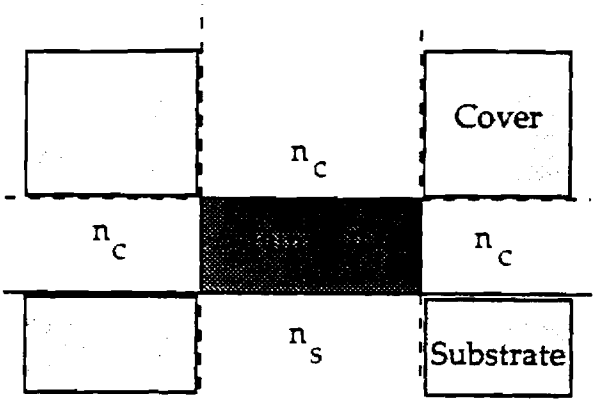

Figure 3.9 Cross section of an asymmetric channel waveguide

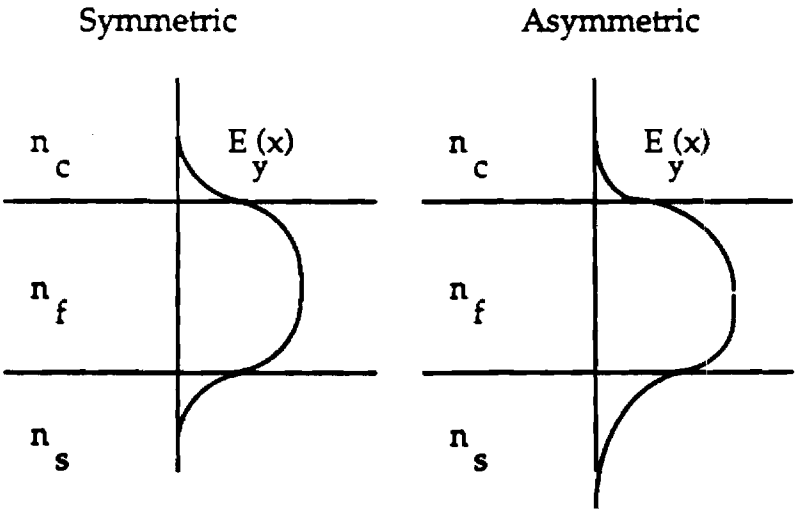

Figure 3.10 The evanescent field extends further into the region where the index of refraction is larger.

picture is more complicated. In addition to a phase shift there is also a lateral shift as shown in Figure 3.11, referred to as the Goos-Hanchen Shift. The relationship between the variables shown in the figure and those defined previously are given by the following equations:

Lateral shift

$$2z_s = \frac{2}{k}(N^2-n_s^2)^{-1/2}\tan(\theta)$$

Penetration Depth

$$x_s = \frac{\lambda}{2\pi(N^2-n_s^2)^{1/2}}$$

This latter parameter defines an effective guide boundary beyond the physical boundary. It also gives the rate of exponential decay of the field outside the waveguide as given by the following expression:

$$E(x) = E_0 \exp\left(\frac{-x}{x_s}\right)$$

The part of the wave outside the guide is referred to as an evanescent wave and is responsible for the coupling of power from the guide into adjacent structures. The greater the rate of decay the more tightly confined the wave. We note that as the mode number gets larger, the mode angle, θ_m, gets smaller and the wave is less confined (has a larger penetration depth). A plot of ray penetration depth into the oxide layer as a function of mode angle is shown in Figure 3.12.. We shall return to this effect again later for analysis of the transfer of energy between adjacent guides, across small gaps and leakage through the oxide into the substrate.

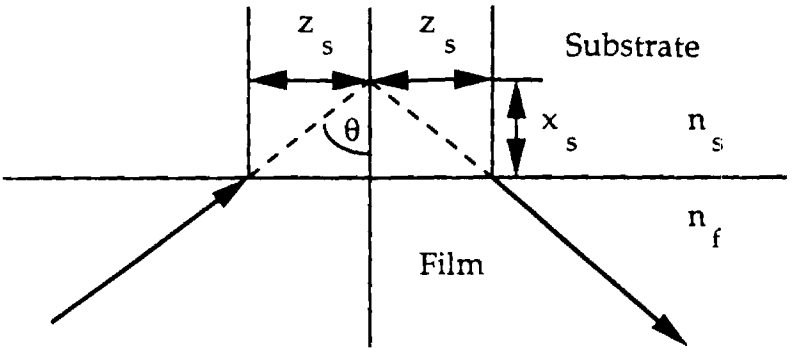

Figures 3.11 Ray Picture of the Goos-Hänchen Shift

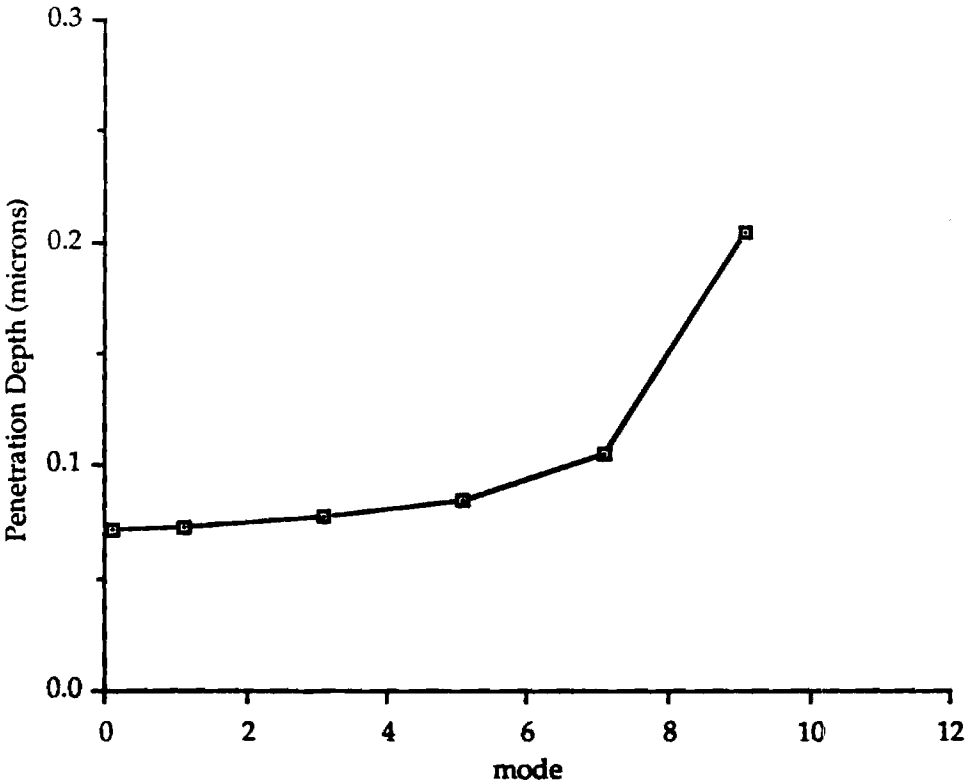

Figure 3.12 Mode versus penetration depth at constant height

3.1.2 Other Passive Structures

A simple straight section of SOI waveguide has been considered as a medium for optical wave propagation. However, a simple straight section of waveguide is not very interesting in and of itself. The routing and distribution of signals between devices is an essential ingredient to sophisticated signal processing. We know that from a silicon process technology point of view, the micro-machining of numerous structures in silicon based materials is well documented and we would be remiss if we ignored this aspect of OIC development.

The routing of signals with minimal loss is a major design goal for OIC interconnect. Electrical IC interconnect typically uses right angle turns because of their geometric simplicity. Right angle turns with optical waveguides would cause significant losses, therefore we have a choice between smooth curves and multifaceted turns. The sharp corners of a multifaceted turn could result in significant losses, therefore from a power loss perspective, smooth curved sections, such as that shown in Figure 3.13, are preferred. From the perspective of geometric simplicity, a 45 ° mirror facet would be preferred and such structures have been implemented in some cases [34]. For analytical purposes a curved section is characterized by a radius of curvature and a guide width. Even in the case of curved structures, optical power is lost to radiative modes as a result of the exponential tail, outside of the guide, being unable to keep up with the wave inside the guide. Thus, modes that are poorly confined and guides with sharp turns produce larger losses.

The combining and dividing of optical power can be performed optically, using a structure referred to as a branch waveguide. The "branch" refers to a structure like that in Figure 3.14. Both symmetric and asymmetric branches are shown. The inclusion of branching structures in this discussion is consistent with the goal of demonstrating a potential new technology, as it is critical to any future switching or multiplexing application. Conceptually, the branch waveguide is a straightforward extension of our previous discussion; ideally, the symmetric branch

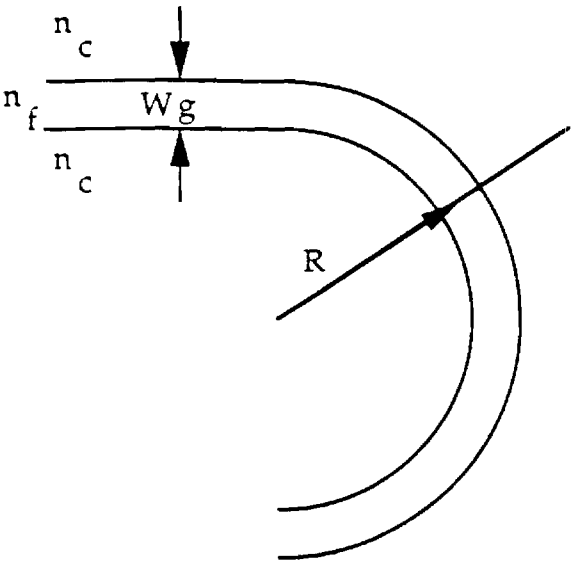

Figure 3.13 Curvature loss model

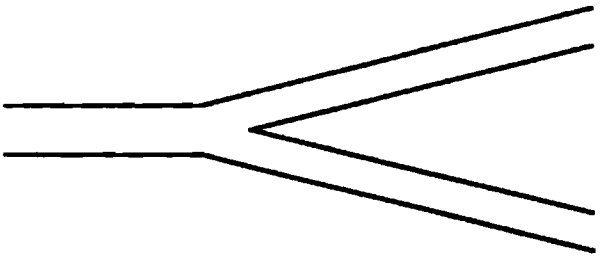

(a) Symmetric

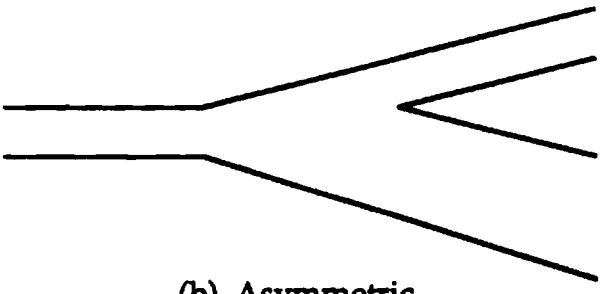

(b) Asymmetric

Figure 3.14 Symmetric and asymmetric branch waveguides

waveguide will divide the guided wave power, without loss, equally between the two branches of the guide. The actual behavior, particularly in a multi-modal guide is beyond the scope of this study. However Marcuse in [18] has shown that--the longer the taper, defined by Lb/Wb--the smaller the losses. For a taper of 10, the radiative loss will be about 10 % or about .5 dB. The degree of symmetry determines the division of power to first order.

3.1.3 SOI Waveguiding Limitations

Up to this point, a geometrically simple, isolated structure has been analyzed. Initial analysis predicts reasonable waveguiding behavior in device structures having producible dimensions. However, we have considered only first order effects where the design variables are not subject to the practical limitations defined by imperfect materials and processes. In order to introduce real world effects and more interesting structures we once again draw upon the literature for relationships between the magnitudes of such effects as a function of process limitations that are inherent to the physical device and fabrication technology.

An important figure of merit for the quality of a waveguide is its attenuation per unit length, with a value of 1 dB/cm considered a benchmark of viability for integrated optical device technology. Sidewall imperfections, bulk defects, free carriers, and abrupt transitions in the confining layers, all cause mode conversion and losses along the signal path. The major losses can be attributed to one of the following causes:

(a) Rayleigh scattering due to surface roughness
(b) Bulk scattering due to bulk defects
(c) Leakage or mode conversion
(d) Absorption
(e) Crosstalk
(f) Curvature

Qualitatively, it is recognized that typical silicon manufacturing process can control short-range surface roughness to a root mean square (rms) value of a few angstroms. SOI films tend to be somewhat rougher. A plot of power transmission loss as a function of guiding angle for several different guide thicknesses for a representative surface figure (rms) is shown in Figure 3.15. It is important to point out that these plots indicate clearly that lower order modes (larger angles) and larger guides improve throughput, i.e., the guided wave interacts less with the surface per unit length of propagation along the axis of the guide.

Bulk defects in waveguide materials produce scattering and consequently transmission losses. This can be a problem in polycrystalline materials or high defect density materials. Improperly prepared SIMOX materials have shown significant losses without a substantial annealing step [7]. However, bulk defect densities for good epitaxial silicon, such as found in BTSOI, are negligible. It is anticipated that any bulk effects can be ignored.

Leakage and mode conversion losses are largely dependent on geometric design parameters. As was discussed earlier, the oxide is in fact not semi-infinite and therefore the possibility of leakage into the substrate is a very real problem. Recalling that decreasing the height of the guide for any given mode causes the mode angle to decrease while the evanescent tail increases, extending further into the substrate, we note that thinner guides will require thicker oxides. However, oxide thicknesses are limited to one or two microns due to process limitations and because the oxide defines the minimum well depth in our active device process, we desire even shallower oxides. An analysis of the attenuation per centimeter due to substrate leakage was made by Kurdi and Hall [32]. The results of this analysis indicate that an oxide as thin as 0.4 microns would be adequate compared to other loss mechanisms for single mode guides (Hg=0.2 microns). In cases where multimode guides are present, discontinuities and odd shapes can cause transfer of optical power between modes. However, an analysis of mode conversion in these structures requires a detailed numerical analysis of the waveguide/guided wave

Figure 3.15 Transmission losses versus guiding angle.

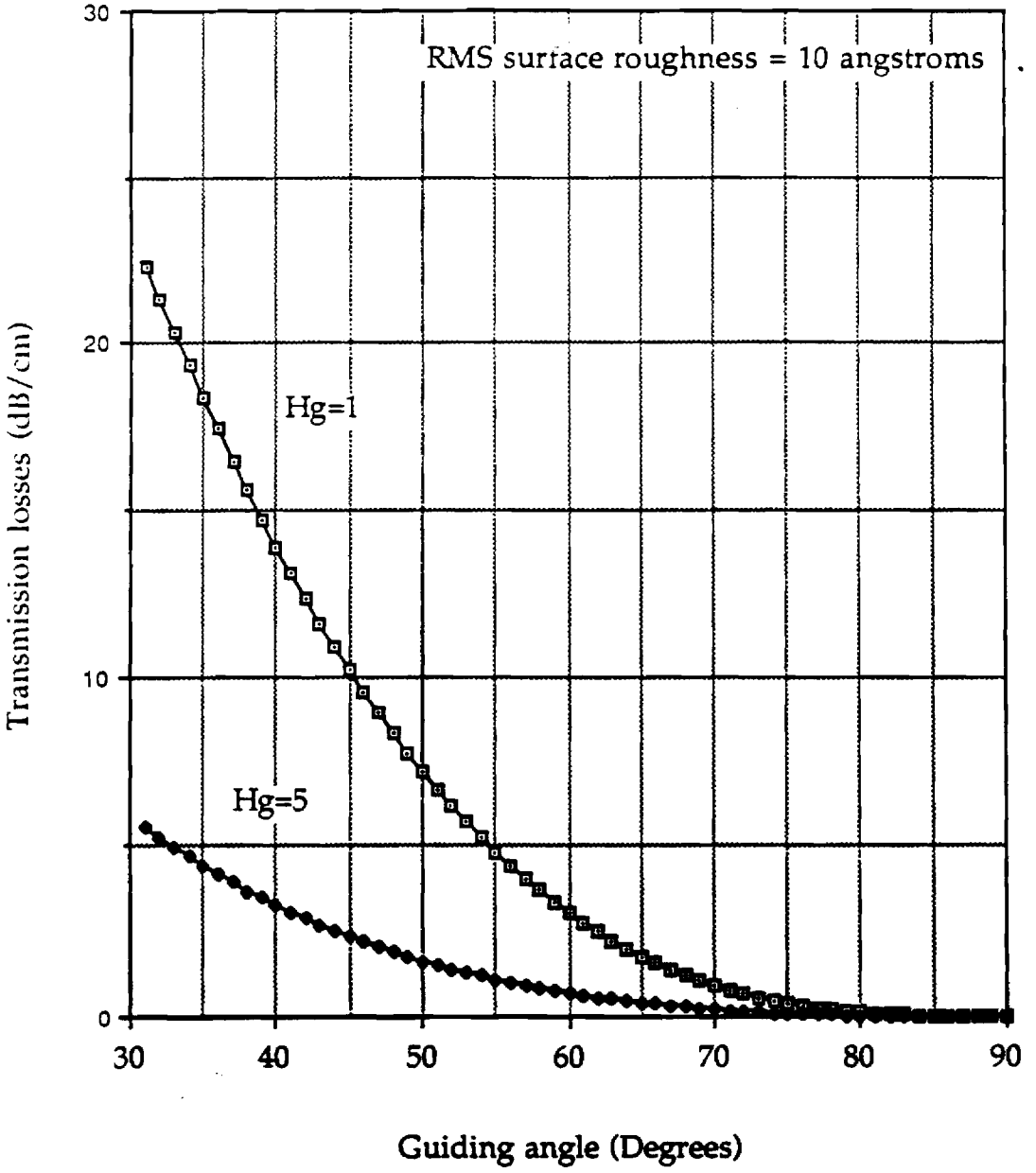

interaction [28] and is beyond the scope of this study.

There is a keen interest in using free carriers for inducing certain types of E-O effects in silicon. It has been pointed out that one of the drawbacks of these techniques is that the presence of free carriers causes signal loss due to absorption. Electrostatic deflection of the proposed mechanical structures will invariably involve some free carriers. One of our process options is to leave the etch stop intact as a natural contacting region. The effects of a sheet of free carriers in the wave guide are readily modeled to first order by computing the fraction of total path length which is represented by the absorbing layer and using a Beer's Law representation with the carrier concentration dependent absorptions reported by Soref et al. [9] to arrive at an attenuation per unit length. The results of this calculation, for a device having an etch stop of approximately 1 micron with an acceptor concentration of roughly 10E+19 carriers per cm^3, a guide thickness of 6 microns and a guided mode having an angle of 74 °, is -26 dB/cm, which is totally unacceptable. However, what happens precisely, when a voltage is applied is another question that would be better investigated experimentally. We know that applied voltages in similar capacitive structures result in high free carrier densities during accumulation or inversion; however, these regions tend to be physically very thin thus it is not obvious how these regions of localized charge would affect wave propagation.

An estimate of crosstalk between adjacent guides requires the computation of an overlap integral according to Burns and Milton [28]. This requires an exact solution of the EM wave equation in the waveguide and thus is directly dependent on the mode of the wave and how much of the wave is outside of the guide. Once again, larger variations in indices and larger guide dimensions result in better confinement. Typical values of the penetration depth for the TE_0 mode in SOI are on the order of .1 microns.

Energy can also be lost as a guided wave turns a corner. A formula for

calculating the loss as a function of the radius of curvature and waveguide width is given in [27] as follows:

$$\Delta n = n_f - n_c$$

$$N = n_f + b\,\Delta n$$

a_R = loss per radians

$$a_R = \frac{8.686 \times 2b(1-b)\Delta n R}{Wg\sqrt{2n_f \Delta n b + \lambda}} \cdot \exp\left\{\frac{-8\pi\Delta n}{3\lambda}\sqrt{\frac{\Delta n}{n_f}}\,R\left[1-(1-b)\left(1+\frac{Wg\,n_f}{4\Delta n(1-b)R}\right)^2\right]^{3/2}\right\}$$

We plot the loss versus radius of curvature for a number of different guide widths in Figure 3.16. We assume that the height of the guide does not affect this loss. The excellent confinement due to the large difference in the index of refraction should facilitate the routing of signals with minimal loss. In fact, because of the excellent confinement it is reasonable to expect comparable performance from simpler geometric structures that perform the same function, such as a 45 ° angle mirror.

3.1.4 Viability of OIC technology in SOI

In the preceding paragraphs we have considered strictly passive devices. The major device design variables for straight sections of waveguide are the waveguide height, width, length, as well as the oxide thickness. Branching and curved sections have also been discussed. Branch parameters include the taper and symmetry while curved sections are characterized by the width and radius of curvature. From the preceding analysis we summarize several important results, concerning the waveguide properties of simple passive SOI structures, to which we will refer again:

(a) The critical angle for the waveguide in the vertical direction is 25 ° which is the same as that defined by the SiO_2/Si interface. The critical angle in the horizontal direction is defined by the air to Si interface and is equal to 16° .

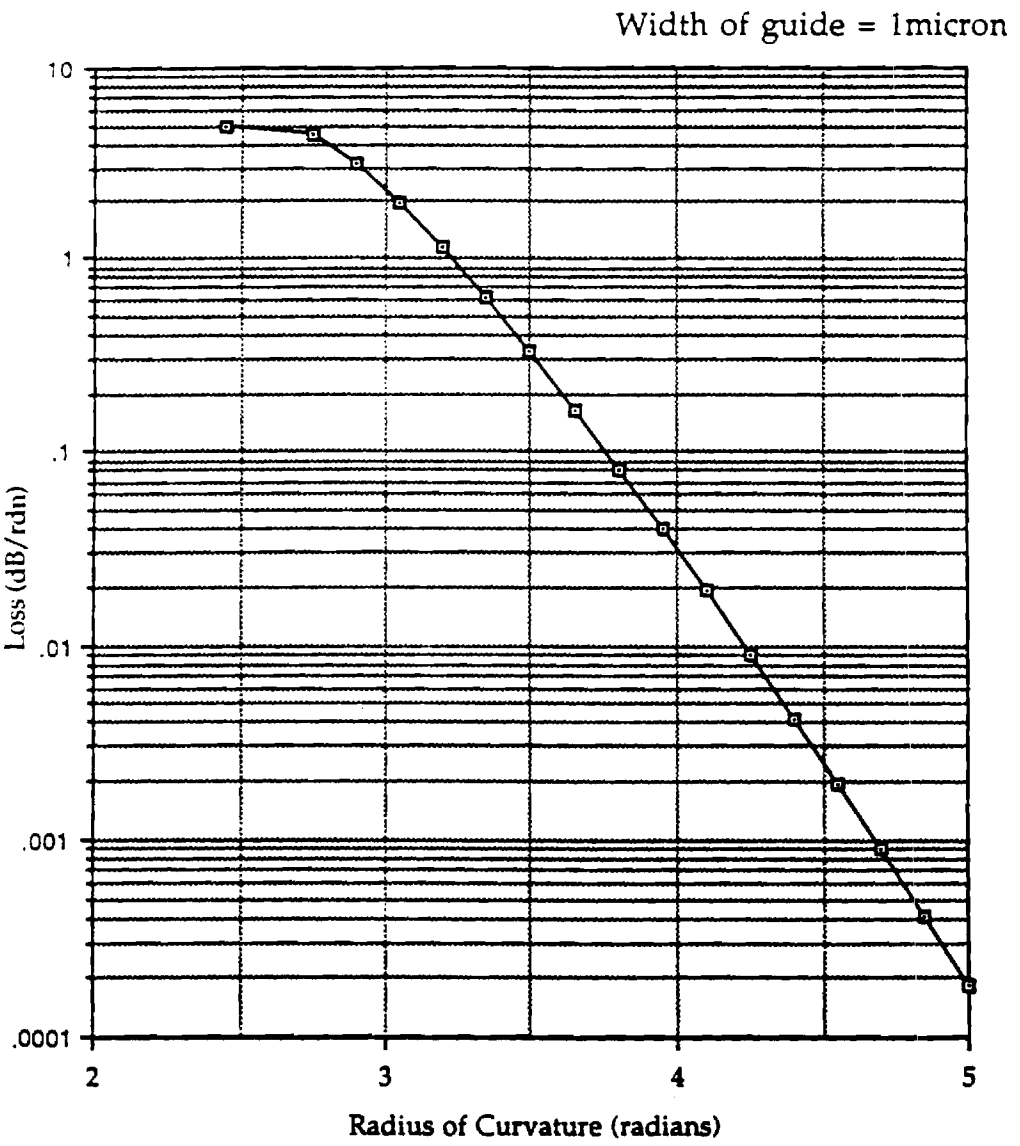

Figure 3.16 Loss due to Curvature in Waveguides

Only rays forming angles, θ_m, that meet the transverse resonance condition and that also exceed the critical angle are guided.

(b) We have defined the complement of the mode angle as the launch angle from which we note that as θ_m gets larger, α_m gets smaller, therefore only rays which meet the resonance condition with launch angles smaller than $90-\theta_c$ will propagate any appreciable distance along the guide.

(c) The number of modes is determined by the wavelength and thickness of the guide. Different modes have different propagation constants. Lower order modes correspond to larger mode angles, therefore the effective velocity of the beam is greater for lower order modes. Single mode operation only is defined for heights between 0.02 μm and 0.2 μm. Both single and multimode structures are realizable without exceeding the limits of current SOI thin film and patterning technologies.

(d) The effective thickness of the guide is defined by the mode of propagation as well as the thickness of the guide. Lower order modes are better confined then higher order modes and hence are effectively thinner.

(e) Numerous structures for routing, combining , and splitting signals can be readily fabricated using SOI technology.

(f) Low loss waveguide structures would appear to be well within the grasp of current silicon micro-machining capability.

In summary, the use of SOI technology for OICs would appear to be viable.

3.2 EMO Device Design Considerations

In contrast to the passive structures discussed in the previous section, the next two sections will consider the phenomenology and design variables of active devices in SOI. The active devices to be considered here are the micro-bridge and the micro-cantilever beam. In addition to the design variables discussed earlier, the bridge structure introduces two additional variables, namely the length of the bridge and the depth of the well. We will presently assume that the width of the well is sufficiently large so that it can be ignored. The micro-cantilever beam provides a more flexible structure given that one end is free to move with the gap length as an additional design variable. Because the mechanical deflection of these devices is the primary effect that enables the optical carrier to be modulated, the effects of deflection will provide the focus of subsequent remarks.

3.2.1 Behavior of a micro-bridge optical waveguide in SOI

The micro-bridge structure has been defined earlier. A three-dimensional perspective drawing that depicts the bridge in its deflected state is shown in Figure 3.17. For the present discussion, we will refer to the two dimensional side view in Figure 3.18 which qualitatively shows the principal additional degree of freedom introduced by the micro-bridge structure. In particular, a vertical deflection at the center of the beam results in an increase in overall path length along the bridge as shown.

We have targeted for study two principal classes of applications, fully acknowledging that there may be others. The two classes are signal processing and signal transduction. Typical signal processing problems would encompass both analog and binary processes (switching).

For signal processing we consider electrostatic deflection of the bridge. Briefly, the bridge and the bottom of the well form two electrodes of a capacitor; when a

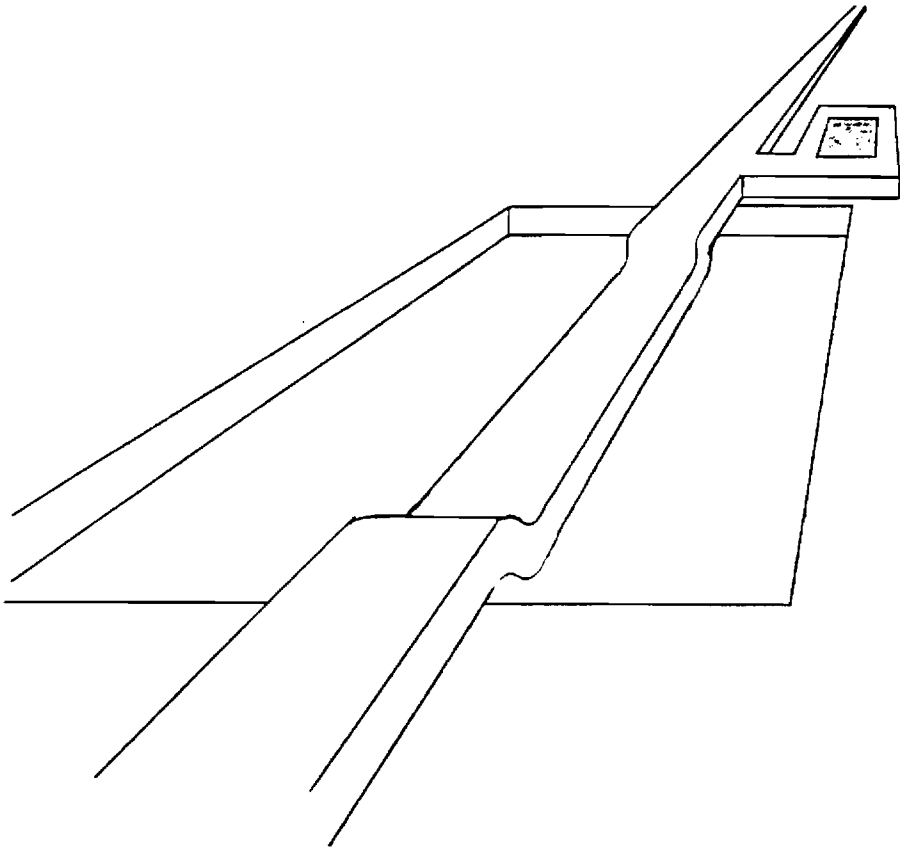

Figure 3.17 Three dimensional perspective drawing of the micro-bridge after deflection

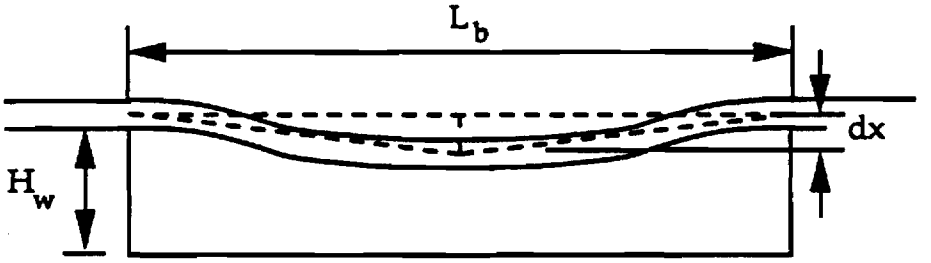

For small deflections $dL_b \cong 2\frac{(dx)^2}{L_b}$

Figure 3.18 Computational model for path length variation as a function of deflection, dx

potential exists between the two electrodes an attractive electrostatic force is developed that causes the bridge to deflect toward the bottom of the well. The deflection depends primarily on the elastic properties of the bridge as defined by the cross section, length and bulk mechanical properties of single crystal silicon, as well as the electrostatic forces developed between the well and the bridge section. Ignoring edge effects, the electrostatic forces depend primarily on the potential, the area of the bridge, and the distance between the bottom of the bridge and the bottom of the well. The deflection of the bridge causes a number of first and second order optical effects. The first order optical effects are an increase in path length, a change in index of refraction due to the photoelastic effect, and for shallow wells an increase in evanescent leakage of radiation into the substrate. Second order effects include variations in the cross section due to bending as well as variations in index of refraction and absorption due to a redistribution of free carriers in the bridge. These second order effects will be ignored for this study.

The use of such a device for signal transduction would rely on forces other than electrostatic such as pressure, acceleration, or mechanical to cause the deflection. Additional structures could be appended to the simple bridge to increase sensitivity to specific types of inputs. Once again the principal mode of transduction would be the variation in optical properties due to deflection. Particular optical quantities capable of signal transfer are: polarization, total power, phase or modal properties. One noteworthy mechanical property of this type of silicon structure is that it has a fairly high Q, with a resonant frequency that is tuneable. These properties makes it particularly amenable to the development of resonant structures and resonant signal processing techniques. The best way to view the simple bridge is as a string having a certain length, tension, and elastic properties that to some extent can be tailored to alter the resonant frequency. Longer, thinner structures will tend to have lower resonant frequencies with larger amplitude fluctuations for a given energy input, at least in the absence of a damping atmosphere. A representative spring constant could be computed by establishing a relationship

between small forces and their effective displacements from equilibrium.

Evanescent coupling between the bridge and the bottom of the well has been shown to depend on the spacing between them. Variations in deflection will result in variations in transmitted signal as a result of this coupling. An important phenomena, particularly in the context of switching applications, is that similar structures exhibit a threshold effect when electrostatically actuated. The origin of this "threshold effect" is best understood by noting that the field induced force depends on the spacing—the smaller the space, the larger the force. Applying an electrostatic force causes the spacing to decrease, which in turn causes the fields to increase which in turn cause the spacing to decrease and so on. At some point a critical field is created which can cause the bridge to spontaneously deflect to the bottom of the well. Optically, this point should be identified by a sudden loss of transmitted power due to direct coupling of light into the substrate resulting in very high off isolation.

Phase is another of several properties of light, propagating in a waveguide, that can be used to carry information. There are several ways in which the phase can be shifted and include:

-electrooptic effect
-path length variation
-photoelastic effect

The electrooptic effect is by far the most prevalent method used for actuation in OICs. The photoelastic effect is also the basis for many acousto-optical devices which use sound waves to modify the index of refraction. The change in index of refraction causes a change in effective path length. One particular method commonly used in macroscopic applications which has not been exploited to date for OICs is the effect of path length variation on the phase of an optical signal. One of the drawbacks to silicon is that it does not exhibit a very prominent electrooptic effect, nor is it the material of choice for acousto optic control methods. However using a micro-

mechanical bridge structure allows the path length to be modified by "stretching" the bridge.

Deflection Formula for Bridge Structure

The micro-bridge is an active device as a consequence of its mechanical motion. This section is included to provide an opportunity to discuss some of the relevant structural mechanics issues associated with our test structures and to present the fundamental relationships between the design variables and the mechanical behavior. We do not intend to derive any results from first principles because the behavior of interest is adequately described by existing formulas. The structure of interest is the micro-bridge, which is an elastic beam that is cantilevered at both ends as shown in Figure 3.19. The term "cantilever" implies that the displacement and slope at the fixed end is zero. This is not actually true, but is a good first order approximation for small deflections. The formulas which will be discussed are true only for small deflections for which Hooke's law holds, i.e. the displacement is proportional to the force. Given that our test structures undergo maximum displacements of only several microns over a length of at least 100 microns, this is an excellent assumption. Another condition for these formulas to be valid is that there be no viscous flow or permanent deformation. Our materials also meet this criteria. The standard formulas are given in terms of deflection as a function of point loads and distributed loads [16]. For non-electrostatic forces the uniform distributed load is an excellent approximation. The appropriate formulas are given in Figure 3.20. For electrostatic forces the situation is significantly more complex because the fields and forces depend on one another. However, a uniform distributed load is a good approximation for small deflections of the double cantilevered beam even for electrostatic forces, when the electrode is continuous as in our test structures. Figure 3.21 contains plots of deflection versus applied voltage for a number of different cross sections and lengths. It is clear that longer, thinner

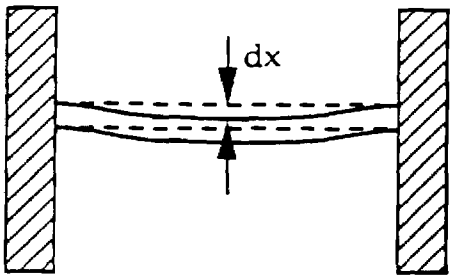

Figure 3.19 Double Cantilevered Beam (Bridge)

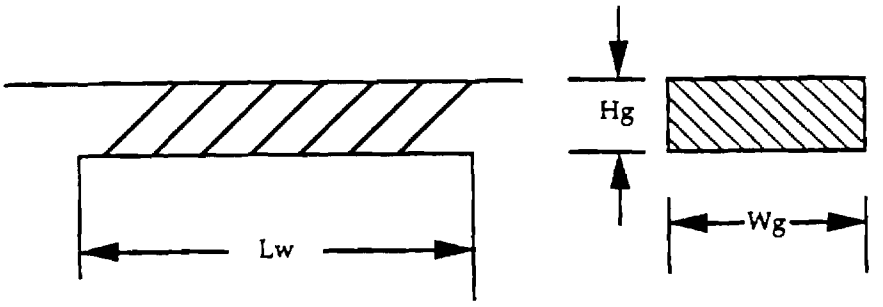

Sideview Endview

Deflection at center $x=\mu\frac{Lw^4}{384YI}$

$\mu \equiv$ uniform distributed load

$I=\frac{WgHg^3}{12}$

Figure 3.20 Geometric specification of a double cantilever beam (bridge)

Figure 3.21 (a) Micro-Bridge deflection versus applied voltage

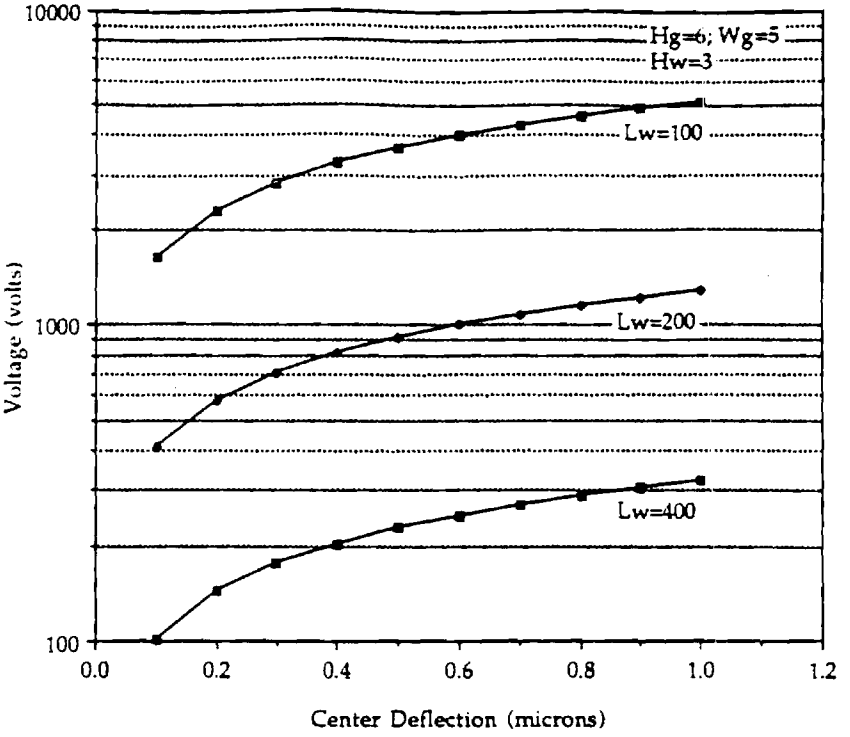

Figure 3.21 (b) Micro-Bridge deflection versus applied voltage

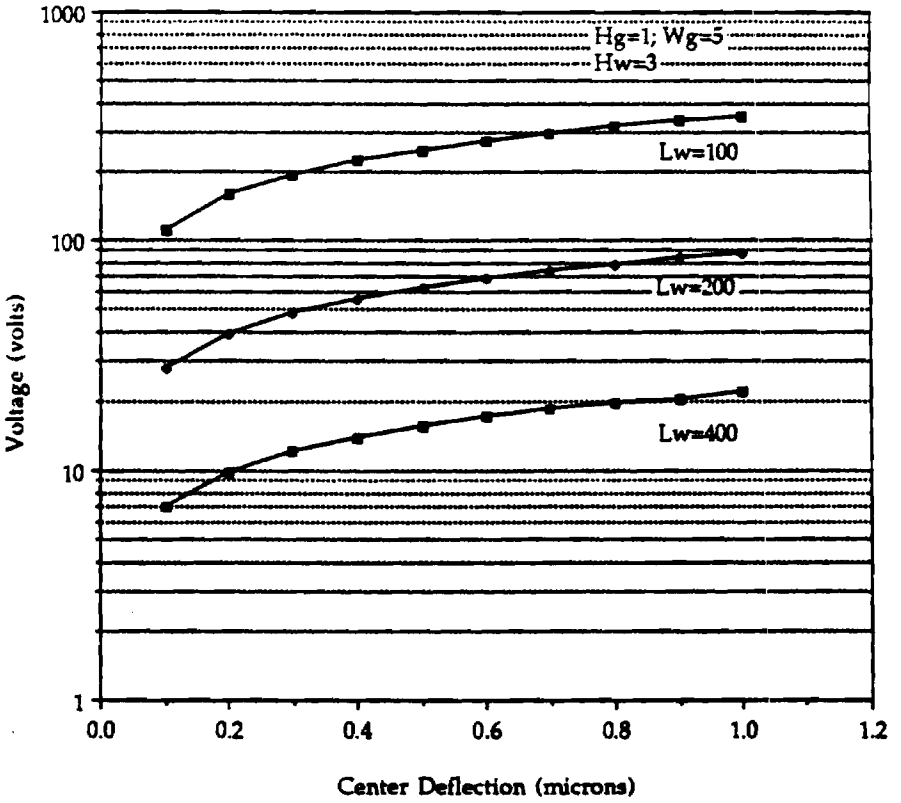

guides require less voltage for a given deflection and that single mode devices (Hg<.2 microns) having lengths of 100 microns require less than 10 volts for large deflections.

Evanescent Coupling

Evanescent coupling is another method whereby the power of the optical carrier can be modified. It was stated earlier that the guided wave is not entirely contained with the physical confines of the guide, but undergoes a mode dependent exponential decay outside of the guide. This evanescent portion of the wave can transfer energy to another structure of equal or higher index. In our case, this other structure can be an adjacent section of waveguide or the silicon substrate. It was reported by Kurdi and Hall [32] that substrate leakage can be significant for thin guides situated on thin oxides. Their analysis involved a four layer structure that included a silicon thin film separated from a silicon substrate by a thin intermediate film of silicon dioxide (index=1.5). Our active devices have a similar four layer structure with air as an intermediate layer (index=1.0) where the thickness of this layer depends on the depth of the well and the deflection of the device (See Figure 3.18). For purposes of estimation we can use the results of Kurdi and Hall to estimate expected attenuation for a given deflection. Their results are replotted in Figure 3.22. Using their results, an order of magnitude calculation of the attenuation for a given deflection could be made by multiplying the length of the device by the attenuation that corresponds to an effective separation between the device and the bottom of the well. For example, a 100 micron device with an effective separation of 0.1 micron would result in an attenuation of 100 dB. If the undeflected state corresponded to a well depth of 0.4 microns the result of a deflection of 0.3 microns would result in a signal variation on the order of 100 dB. A more precise analysis would require that we adjust the data of Kurdi and Hall for air and then incorporate the z dependent variation in guide/substrate separation by

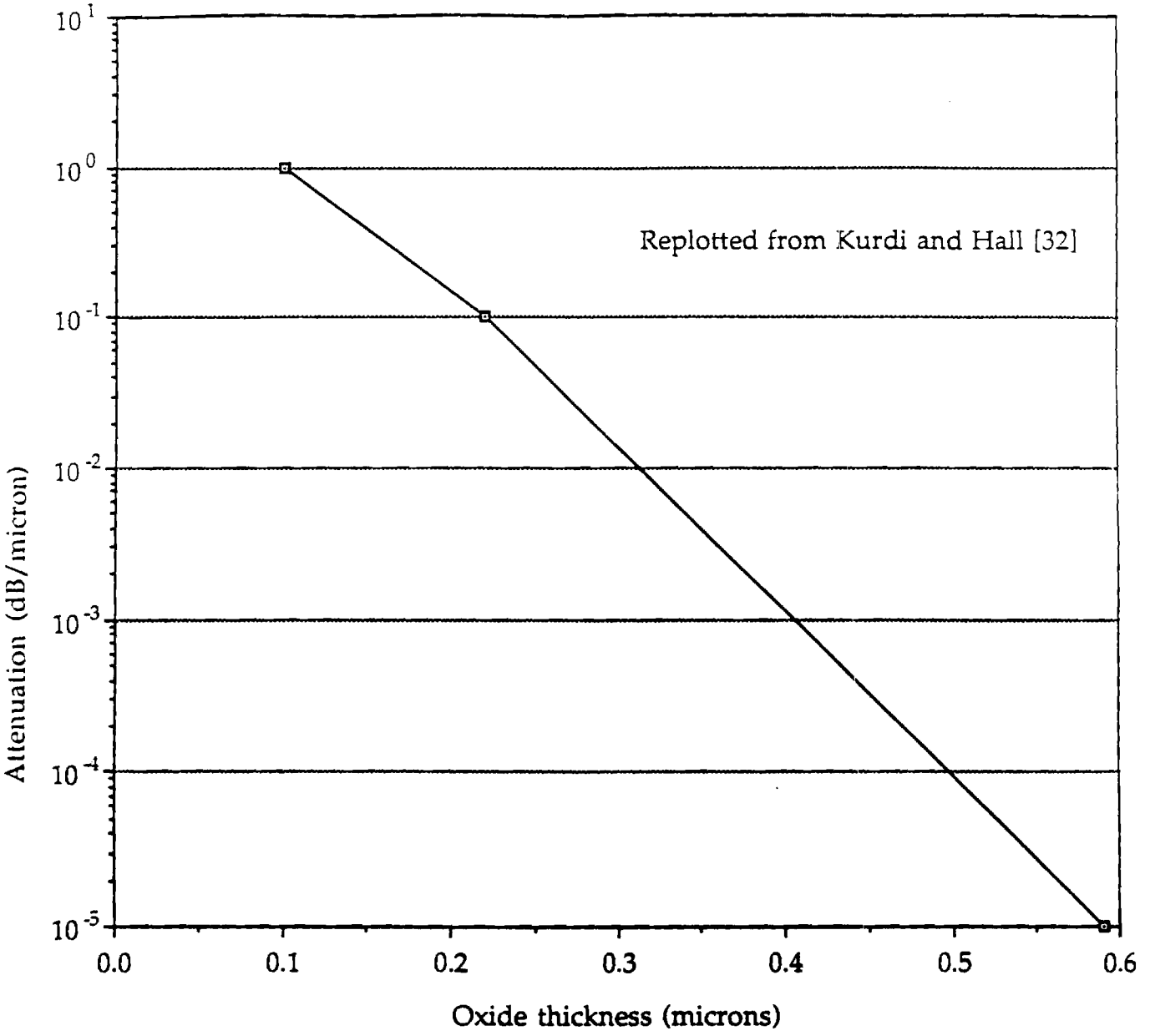

Figure 3.22 Attenuation due to evanescent coupling through the oxide to the silicon substrate

integrating the position dependent attenuation over the length of the device. Nonetheless, considering that typical integrated EO devices only exhibit off isolation on the order of 20-30 dB, this device possesses the potential to provide a substantial improvement.

Photoelastic Effect [24]

One of the important consequences resulting from the deflection of the bridge is a strain induced variation in index of refraction referred to as the photoelastic effect. A cubic crystal such as silicon is isotropic with regard to the propagation of radiation. However, when the crystal lattice is deformed this is no longer true because the symmetry is removed. The purpose of this section is to present the theory of this phenomena in sufficient depth to enable a first order estimate of the magnitude of index variations as a function of mechanical deformation.

In a mechanically isotropic material, the elastic deformation of the structure can be completely defined by the externally applied forces, Young's modulus and the Poisson ratio which relates stresses to strains. Once the stresses and strains have been determined, the variations in indices can be ascertained by direct application of the Neumann-Maxwell [24] stress-optical equations if the stress-optical constants are known. These stress optical equations assume that Hooke's law is valid, which we have already determined is a good assumption in this case. For a crystal lattice, the elastic constants are not necessarily the same, as is the case for silicon, so that the computation of the stresses and strains requires evaluation of the tensor product of two second rank tensors. Assuming silicon is isotropic for this first order analysis will be adequate. With this assumption, we can obtain a first order estimate of the magnitude of the variation of the index of refraction simply by multiplying the stress by the largest of the stress-optical coefficients (which is typically within a factor of three of the other constants).

To obtain the necessary stresses we follow the discussions in Timoshenko and

Gere [25]. For the structures under consideration, the stress is found by first determining the shape of the neutral plane after deformation. The bending moment is then determined by calculating the radius of curvature at any particular point and then substituting into the relation that follows:

Bending Moment

$$M = \frac{Y I}{\Gamma}$$

Γ=radius of curvature

Y= Young's modulus

I = Moment of Inertia

The relationship between the stress and the bending moment is then given by:

Stress

$$\sigma = \frac{M y}{I}$$

y= distance from neutral plane

And the relationship between the stress and strain is given by :

Longitudinal Strain

$$\varepsilon_L = \frac{y}{\Gamma}$$

Latitudinal Strain

$$\varepsilon_T = -\nu\varepsilon_L$$

υ = Poisson ratio

An important point is that even for isotropic materials the stress and strain vary from point to point within the beams. We can compute the maximum variation in

index by finding the maximum stress. For these structures the maximum stresses are given by

Bridge

$$\sigma_{max} = \frac{\mu l^2}{48} \cdot \frac{Hg}{I}$$

Unable to find the stress optical constants for silicon, we used those for diamond which has an almost identical crystal structure [26]. The resulting maximum index variations are plotted for a number of representative cases in Figure 3.23. The magnitude of these changes are commensurate with E-O induced (Pockels effect) index variation reported in the literature [1] for comparable applied potentials on such mainstream OIC materials as lithium niobate.

3.2.2 Behavior of a Micro-cantilever (MC) beam optical waveguide in SOI

The major difference between the behavior of the micro-bridge and the micro-cantilever beam is due to the presence of the gap at the end which allows the free movement of one end of the beam as shown in Figure 3.24. Mechanically, it is much easier (requires less force) to deflect just one end of the beam a given distance rather than stretch the bridge structure for a given device geometry. The presence of the gap also introduces two additional degrees of freedom in that it can vary the offset and the tilt. Optically the presence of the gap represents a number of loss mechanisms which were not present in the bridge structure. Because of these additional loss mechanisms and the relative ease of deflection, it appears that the micro-cantilever beam would be an effective optical switch with very high off isolation, although this structure could equally be used for analog signal processing and transduction. Because of the importance of the gap to the behavior of this device a special section has been included to define this behavior.

Once again, the micro-cantilever beam exhibits many of the same types of behavior as the micro-bridge although the analytical relationships between the

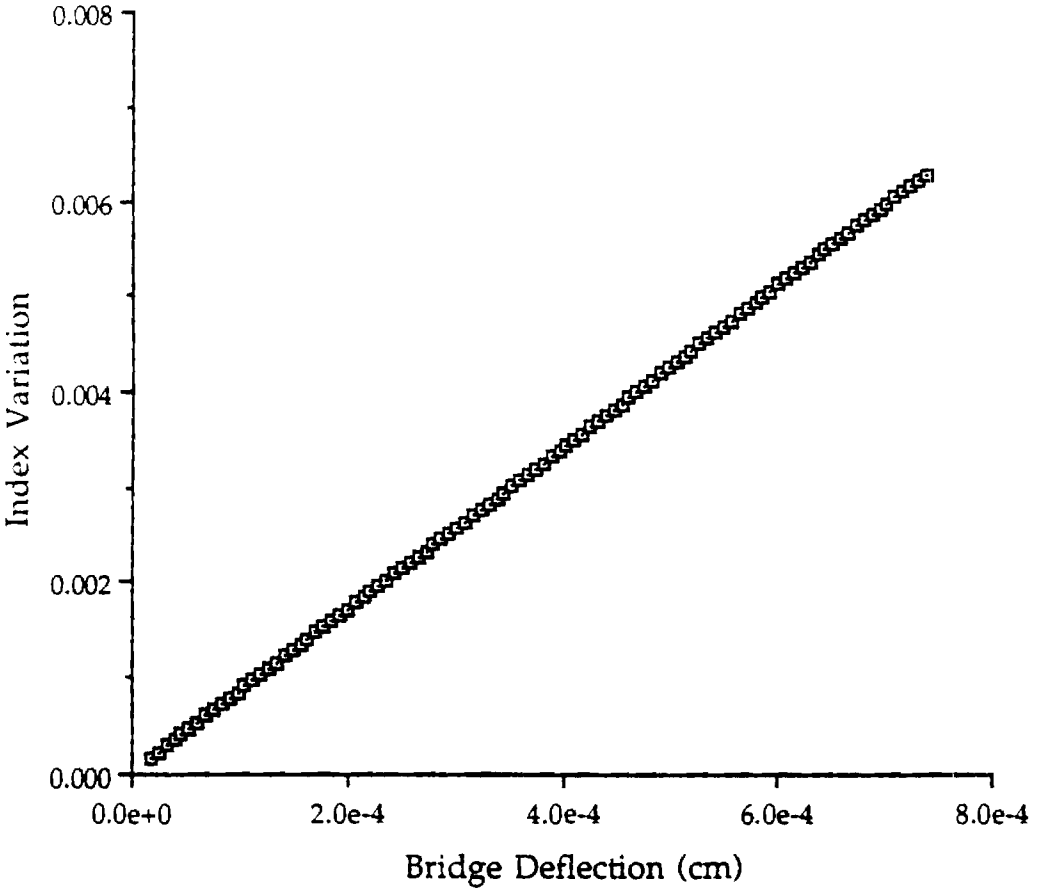

Figure 3.23 Index Variation as a function of Micro-Bridge Deflection

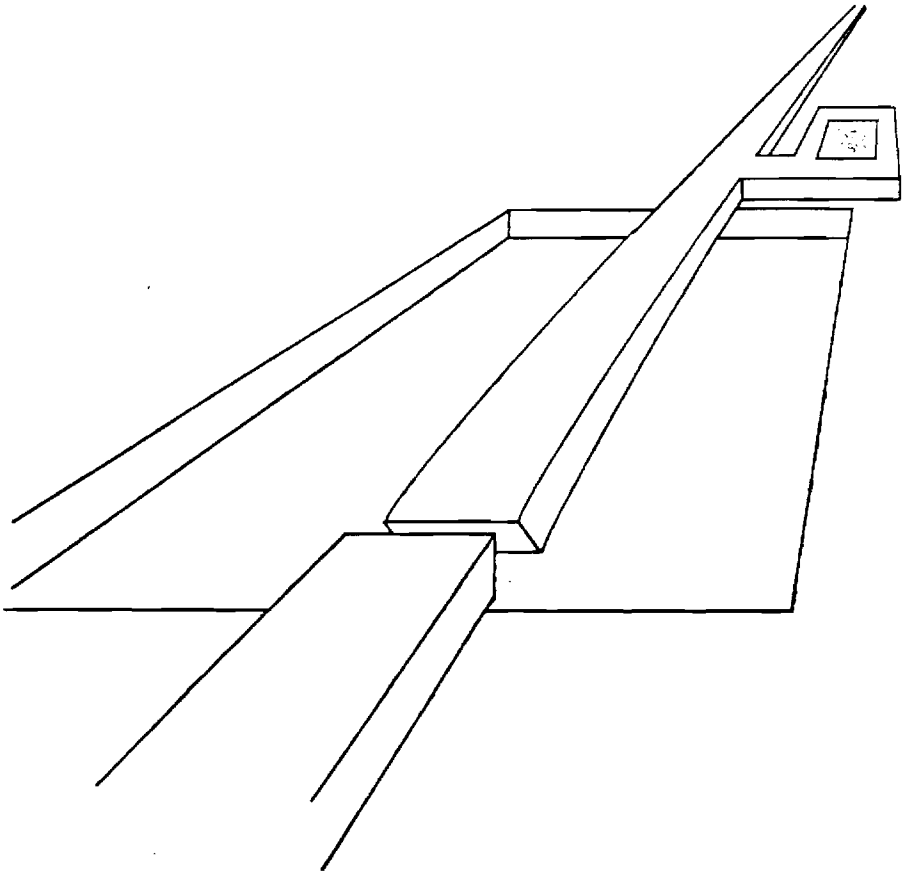

Figure 3.24 Three dimensional perspective drawing of the micro-cantilever beam after deflection

design variables are somewhat different. For purposes of resonance based processes the MC beam would be considered in the same vein as the tine of a tuning fork rather than a string. The photoelastic effect would be even more significant for a given cross section, length, and deflection where the maximum stress is given by:

$$\sigma_{max} = \frac{\mu l^2}{4} \cdot \frac{Hg}{I}$$

While the threshold phenomena is completely equivalent to that of the bridge, the voltage at which threshold occurs will be much less.

Deflection Formulas for a Micro-cantilever Beam

A development similar to that of the micro-bridge can be applied to illustrate some of the relevant structural mechanics issues associated with the MC beam, in particular the fundamental relationships between the design variables and its mechanical behavior. In this case, the structure of interest is an elastic beam which is cantilevered only at one end as shown in Figure 3.25. Once again, the formulas that will be discussed are true only for small deflections for which Hooke's law holds, i.e. the displacement is proportional to the force. The standard formulas are given in terms of deflection as a function of point loads and distributed loads [16]. For non-electrostatic forces the uniform distributed load is an excellent approximation. The appropriate formulas are given in Figure 3.26. For electrostatic forces the situation is significantly more complex because the fields and forces depend on one another. A relationship to describe the deflection as a function of voltage has been derived and is applied here[17]. We also define a threshold voltage, above which, the beam spontaneously deflects to the bottom of the well.

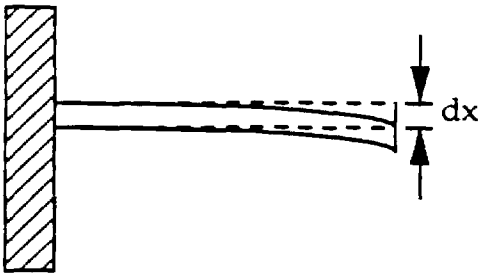

Figure 3.25 Single cantilevered beam

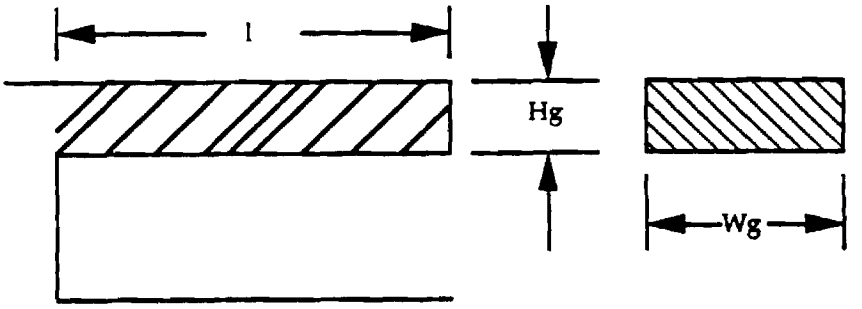

Sideview Endview

Deflection at tip: $x=\mu\frac{l^4}{8YI}$ μ=uniform distributed load

Angle at tip: $\theta=\mu\frac{l^3}{6YI}$ $I=\frac{WgHg^3}{12}$

Figure 3.26 Geometric specification of a cantilever beam

Deflection as a function of voltage

$$I = \frac{Wg\ Hg^3}{12}$$

$$\varepsilon_o \frac{Wg\ l^4\ V^2}{2\ Y\ I\ Hw^3} = 4(dy)^2\left(\frac{2}{3(1\text{-}dy)} - \frac{\tanh^{-1}\sqrt{dy}}{\sqrt{dy}} - \frac{\ln(1\text{-}dy)}{3dy}\right)^{-1}$$

Threshold voltage.

$$V_{th} \equiv \sqrt{\frac{18\ Y\ I\ Hw^3}{5\ \varepsilon_o\ l^4\ Wg}}$$

A number of plots are presented in Figures 3.27 and 3.28 to provide some quantitative understanding of how our test structures (Hg=6 microns) will behave or how they might be modified to improve their behavior for specific cases of interest (Hg=1 and Hg=.2 microns).

We note that the guides with large cross sections (Hg = 6 μm) require very large voltages (hundreds of volts) to produce substantial deflection even for long devices (hundreds of microns). In contrast, the threshold voltages for single mode devices are quite reasonable (less than ten volts for guides one hundred microns in length).

3.2.3 Gap Effects

The gap at the end of the cantilever beam is integral to the functioning of the beam as a transducer or switch. By deflecting the beam we change the character of radiation which continues along the waveguide. For switching applications the "on" state should be characterized by zero loss while the signal should go to zero (100% loss) for a switch in the "off" state. This doesn't necessarily imply that the radiation must not traverse the gap if, for example, polarization was being used as

Figure 3.27(a) Threshold Voltage versus Beam Length
Hg = 6 microns
Hw = 3 microns
Wg = 5,10,20

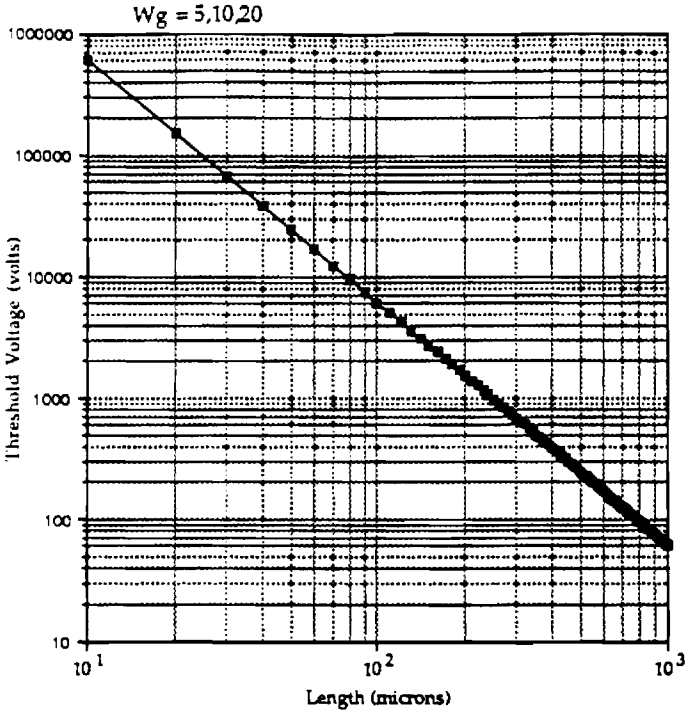

(b) Threshold Voltage versus Beam Length
Hg = 1 micron
Hw = 3 microns
Wg = 5,10,20

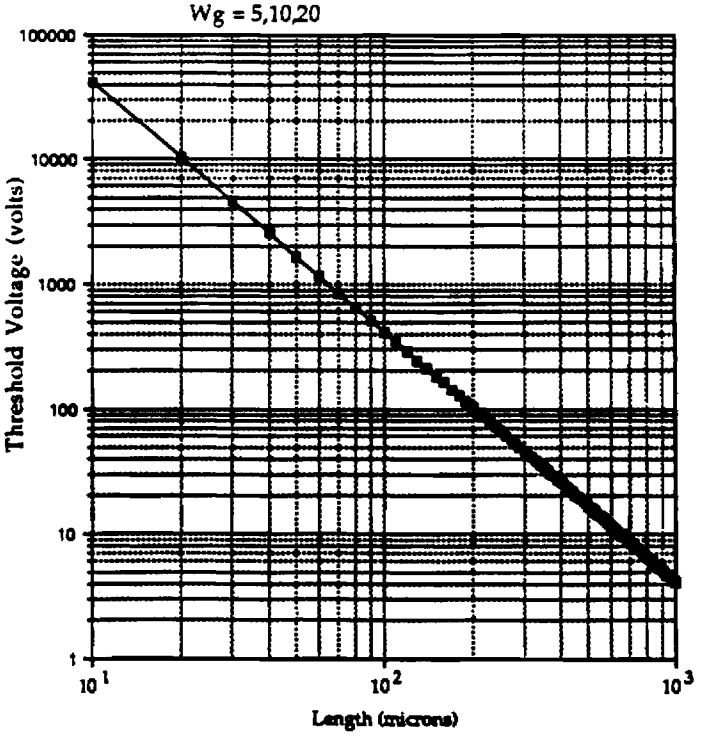

(c) Threshold Voltage versus Beam Length
Hg=0.2 microns
Hw=3 microns
Wg=5,10,20

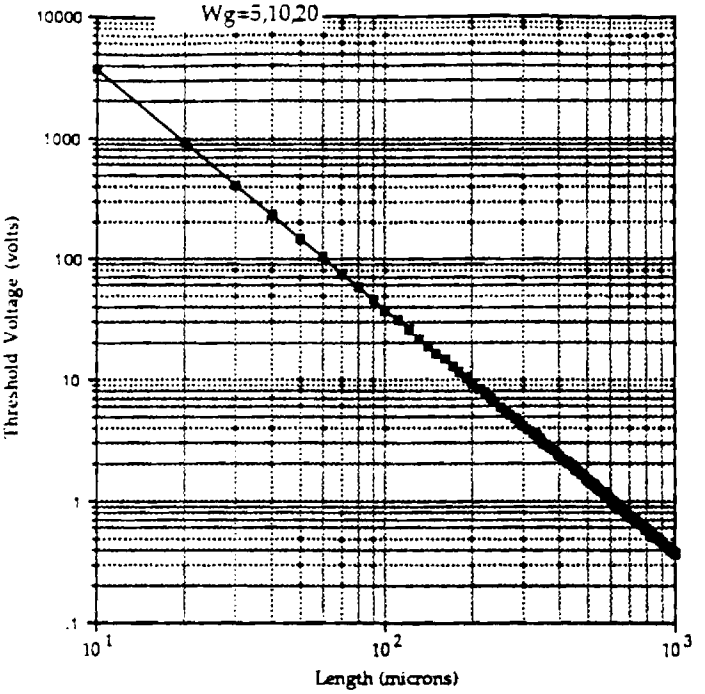

(d) Threshold Voltage versus Beam Length
Hg=0.2 microns
Hw=1micron
Wg=5,10,20

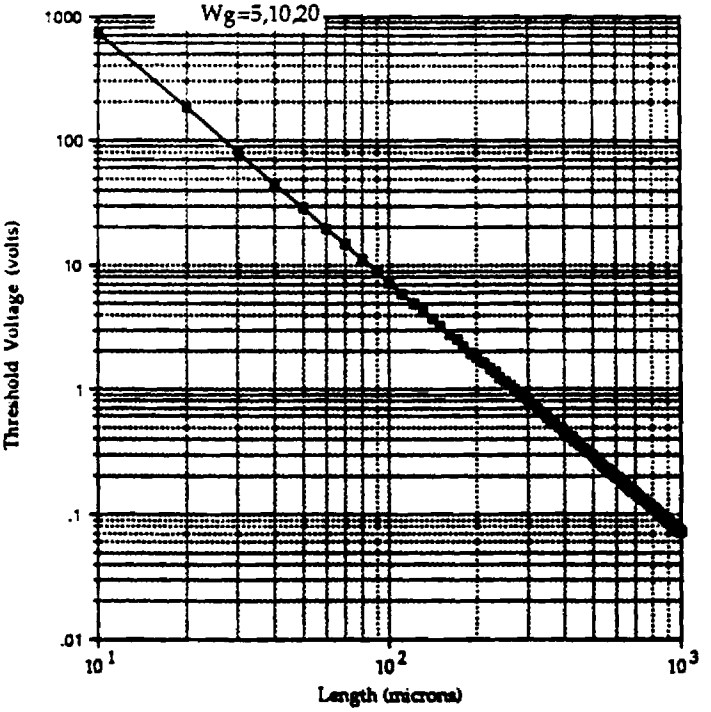

Figure 3.28 (a) Deflection of micro-cantilever beam as a function of voltage

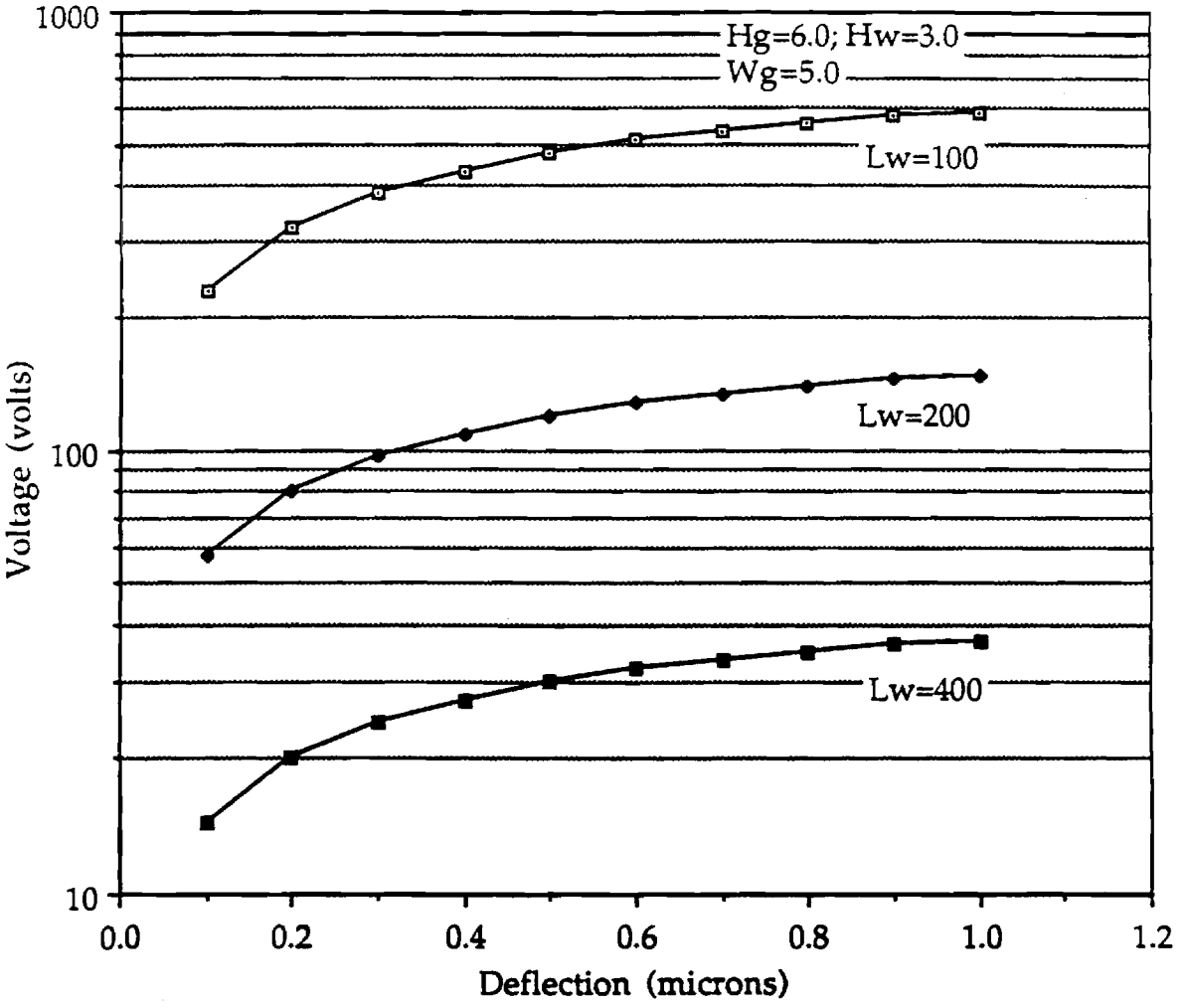

Figure 3.28 (b) Deflection of micro-cantilever beam as a function of voltage

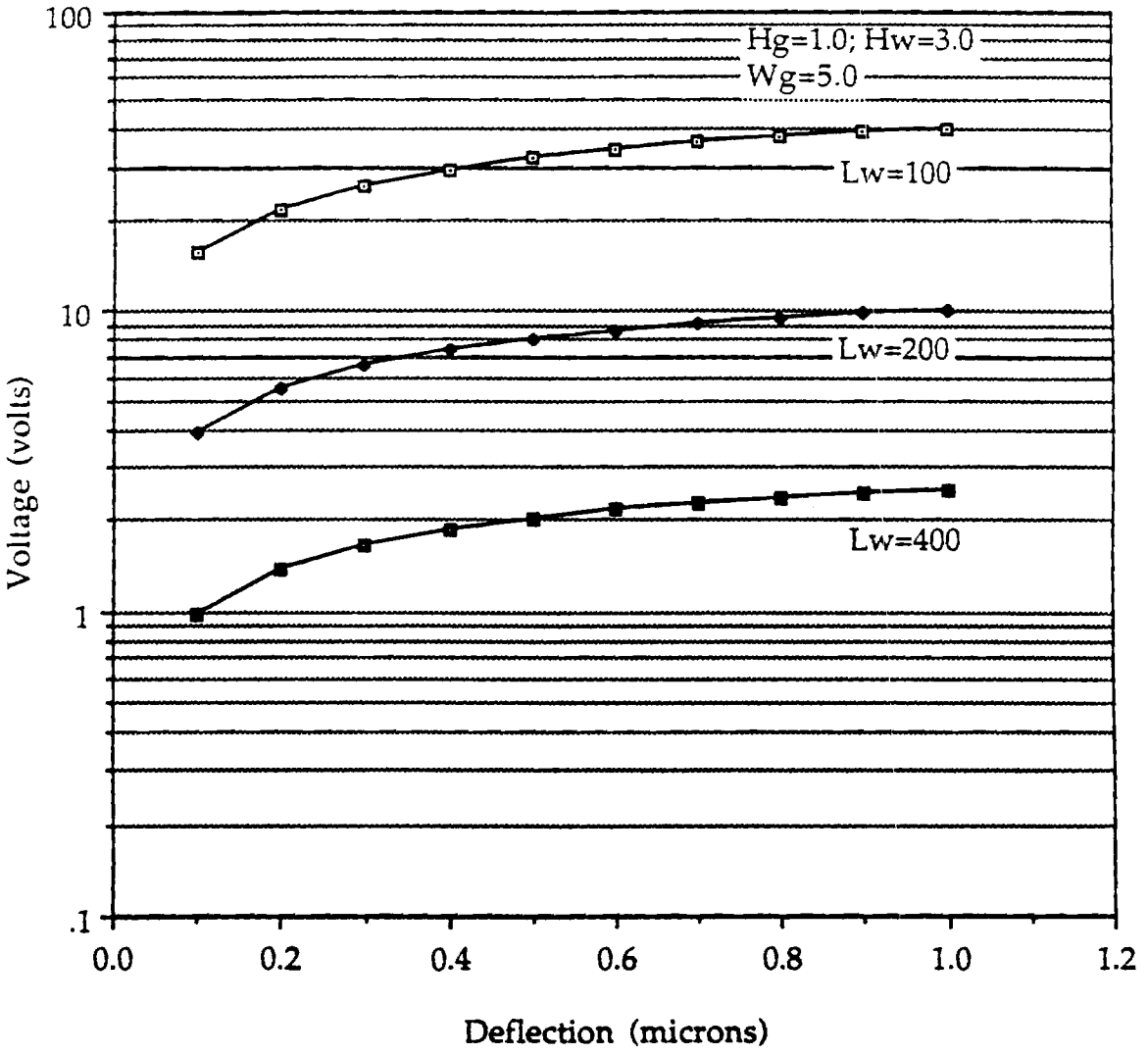

the signal carrier. A linear relationship between the measured variable and the signal would be the ideal relationship for a transducer application; however, any monotonic function would probably suffice. It is the purpose of this section to look at the effect of the gap on the guided wave. In particular, variations in transmitted power will be considered for each of the effects discussed below. Under ideal circumstances each of these effects would be independent of the others so that one could obtain the total change in power by simply summing the individual changes. Later we will look at the relationship between design variables and see how they relate to affect the properties discussed here.

The important effects of the gap on guided waves, which have been discussed in the literature [18], are listed below:

- Diffraction
- Scattering at surface
- Geometry
- Fresnel
- Total Internal Reflection (TIR)

It is possible that there are other significant effects which have been ignored here. The abrupt transition of the active waveguide from its asymmetric form ($n_c \neq n_s$) to its symmetric form ($n_c = n_s$) over the well is one particular aspect of the problem which will be ignored. Experimental results may cause us to reconsider this approach. In this section we will consider only the five effects listed above.

We begin with a qualitative discussion of each of these effects and then follow with quantitative analysis where appropriate. Quantitatively, we will follow the development of Marcuse [19] and assume that the fundamental mode is Gaussian in nature. Ultimately, experimental evidence will be needed to determine the validity of this assumption. The relationships between the effects cited above and the waveguide and gap parameters, shown in Figure 3.29, are of particular importance. Ultimately, we would like to have the capability to optimize these

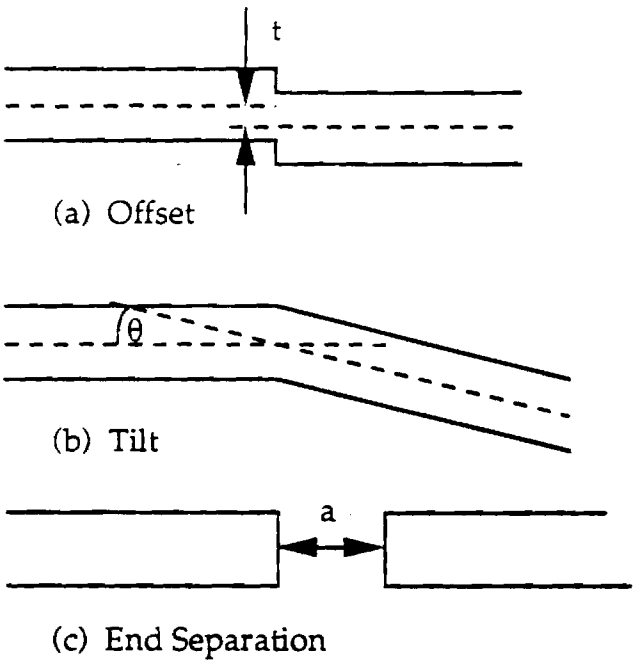

Figure 3.29 Geometric definitions of tilt, offset and end separation

effects to best suit a particular application by proper specification of the gap geometry.

Diffraction

Diffraction is a fundamental physical effect which results from waves passing through a finite aperture. Diffraction theory is used to describe the spreading of the wavefront as it leaves the aperture (waveguide exiting surface). As the beam spreads, less power will be intercepted at the other end of the gap. Hunsperger [2] attributes to Miller [36] that light emitted into a medium from an abruptly terminated waveguide remains collimated to within a waveguide thickness over a length, Zc given by

$$Z_c = \frac{H_g^2}{\lambda^2}$$

where Hg is the height of the guide, and λ, the wavelength [2]. For a wavelength of 1.3 microns we calculate the following three values:

1) Zc = 27.7 μm at Hg = 6 μm,

2) Zc = .77 μm at Hg = 1 μm, and

3) Zc = .03 μm at Hg = .2 μm.

Diffraction effects are decidedly more significant for guides smaller than a wavelength.

Surface Scattering

If the end faces of the two portions of the waveguide are not "smooth" then the wavefront will be distorted and energy will be lost. The "smoothness" of an optical surface is usually given in fractions of a wavelengths. One tenth of a wavelength is usually considered acceptable while one hundredth is exceptional. For our analysis we will assume that both faces are planar, parallel and perfectly

smooth, since we presently have no reason to believe that to first order it will be otherwise.

Geometry

The geometry problem to be discussed here is basically the same as the coupling between two fibers. It has been treated by a number of researchers and is typically broken down into three separate effects--tilt, offset and end separation [19,20,1,2]. All three of these effects are relevant to the operation of a cantilever beam and a quantitative understanding of each will ultimately be necessary to estimate the effect of beam deflection on the guided energy. These variables are defined in Figure 3.29. The end separation, a, is the gap and is relatively fixed given that the ratio between the maximum deflection and length of the beam is small. It is assumed for this discussion that the two opposing gap faces are parallel to one another and orthogonal to the other adjacent surfaces. The presence of the gap can introduce diffraction and Fresnel losses which are discussed in other sections. Both tilt, θ, and offset, t, are present when the beam deflects and both can contribute significantly to the losses. For the analysis that follows, we will assume that the static alignment is perfect, with all dimensions defined by the masks and film thicknesses. Furthermore, our treatment will be one-dimensional in nature since the waveguides which we have designed have a large width-to-height aspect ratio. To obtain the two-dimensional result we will assume that the one-dimensional analysis is valid along the entire width of the guide (no edge effects).

Fresnel Losses

In general, when light propagates across a boundary between two media having different indices of refraction, the light is only partially transmitted. This is a direct result of applying Maxwell's laws with the appropriate boundary conditions to

EM wave propagation across a planar boundary between two different dielectric materials. The equations which result are called the Fresnel equations and can be used to derive precisely the amount of power that is reflected and transmitted (absorption is ignored). For waves that have an angle of incidence equal to zero with respect to the surface normal, the transmitted power associated with each isolated interface is given by the following equation [21] :

Transmitted Power per Face

$$T = \frac{4n_1 n_2}{(n_1+n_2)^2}$$

For waves that are off axis this relationship is different for the two polarizations resulting in partial polarization. An important assumption for the application of these equations is that the dielectrics are considered semi-infinite and that they are isolated, i.e. the next nearest interface is many wavelengths away. When two semi-infinite layers are separated by one or more finite layers then the problem can have a significantly different result--anywhere from zero to a 100 percent loss. In our case, we have a gap that is on the order of several wavelengths which is a grey area due to the fact that the materials are neither semi-infinite nor isolated. We must note that when passing from a high index media into a low index media (such as silicon into air) that these relationships are valid only for angles less than the critical angle for which total internal reflection does not occur.

Total Internal Reflection (TIR)

Most OIC applications combine materials that have similar indices; the result is, that the light is not tightly confined unless it is on axis and if it is on axis, then it is readily emitted at the end of the waveguide. This is not necessarily true for cases

where the difference in indices is large, as is true in our case. In our case, there are two distinct ways to characterize reflection at an extremity of a waveguide, such as the gap. First, for guided modes with launch angles that are smaller than the silicon/air critical angle (16 °), the use of the Fresnel equations cited above is appropriate. Second, for guided waves incident on the exit plane into the air gap at angles greater than this critical angle, TIR can result. A simple "gedanken" experiment based on Figure 3.30 will allow us to illustrate this point. First we note, from previous calculations, that for the material system here, we have total internal reflection at the air-silicon boundary for angles of about 16 degrees and greater, while at the silicon-silicon dioxide interface we obtain TIR at angles of 24 degrees and greater, thus the waveguide can sustain guided modes only at mode angles greater than 24°. This translates to launch angles less than 66° with respect to the guide axis. We must also remember that no consideration was given to how these modes were excited, i.e. there is no guarantee that a guided mode can be extracted from the guide. In fact, at the exit plane (assumed to be orthogonal to the guide axis), any modes which have a launch angle greater than sixteen degrees will, in general, undergo TIR unless the gap is very small, resulting in an effect similar to quantum mechanical tunneling. If the gap is large, it can act as a mode filter for higher order modes that invariably have larger launch angles. It should not be surprising that, because of the large index of silicon relative to air, it is relatively easy to couple light into the guide rather than out.

Gap Loss Reduction

TIR and Fresnel losses can cause a substantial reduction in signal to noise ratio if a number of devices with gaps are cascaded together. The Fresnel equations are only valid for guided modes which are within 16 ° of being on axis and result in losses on the order of .77 dB per face. For modes with launch angles greater than this, TIR applies, resulting theoretically in total signal loss. However we know that,

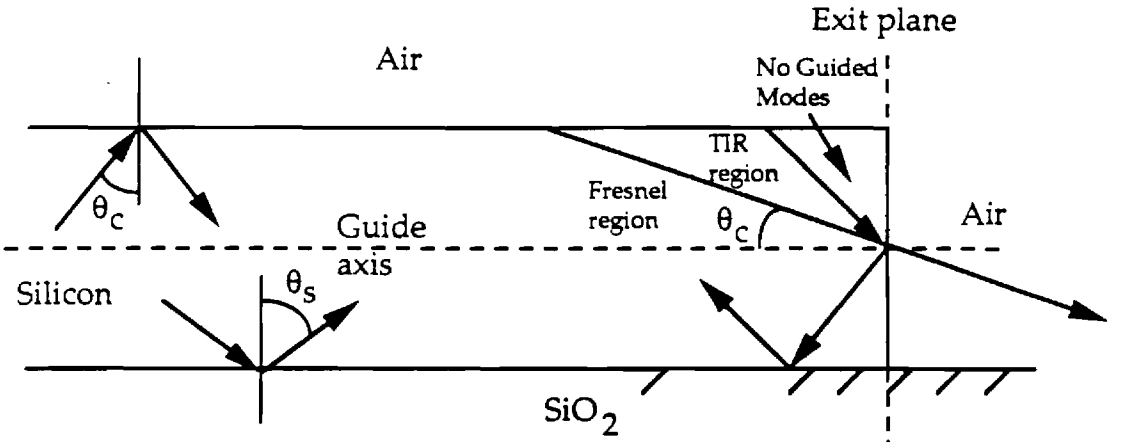

θ_c = silicon/air critical angle (16°)

θ_s = silicon/silicon dioxide critical angle (24°)

Figure 3.30 Total internal reflection at the exit plane

in the limit, as the gap disappears, these losses go to zero for both cases. A question that arises is, how small must the gap separation be before these losses become insignificant? To answer this question we have performed an analysis similar to that of Huppert and Ott [22] which treats this as an electromagnetic analog of the quantum mechanical (QM) tunnel effect. Although this analysis specifically addresses the case of TIR, it also has some applicability to the Fresnel losses, for gap lengths that are significantly less than a wavelength.

The problem formulation requires that we solve the wave equation in three regions shown in Figure 3.31. Region I assumes the presence of an incident and reflected wave, region III assumes only a transmitted wave, while region II (the gap) assumes an exponentially decaying evanescent wave. The solution to this QM tunneling problem is given in many standard texts on Quantum Mechanics.. Transmitted power is given in Anderson [23] as follows:

Transmission equation

$$k_2=\beta \quad k_1=\frac{2\pi}{\lambda} \quad a=\text{gap spacing}$$

$$T = \frac{1}{\cosh^2[k_2 a] + \frac{1}{4}\left[\frac{k_2}{k_1} - \frac{k_1}{k_2}\right]^2 \sinh^2[k_2 a]}$$

The resulting worst case losses are shown for the smallest guided mode angle (launch angle=66°; mode angle=24°) as a function of gap separation in Figure 3.32. Due to TIR at the exit plane and Fresnel losses one can conclude that transmission across the gap is more favorable for lower order modes where the mode angle is greater than 74 ° and thus the gap acts as a mode filter. Note that if no mode exists with a mode angle greater than 74° and the gap is large, then no power will traverse the gap. Thus a large gap defines a new minimum height at which the waveguide can operate effectively, namely the height at which the zero order mode has a mode

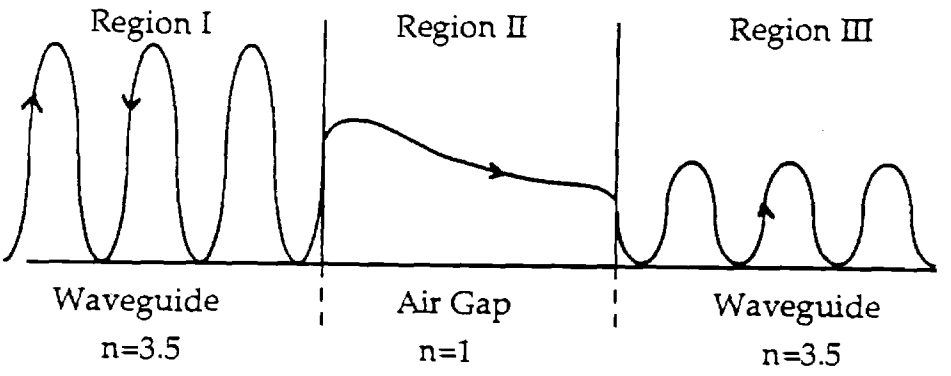

Figure 3.31 Wave Penetration of a finite potential barrier

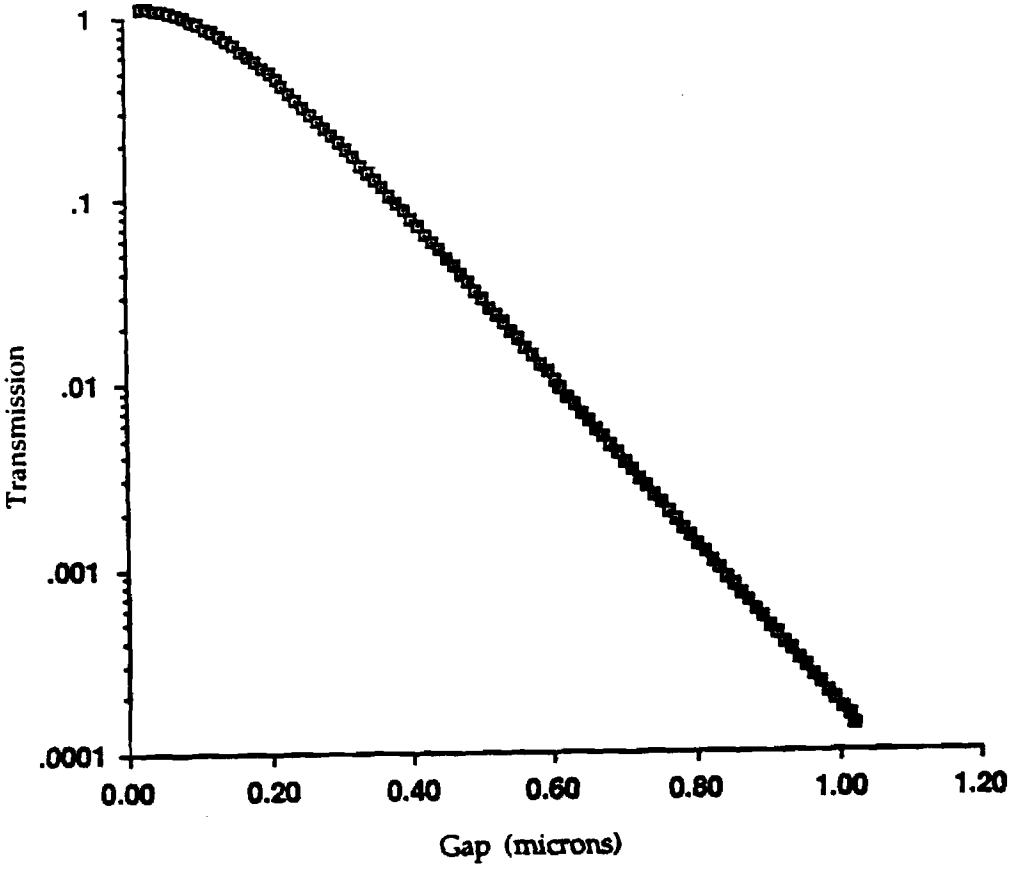

Figure 3.32 Transmission as a function of gap separation

angle of at least 74 ° (approximately 1 micron at λ =1.3 μm). However, by reducing the gap to approximately one tenth of a wavelength, the mode filtering and Fresnel losses at the gap are no longer significant.

3.3 SOI Waveguide System Level Considerations

The major part of the preceding analysis was directed at isolated structures and devices based upon producible waveguiding structures in SOI. In order to introduce real world effects we consider those constraints which arise when several waveguide structures must be integrated into a sophisticated multi-function OIC. The inherent limitations are two fold: one concerns the transmission of the signal in the guide which we have expressed in terms of power loss per unit length or throughput. The second important limitation concerns our ability to couple power into and out of the structure, which we define in terms of the coupling efficiency. Other limitations associated with integration of several devices which are layout dependent can be defined in terms of packing density and routing efficiency. Packing density addresses the issue of the sizes of devices and crosstalk between neighboring devices. Routing addresses the problem of interconnect and guide curvature.

3.3.1 Inherent Limitations

There are two type of losses associated with dielectric waveguides: I/O and transmission losses. The former we define in terms of a coupling efficiency, the latter we define as throughput efficiency. Coupling efficiency is subject to a number of physical constraints, such as the size of the source, the aperture of the guide as well as impedance mismatches between the external source and film dielectrics. Coupling efficiency also depends significantly on the particular method of coupling used.

There are a number of mechanisms which contribute to transmission losses. These are:

substrate leakage

absorption

scattering

bending (curvature)

The physical mechanisms for these phenomena are readily explained. Substrate leakage refers to the process whereby the evanescent tail of the guided wave interacts with the silicon substrate below the oxide layer resulting in a transfer of power from the film to the substrate. The primary cause of absorption in silicon is free carriers. Scattering occurs due to imperfections in the bulk or at the surface of the guide. Bending or curvature causes loss to due to variations in path lengths along the inner and outer curve.

Coupling Efficiency

One of the key concerns from a system's perspective is how does one couple energy (the signal) into and out of the device. Coupling efficiency is a term used to address the effectiveness of coupling light into and out of these structures. Several methods of coupling light into and out of waveguides have been reported and analyzed with regard to their efficiency. One way, is to integrate detectors and transmitters onto the same substrate. One of the drawbacks of a silicon-based OIC technology is that there are no mature technologies for fabricating optical detectors and emitters at wavelengths beyond 1.2 microns in silicon. Silicon Schottky barrier detectors are known to operate at these wavelengths and have been demonstrated, however, they require cryogenic cooling and have relatively low quantum efficiencies. Some successes in developing efficient emitters using Si-Ge compounds have been reported, but the work which integrates III-V technologies with silicon [35] appears to hold greater potential for near term realization.

Alternatively, a wide variety of techniques using passive structures such as lenses, gratings, and prisms have been used to couple radiation into and out of OIC's [1]. In general, this should not be a major concern, although problems have been reported when trying to couple radiation in to very small structures in part due to the required alignment accuracy. Carefully designed tapered integrated structures can be used to alleviate this problem [27]. The principal tradeoff in coupling efficiency is that having smaller detectors and transmitters facilitates improved coupling efficiency but only at the expense of requiring more precise alignment. The cost of the latter would probably override any benefits of the former.

Using simple geometrical optical (ray-optics) arguments, it can be shown that the excitation of certain guided modes requires consideration of both the guide and its input coupling mechanism. Earlier we showed the relationship between the height of a slab waveguide, the angle and the modes which can be sustained for our system of air/Si/SiO_2 in Figure 3.8. During our discussion of the gap (Section 3.1.3) we showed that for guided modes with mode angles less than 74 ° total internal reflection occurred at an exit plane that was perpendicular to the plane of propagation unless a high index material was brought close (~ 1000 Å) to it. This same problem can exist at any cleaved surface and could make it difficult to couple out any higher order modes which don't satisfy the angular constraint. The reciprocal problem is represented by limitations on excitation of modes at the input to a cleaved face such as in an end fire application, shown in Figure 3.33, commonly used for testing purposes. In this figure we show several incident and transmitted rays. Based on Snell's law the extreme incident ray (90 °) can at most produce a transmitted ray that makes an angle of 16° with the axis which translates to a guided mode angle of 74°. In a perfect guide, where there is no cause for mode conversion, this mode excitation limitation would also require a height of at least 1 micron before one could excite the fundamental mode. The implication of this result is that single mode operation is determined by the input/output (I/O) constraints and can be maintained for waveguide heights that are significantly larger than those

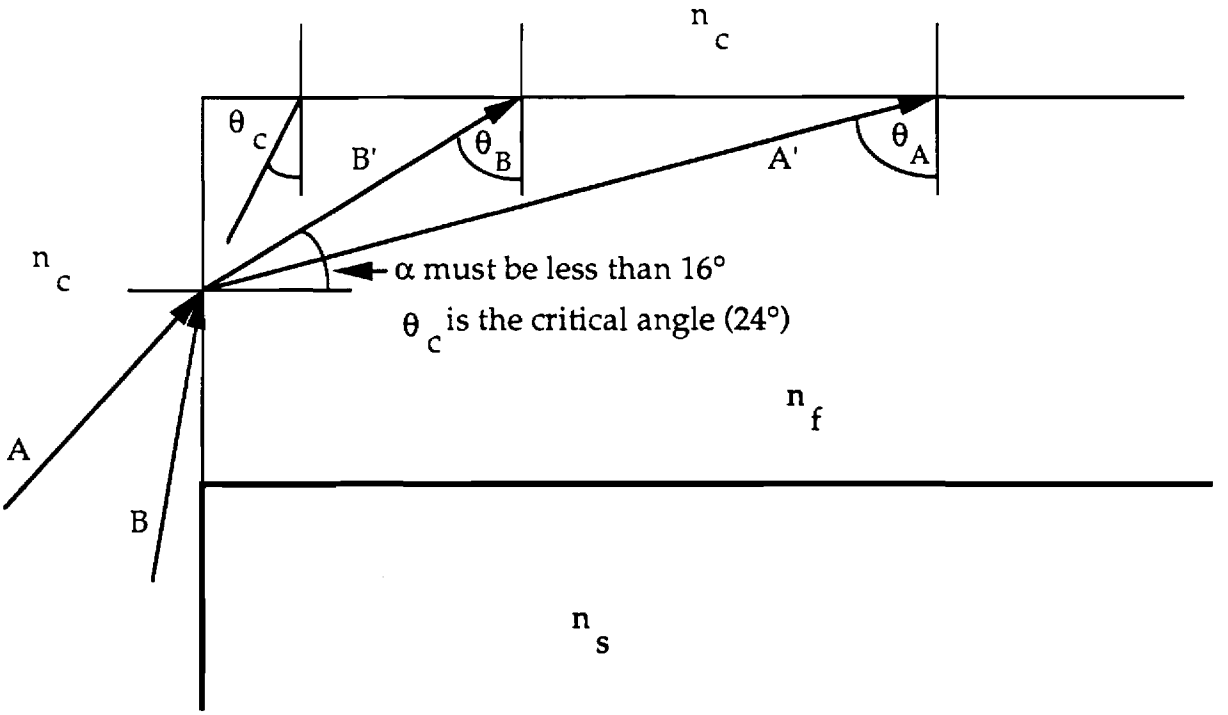

Figure 3.33 Because of the large index difference there is no input ray (A or B) that provides a guided mode angle (θ_A or θ_B) between the critical angle and 74 °. Therefore the endfire coupling mode requires a guide height such that the TE_0 mode angle is at least 74° (Hg ≈ 1μm).

determined earlier when the I/O problem was ignored. If this is true, then single mode operation would be simpler from a silicon processing point of view and furthermore because of the likelihood of mode conversion due to mechanical perturbations, the sensitivity to these perturbations would be greatly enhanced because of the natural suppression of higher order modes (smaller angles) at the exit plane due to TIR.

Throughput

An important figure of merit for the quality of a waveguide is its attenuation per unit length. Sidewall imperfections, bulk defects, free carriers, and abrupt transitions in the confining layers, all cause mode conversion and losses along the signal path. Throughput addresses the issue of how efficiently the signal is conducted through the structure. The major sources of signal attenuation have been listed and discussed earlier. Because of the large index of refraction of silicon, leakage should not pose a problem for the raised strip channel guide. However for the two active devices, where a well has been introduced under a section of the guide to enable mechanical displacement, several additional losses arise, due to

-impedance mismatch
-coupling of evanescent mode
-Fresnel losses at the gap
-gap misalignment

The impedance mismatch occurs at both ends of the bridge where there is a transition between an asymmetric guide to a symmetric guide. Although in this case the difference is not exceptionally large it is anticipated that this mismatch will result in some reflection of the incident power as well as some redistribution of power into other modes. Because the index of air is lower than that of silicon dioxide the leakage effect due to the presence of the evanescent wave should be no more significant than that of the straight guide provided that the bridge is not

deflected. The gap, present as an integral part of the microcantilever beam, can act as a mode filter, eliminating higher order modes and attenuating lower order modes due to diffraction and Fresnel losses. Maintaining a small gap distance (fractions of a wavelength) can significantly reduce these losses.

3.3.2 Limitations to Large scale integration

Packing Density

The smaller the device, the greater the density up to a point at which crosstalk between adjacent devices becomes significant. Packing density is a measure of (1) how closely these structures can be placed, and (2) how small can they be made. Both requirements distill down to the issue of how well the light is confined. In general, the larger the index difference, the better the confinement for any given mode angle.

An estimate of crosstalk requires the computation of an overlap integral according to Burns and Milton [28]. This requires an exact solution of the EM wave equation in the waveguide and thus is directly dependent on the mode of the wave and how much of the wave is outside of the guide. Once again, larger variations in indices result in better confinement. Typical values of the penetration depth are on the order of .1 microns.

There are limits to how small one can make these devices. Theoretically this is not true for symmetric waveguides, although what one can achieve technologically is another matter. For the silicon waveguide under consideration here, the minimum dimension for a guided mode is about 200 angstroms. This size is considered technologically infeasible; however single mode propagation is also supported up to about 2000 angstroms (and perhaps even a micron when the guide is I/O limited), which is considered to be attainable. For waveguides having transverse dimensions greater than .2 microns multi-mode operation is applicable. If we wish to maintain reasonable switching voltages (less than 15 volts), then

typical single mode (assumed to be < .2 microns in height) beam lengths must be on the order of 100 microns. The equivalent constraint for 1 micron high guides is 500 microns, while our test structures, at 6 microns in height and 400 microns in length, require a threshold voltage of several hundred volts. Reducing the depth of the well will reduce the required deflection voltage. The primary problem with thicker guides is that not only are they more difficult to bend but they also require deeper wells to allow an offset at least equal to the thickness of the guide for switching. Furthermore, multimode devices are less desirable because of the pulse broadening effects due to modal dispersion.

Routing

Another key issue, which has always been problematic for high density circuit development, is how to route signals from one device to another. A key difference between optical waveguides and electrical conductors is that the confinement of the waves is only limited by the difference in refractive indices between the guide and the adjacent material—energy can be lost as a guided wave turns a corner. The ability to route signals is limited by this phenomenon. Routing is an indication of how readily or efficiently light can be redirected. This property has been characterized by a consideration of the loss as a function of the radius of curvature for guides of different thicknesses. In this particular instance the large difference in indices of refraction is a considerable advantage.

Another challenging problem is how to develop crossover interconnects. The use of a simple cross section, like that in Figure 3.34, has been reported in [34] and represents a possible solution, if crosstalk between orthogonal channels is small enough. Alternatively, the multiplexing afforded by the presence of switches and branches can be readily used as a reconfigurable interconnect, however the ability to implement a truly effective crossover structure, as versatile as those used in

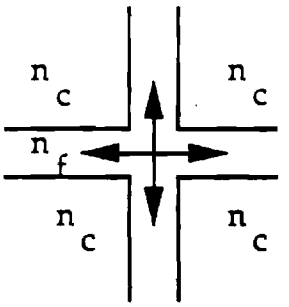

Figure 3.34 One potential method of interconnect is a simple right angle cross.

electronic integrated circuits, will probably require further development and experimentation.

3.3.3 Summary

In light of previous computations, we can conclude that the inherent limitations can be reduced to insignificance for the following conditions:

Oxide thickness greater than .4 microns

Dopant density less than 10E+15 per cubic centimeter

Radius of curvature greater than 5 microns

Rms surface roughness less than 10 Å

Coupling efficiency, on the other hand, remains a problem for single mode guides. Because of the large index of silicon, single mode guides are quite small making alignment difficult. Integral emitters and detectors at wavelengths of interest are not available therefore grating structures would appear to hold the most promise for coupling into SOI waveguides.

Throughput for the bridge structure should be quite good compared to the cantilever beam due primarily to the absence of the gap's fixed losses. In contrast, the cantilever beam is likely to represent a more sensitive indicator of deflection because it is more mechanically compliant and the resultant tilt and offset should accentuate the optical attenuation for a given deflection.

Packing density depends on the area of the devices, their interconnect and the required isolation. To maintain relatively low voltage operation, these devices will need to be relatively long (~100 μm) particularly if multimode devices are used. However, the large index variation should allow devices and signal paths to be closely spaced (only .4 micron between adjacent devices). Furthermore the large index variation results in excellent confinement which simplifies the low loss distribution of signals.

CHAPTER IV

CONCLUSIONS AND SUGGESTIONS FOR FURTHER RESEARCH

The potential for EMO devices for development of OIC's appears very promising. Initial first order analysis indicates that the physical basis for these types of devices is within reason. Furthermore, the available silicon process technology is adequate for fabrication of these devices. It remains to be seen how well these devices perform with respect to the first order model results.

Based on the analysis and results of this directed study the following conclusions are made:

1. BESOI shows considerable potential as a material for producing low loss high performance waveguides at wavelengths beyond 1.2 microns. Devices based on this material have the potential for high levels of integration due to the large index of refraction for silicon compared to its surroundings.

2. Electro-Mechanical control of guided waves is well within the capabilities of current process technologies. A fabrication sequence has been developed and test devices are near completion. First order analysis indicates that these test structures are capable of providing measurable results without exceptional effort. In effect, the initial "best guess" appears to have provided a good starting point for further investigations into this technology.

3. Mechanical transduction with optical readout using silicon micro-cantilever beans and micro-bridges also appears to hold significant potential.

4. A quantum mechanical motivated analysis of evanescent wave propagation across the gap in the micro-cantilever beam structure indicates that the losses due to gap spacing or end separation can be significantly reduced for gap dimensions below a 1000 angstroms.

5. Design tradeoffs indicate that performance should improve as devices approach single mode operation for layers thinner than .2 microns, although coupling energy into and out of the structures will be more difficult. Deflection voltages are reduced because the layers are thinner and the wells can be shallower.

In summary, we conclude that the control of guided waves using EMO devices appears feasible. An assessment of the advantages of this approach to guided wave fabrication and control will depend on the ease with which good devices can be fabricated.

The predicted analytical results and fabrication process development progress to date are encouraging. There is considerable work yet to be done in the area of modelling and experimentation. The most important steps are the completion of the fabrication sequence and characterization of actual device behavior. Measurements on working devices is the first step to improving on first order modelled results. A second round of device fabrication should include single mode operation devices. As a precursor to single mode devices, better control over film uniformity is essential for improved yield and better experiment design. Electrochemical etching or wafers that have been pre-processed to have parallel faces may prove fruitful in this regard. Ultimately the integration of structures to couple radiation into and out of the structure would expedite the potential application of these types of devices for optical switching and transduction. As experimental results accumulate more sophisticated modelling may be required. However, simulation of these types of devices would probably require a significant effort, in

that device operation depends simultaneously on free carrier distributions, electrostatic forces, electro-magnetic wave propagation, structural mechanics and to an unknown extent on anisotropic crystallographic effects. It is possible that all of these effects could be incorporated in a single package, starting with a mechanical finite-element simulation program.

BIBLIOGRAPHY

[1] H. Nishihara, M. Haruna, and T. Suhara, Optical Integrated Circuits, McGraw-Hill 1989.

[2] R.G. Hunsperger, Integrated Optics: Theory and Technology, Springer-Verlag 1985.

[3] IEEE Micro-Electro-Mechanical Systems Workshop, Salt Lake City, Utah 1989.

[4] D.G. Hall, "Survey of Silicon-Based Integrated Optics", Computer, pp. 25-32, December 1987

[5] F.S. Hickernell, "Optical Waveguides on Silicon", Solid State Technology, pp. 83-87 November 1988

[6] R.A. Soref, and J.P. Lorenzo, "All-Silicon Active and Passive Guided Wave Components for λ=1.3 and 1.6 micron",IEEE Journal of Quantum Electronics, VOL. QE-22, NO.6 pp. 873-879 June 1986

[7] D.E. Davies et al, "Optical Waveguides and SIMOX Characterization" ---- 1989

[8] W.P. Maszara, G. Goetz, A. Caviglia, and J. McKitterck, "Bonding of silicon wafers for silicon-on-insulator" J. Appl. Phys. 64 (10), 15 November 1988, pp. 4943-4950.

[9] R.A. Soref and B.R. Bennet,"Electro-optical Effects in Silicon",IEEE Journal of Quantum Electronics, Vol. QE-23, No. 1, pp. 123-129 January 1987.

[10] R.D. Black, S.D. Arthur, R.S. Gilmore, N. Lewis, and R.D. Lillquist, "Silicon and silicon dioxide thermal bonding for silicon-on-insulator applications", J. Appl. Phys. 63(8), 15 April 1988, pp. 2773-2777.

[11] D. Lu, J.J. Wortman, "Bonding Silicon Wafers by use of Electrostatic Fields Followed by Rapid Thermal Heating"' Materials Letters, Vol. 4, No. 11,12 October 1986 pp. 461-464.

[12] A. Reisman, M. Berkenbilit, S.A. Chan, F.B. Kaufman, and D.C. Green, "The Controlled Etching of Silicon in Catalyzed Ethylenediamine-Pyrocatechol-Water Solutions", J. Electrochem. Soc.: Solid-State Science and Technology, August 1979 pp. 1406-1415

[13] C. Spangler, Practical Silicon Etching Technology, University of Michigan, January 1987.

[14] B. Koeck, S.D. Collins, N.F. De Rooij, and R.L. Smith, "Study of Electrochemical Etch-Stop for High-Precision Thickness Control of Silicon Membranes", IEEE Transactions on Electron Devices, Vol. 36. No. 4, April 1989, pp. 663-669.

[15] H. Kogelnick, "Theory of Optical Waveguides", Guided-Wave Optoelectronics, T. Tamir (ed.) Springer-Verlag 1988

[16] R.J. Roark, Formulas for Stress and Strain, McGraw-Hill 1975.

[17] K.E. Petersen,"Dynamic Micromechanics on Silicon: Techniques and Devices," IEEE Trans.on Electron Devices, Vol. ED-25, NO. 10, pp. 1241-1250, October 1987.

[18] D. Marcuse, Light Transmission Optics, Van Nostrand Reinhold 1982.

[19] D. Marcuse, "Tilt, Offset, and End-Separation Loss of Lowest-Order Slab Waveguide Mode", Journal of Lightwave Technology, Vol. LT-4, No. 11, November 1986, pp. 1647-1650.

[20] M.K. Barnoski, "Fiber Couplers" Semiconductor Devices for Optical Communications, Topics in Applied Physics, Vol. 39, Springer-Verlag 1982.

[21] E. Hecht and A. Zajac, Optics, Addison-Wesley 1974.

[22] J.J. Hupert and G. Ott, "Electromagnetic Analog of the Quantum-Mechanical Tunnel Effect" ----- 1966.

[23] E.E. Anderson, Modern Physics and Quantum Mechanics, W. B. Saunders 1971.

[24] P.S. Theocaris and E.E. Gdoutos, Matrix Theory of Photoelasticity, Springer-Verlag 1979

[25] S.P. Timoshenko and J.M. Gere, Mechanics of Materials, Van Nostrand 1972.

[27] F.J. Leonberger and J.F. Donnely, "Semiconductor Integrated Optic Devices", Guided-Wave Optoelectronics, T. Tamir (ed.) Springer-Verlag 1988

[28] W.K. Burns and A.F. Milton, "Waveguide Transitions and Junctions", Guided-Wave Optoelectronics, T. Tamir (ed.) Springer-Verlag 1988

[29] K. Hogari and T. Matsumoto, "Electrostatically Driven Fiber-Optic Micromechanical On/Off Switch and Its Application to Subscriber Transmission Systems", Journal of Lightwave Technology, Vol. 8. No. 5. May 1990, pp. 722-727.

[30] R.S. Muller and T.I. Kamins, Device Electronics for Integrated Circuits, John Wiley and Sons 1986

[31] The IR Handbook, ed. G. Zissis and W. Wolfe, ONR 1978.

[32] B. N. Kurdi and D. G. Hall. "Optical Waveguides in Oxygen-Implanted Buried-Oxide Silicon-on-Insulator Structures". Optics Letters, vol. 13, no. 2, pp.175-177,1988.

[33] J. Haisma, G. Spierings, U. Bierman, and J. Pals, "Silicon-on-Insulator Wafer Bonding-Wafer Thinning Technological Evaluations", Jap. Journal of Appl. Phys. Vol. 28, No. 8, August, 1989, pp. 1426-1443

[34] R. Selvaraj, H. T. Lin, and J. F. McDonald, "Integrated Optical Waveguides in Polyimide for Wafer Scale Integration", IEEE Journal of Lightwave Technology, Vol. 6, No. 6, pp. 1034-1043, June 1988.

[35] D. G. Hall, "The role of silicon in integrated optics", Optics News, pp.12-15, February 1988.

[36] S.E. Miller, Bell Syst. Techn. J. 43, 1727 (1964)